The MicroSkyshine Method For Gamma-Ray Skyshine Analysis

by

R. E. Faw and J. K. Shultis

Nuclear Engineering Department
Kansas State University
Manhattan, KS 66506

February 1987

Kansas State University
College of Engineering
Engineering Experiment Station

Report 188

The MicroSkyshine Method for Gamma-Ray Skyshine Analysis

-- TABLE OF CONTENTS --

1. Summary

A method is presented for the calculation of gamma-ray skyshine radiation dose rates arising from point, monoenergetic, isotropic sources in two fundamental geometries. Specifically, the source may be placed on the axis of a cylindrical silo or behind an obliquely oriented wall. There may also be a horizontal slab shield above the source. The method, because of its inherent simplicity, is ideally suited for implementation on microcomputers.

This skyshine method, termed MicroSkyshine, is based on line-beam response functions which were determined by empirical fits to Monte Carlo skyshine calculations [La79]. These response functions, as adapted for use in the MicroSkyshine method, cover the gamma-ray energy range from 0.1 to 10 MeV. In terms of source-to-detector distances, the nominal range of validity of the response functions is 0 to 1500 m. However, for the high-energy gamma rays from ^{16}N sources, the response functions may be used for distances as great as 2500 m. Although the MicroSkyshine method is developed for point monenergetic sources in the two fundamental skyshine geometries, it can readily be applied to polyenergetic source, line and area sources, and to geometries with different source collimations.

To verify the accuracy of the MicroSkyshine method, its results are compared to many different skyshine results. Results from a benchmark skyshine experiment and calculations for two ANSI-Standard reference skyshine problems verify that the MicroSkyshine method yields predictions with precision comparable to that achieved by other "standard" methods. The validation of the MicroSkyshine method is further supported by comparisons to skyshine calculations obtained by (1) the moments method, (2) the G^3 point-kernel code, (3) the K-SHINE

point-kernel skyshine code, and (4) a combination of the ANISN code and the SKYSHINE-II code.

From these comparisons, it is found that the MicroSkyshine method produces results that are, in nearly all cases, conservative and within 50 percent of authoritative reference values. For shielded-source problems, there are too few reliable reference values to quantify the accuracy of the MicroSkyshine method over the entire ranges of permissible source energies, of various source-to-detector distances, and of possible shield thicknesses. The most authoritative reference values for a shielded geometry are provided by the benchmark skyshine experiment (^{60}Co source, source-to-detector distances of 0 - 700 m, and 21-cm and 43-cm concrete shields). For the thinner shield, MicroSkyshine overestimates the skyshine by about 50% for distances greater than 300 m, while for the thicker shield MicroSkyshine is in good agreement with experiment at large distances although somewhat underpredictive at smaller source-to-detector distances.

The MicroSkyshine method is thus shown to be a simple, accurate, and robust method for predicting the skyshine radiation doses for many practical problems. As such, it affords the shielding analyst with an inexpensive alternative to the many computationally intensive mainframe codes presently used for skyshine analyses.

2. Introduction

The term *skyshine* refers in general to radiation originating from a fixed source and scattering in the atmosphere before reaching a receiver or detector. It becomes important when sufficient material shielding is present along the direct path from the source to the receiver so as to prevent any significant radiation from reaching the receiver through the shielding material. In such circumstances, the elementary technique of ray analysis and the application of buildup-factor concepts fail. The shielding designer or analyst must resort to more specialized if not more sophisticated techniques.

This report describes the evolution of methods of gamma-ray skyshine analysis. It describes in detail and supports the verification of one particular method synthesized from more general methodologies used in mainframe computer codes. This particular method, called the *Micro-Skyshine* method, has been developed specifically for microcomputer implementation and is intended to provide the shielding analyst with a simple, accurate, and inexpensive means of performing gamma skyshine calculations for elementary problem geometries.

2.1 Methods of Skyshine Analysis

The Monte Carlo method was the first of the radiation-transport methods applied to the analysis of gamma-ray skyshine. Lynch, Benoit, Johnson, and Zerby [Ly58] at Oak Ridge National Laboratory computed the air dose as a function of distance from point-monodirectional sources emitting photons at angles up to 180 degrees from the source-receiver axis. The resulting "line-beam" response functions were suitable for use in skyshine analysis. More recently, Radiation Research Associates

carried out much more extensive Monte Carlo calculations of line-beam response functions for use with the SKYSHINE and SKYSHINE-II codes [Pr76, La79]. These response functions, which are in the public domain, have been incorporated into the MicroSkyshine method and are described in detail in this report.

Availability of Monte Carlo generated line-beam response functions stimulated investigations of the suitabililty of more elementary "single-scatter" calculations of response functions and the extension of single-scatter techniques to more comprehensive skyshine analyses. Trubey [Tr61], and later Kitazume [Ki68], made direct comparisons between Monte Carlo and single-scatter line-beam response functions. The success of their work has led to the further development of single-scatter methods to apply to more complicated skyshine geometries.

Both Monte Carlo and single-scatter methods have supported the evolution of skyshine analysis techniques. The more general-purpose Monte Carlo codes such as OGRE ,COHORT, and MORSE have been applied directly in skyshine calculations, while codes specifically designed for skyshine calculations, such as SKYSHINE and SKYSHINE-II, make use of Monte Carlo generated response functions. Evolution of the QAD and G^3 series of codes exemplify the application of the single-scatter method to general gamma-ray problems. More specific application of the single-scatter method to skyshine analysis is exemplified by the work of Roseberry et al. [Ro80, Ro82] and by Chou et al. [Ch83].

Also finding use in skyshine analysis are transport codes based on the discrete-ordinates method, such as the DOT and ANISN codes. These general-purpose transport codes, like the general-purpose Monte Carlo codes, directly solve the governing transport equation for the radiation, and generally require great computational resources. To reduce the computational effort, Keck and Herchenroder [Ke82] have combined the discrete-ordinates and line-beam response-function methods in skyshine analysis by using ANISN for in-structure radiation transport and then SKYSHINE-II for atmospheric transport of gamma rays.

2.2 Development of the MicroSkyshine Method

Adoption of the personal microcomputer as a tool for engineering design and analysis has led to the demand for codes which take full advantage of capabilities of such a tool. This is true for radiation-shielding design and analysis and an important application in this area is the analysis of gamma-ray skyshine. Unfortunately, many of the mainframe-based methods used for skyshine analysis are far too computationally intensive for microcomputer execution. Thus, the MicroSkyshine method was devised to meet the need for a technique which is not only accurate in prediction of skyshine dose rates for practical geometries but also well-suited for implementation on microcomputers.

2.2.1 The Principles of the MicroSkyshine Method

The method developed in this study is directed towards skyshine gamma radiation arising from isotropic, monoenergetic point sources that are occluded from the point of interest (detector) by simple structures. In particular, two simple problem geometries are considered. In the first, the point source in placed on the axis of a cylindrical silo. In the second, the source is placed behind a vertical plane wall (which may be oriented obliquely to the source-detector axis). In both cases, radiation may be emitted skyward directly into the air or may first have to penetrate a horizontal slab of shielding material placed over the source.

The MicroSkyshine method presented here for these two fundamental skyshine geometries makes use of line-beam response functions developed from Monte Carlo calculations and employed in the Radiation Research Associates' SKYSHINE II code [La79]. These response functions give the dose at a specified detector location for a gamma-photon beam of a given energy and angular orientation. Thus, to calculate the skyshine dose resulting from radiation emitted upwards for either of the unshielded silo or wall geometries considered here, it is only necessary to integrate these line-beam response functions over all directions allowed by the silo or wall collimation.

For cases in which the point source is shielded above by a horizontal slab, the radiation emitted skyward is first attenuated and corrected for buildup of scattered photons as it passes through the shield. While this correction for the shield effect is not rigorously justified, it is found to produce reasonable results for shields typical of roof structures encountered in many radiation facilities.

Overhead shielding is not accommodated in the SKYSHINE-II code. It is in the G^3 code. However, in G^3, while photon attenuation is properly accounted for, no corrections are made for the buildup of photons scattered in the overhead shield. This *necessarily* leads to *underprediction* of skyshine dose rates by the G^3 code, as is shown in this report.

2.2.2 Extensions of the MicroSkyshine Method

While the MicroSkyshine method presented in this report is restricted to monoenergetic point sources in the silo or single-wall geometries, the method can readily be extended to other situations. First, any source emitting gamma photons of different energies can be treated easily as a series of monoenergetic problems. The method can also readily be extended to line and area sources by treating such sources as a series of point sources. Finally, the problem geometry defining the degree of upward collimation of the emitted radiation can be extended to more restrictive situations than the silo or single-wall cases by using different (and more complicated) algebraic expressions to define the boundaries of the vertically collimated photon beam. For example, the point source can easily be placed anywhere inside a rectangular building (see Section 6.3.2).

Thus the two specific skyshine problems considered in this report represent basic or fundamental skyshine problems with which solutions to more complicated skyshine problems may be obtained.

2.2.3 Limitations of the MicroSkyshine Method

The MicroSkyshine method has several inherent limitations and

restrictions. The method is only as good as the line-beam response functions upon which it is based. These response functions cover a wide range of source-to-detector distances and photon energies. Specifically, the calculated skyshine doses are valid for photon energies between 0.1 and 10 MeV and for source-to-detector distances nominally from 0 to 1500 m. However, as is shown in Chapter 6, for the high-energy gamma rays of ^{16}N sources, results are valid in most cases for distances to 2500 m. For gamma-ray energies less than about 0.5 MeV, The MicroSkyshine results may be over-conservative for distances greater than about 1000 m. Chapter 6 examines the extremes of source-to-detector distances for which the MicroSkyshine method is applicable and offers recommendations for extrapolation of MicroSkyshine results beyond these extremes.

Finally, the MicroSkyshine treatment of the overhead shield is only approximate, and while it has been verified for shield thicknesses less than about six mean-free-path lengths (or attenuation factors $\leq$ 400) the shield correction must be used with caution for thicker shields. The following table summarizes shield thicknesses corresponding to six mean free paths.

Photon Energy (MeV)	Equivalent thickness (cm) for 6 mean free paths			
	Water (1 g/cm^3)	Concrete (2.35 g/cm^3)	Iron (7.86 g/cm^3)	Lead (11.3 g/cm^3)
1	85	40	13	8
2	122	57	18	12
5	198	88	24	13
10	270	111	26	11

Despite these limitations, the MicroSkyshine method, when applied to shielded sources, is no doubt more precise than other codes such as G^3 which are routinely applied to skyshine analyses.

2.3 Validation of the MicroSkyshine Method

Of prime importance in the development of a new analysis method is the determination of its accuracy. Such verification or validation is generally very difficult when, as in the skyshine problem, there are no known "exact" results against which the method may be compared. In lieu of such exact standards, one must compare against, (1) results of experiments which usually have inherent features which are difficult to model exactly, (2) reference calculations for standard benchmark problems which seldom are in complete agreement with each other, and (3) values obtained by independent calculational methods which have unknown limitations for the class of problems being considered. In this study all three validation comparisons are used to test the MicroSkyshine method.

2.3.1 Skyshine Benchmark Experiments

To the authors' knowledge, only one series of experiments has been widely documented. That is the series conducted at the Kansas State University Nuclear Engineering Shielding Facility, under the auspices of Radiation Research Associates and the Japanese Nuclear Safety Research Association. That work, based entirely on ^{60}Co sources, is described in detail in this report and provides an important set of benchmarks for verification of the MicroSkyshine method.

2.3.2 Skyshine Benchmark Calculations

ANSI/ANS-6.6.1-1979, the "American National Standard for Calculation and Measurement of Direct and Scattered Gamma Rays from LWR Nuclear Power Plants," contains results of a number of reference skyshine calculations for ^{16}N sources. Results of those calculations are described in this report and further support the verification of the MicroSkyshine method.

2.3.3 Skyshine Calculations By Other Methods

The above benchmark experimental results and reference problem calculations are for very specific skyshine problems. To test the MicroSkyshine method for for different problem parameters (e.g., different source energies, different overhead shielding, different degrees of vertical collimation, etc.) it is necessary to compare MicroSkyshine results against values obtained with methods which have previously been found useful for skyshine calculations. In this study four different calculational codes are used to obtain results for the two skyshine geometries considered and against which the MicroSkyshine results are compared. Included as comparison methods are (1) the moments method [Ch80], (2) the G^3 point-kernel code [Ma73], (3) the K-SHINE point-kernel skyshine code [Ge87], and (4) a hybrid method which combines the ANISN and SKYSHINE-II codes [Ke82].

2.4 Objective and Scope of Report

This report has two main objectives. The first is to provide documentation for the analysis techniques and the data used in the MicroSkyshine method for calculation of gamma-ray skyshine dose. The second is to provide documentation supporting the verification of suitability of the MicroSkyshine method for general purpose gamma-ray skyshine dose calculations.

Chapters 3 and 4 respectively describe benchmark skyshine experiments and calculations. Chapter 5 describes the MicroSkyshine method and examines in detail the line-beam response functions used in MicroSkyshine computations. Chapter 6 deals with verification, comparing skyshine doses calculated by the MicroSkyshine code with results of benchmark experiments and calculations. For shielding conditions for which no benchmarks are available, new verification calculations are described and documented. Chapter 7 and Appendix B provide full documentation of the data employed in the shielding calculations performed using the MicroSkyshine code. Other appendices provide documentation of the results of all verification calculations.

3. Skyshine Benchmark Experiments

3.1 Description of Experiments

There are few experimental skyshine measurements which can serve as benchmarks for the skyshine problem. Most measurements have been taken relatively near the source ($\lesssim$ 1 mean free path in air) or involve geometric configurations which are too difficult to model accurately. To alleviate this deficiency, several years ago a major experimental program, designed for ease of simulation, was performed to measure the skyshine radiation over a source-to-detector baseline from 30 to 700 m [Na81]. Data from this experiment serve as standards against which calculational models can be tested. In this chapter, this benchmark experiment is reviewed, and pertinent results tabulated.

The benchmark experiment described here was performed at the Kansas State University Nuclear Engineering Shielding Facility as part of a project managed by Radiation Research Associates under support and guidance of the Japanese Nuclear Safety Research Association Study Committee on Air-Scattered Gamma Rays in Nuclear Facilities. Compact cobalt-60 sources with activities up to 140 GBq (5200 curies) were positioned on the axis of an annular concrete silo with walls sufficiently thick to preclude significant radial penetration of radiation. Two basic experimental geometries were used. In the "unshielded" geometry, wedge-shaped collimator concrete blocks were placed around the top edge of the silo wall so as to define an open conical aperture with a full-angle of 150.5 degrees and with the source at the apex. In the "shielded" geometry, concrete shielding slabs of two thicknesses (21 or 43 cm) and of density 2.13 g/cm^3 were placed atop the silo.

With the above source geometries, two types of skyshine measurements were made. With a well-collimated and shielded NaI detector, energy spectral measurements of the skyshine 2.2 m above grade were

obtained radially outwards in 100-m increments out to 700 m from the source. In a second set of measurements, which are of more interest to the present study, a high-pressure ionization chamber was used to measure directly the 4π-skyshine-exposure rate 1 m above grade at distances from 30 m out to 700 m from the silo axis.

3.2 Experimental Results

Several corrections were made to the raw experimental data. Although the energy sensitivity of the high pressure ionization chamber was relatively flat for high gamma-ray energies (> 300 keV), it varied significantly for lower energies (where the measured skyshine spectra was found to peak). Using the measured skyshine energy spectra, a correction factor to account for the non-uniform energy response of the detector was calculated. Typically, less than a 10% correction was needed to obtain the true skyshine exposure rate.

It was also possible to infer exposure rates from the NaI spectral measurements. Using measured energy response functions based on NBS calibration sources, the NaI spectra were unfolded. The unfolded spectra were then integrated over energy to give exposure rates and then further corrected for the NaI collimation. These secondary or derived skyshine exposure rates were found to be in excellent agreement with those obtained with the high-pressure ionization chamber.

3.2.1 Results From The Unshielded Silo Benchmark Experiment

The skyshine exposure rates for the unshielded-silo geometry, as measured by the high-pressure ionization chamber, are listed in Table 3.1. In Table 3.2, the NaI-derived exposure rates are tabulated. In order to facilitate intercomparison of experimental data, comparison of experimental data with calculations, and extrapolation of results to situations other than those investigated experimentally, the raw experimental data have been multiplied by the square of the source-to-

detector distance, divided by the solid angle of collimation, and normalized by dividing by the source strength. Multiplication by the square of the distance recognizes the strong influence of the inverse-square law on radiation dose, even in the geometries associated with skyshine. Division by the solid angle recognizes that skyshine dose from a point source in a silo varies approximately in proportion to the solid angle of collimation. Indeed, as the solid angle approaches zero, a linear relationship becomes more and more exact. Finally, the source-to-detector distance r is multiplied by the air density (i.e., $r \times \rho_{air}$, the product being called the aerial density) This reexpression of the experimental exposure rates permits intercomparison of data taken under conditions of day-to-day air-density variations, and is used only as a convenience in the presentation of results. Such a renormalization procedure is not part of the MicroSkyshine method; however, it is sometimes applied to MicroSkyshine results in this report when they are compared directly to experimental results.

3.2.2 Results of The Shielded Silo Benchmark Experiment

Two thicknesses of concrete shielding above the source (21.0 and 42.8 cm) were used in the KSU benchmark skyshine experiment. Exposure rates (normalized as above for the unshielded results) are presented in Table 3.3 for the high-pressure ionization-chamber measurements, and in Table 3.4 for the normalized NaI-inferred exposure rates.

The exposure rate measurements are generally accurate to within a few percent except for the largest source-to-detector distances where the skyshine signal was the weakest. The unnormalized results for the the shielded and unshielded case and the associated errors can be found in Ref. [Na81].

3.2.3 Calculations for Benchmark Experimental Conditions

Besides the experimental phase of the skyshine experiment, the skyshine energy spectra and exposure rates for the unshielded case were calculated at two different levels of detail by the discrete-ordinates

code DOT 3.5 [Rh73]. The first, and most elaborate of these calculations, used 39 energy groups, P-5 cross-section expansions, and an S-16 (160 angles) angular quadrature set. The second calculation used only 10 energy groups, P-3 expansions, and S-12 (96 angles) quadrature. The generation of group cross sections for these calculations is described by Nason [NaS1].

For these DOT calculations, cylindrical r-z geometry was used (r = 0 being the silo axis). Vacuum boundary conditions were used except at r = 0 where a reflecting boundary was employed. For the 39-group calculation, a 0.2-m-thick ground interface (z = 0) was used, while for the 10-group calculation, the ground was replaced by an absorbing boundary.

For the shielded geometry case, only the 10-group DOT model was used. First the ANISN-ORNL one-dimensional discrete ordinates code (RSIC code package CCC-254) was used to calculate the energy spectrum of the radiation penetrating the roof shield. This penetrating radiation was then used as a source for the DOT calculations.

Detailed comparisons of these DOT calculations with the measured energy spectrum of the skyshine radiation are found in Ref. [NaS1]. Of concern in this study are the 4π-skyshine exposure rates. The measured values and the DOT calculated values are shown in Fig. 3.1. It is seen that the 39-group DOT calculations are in excellent agreement with the unshielded experiment for distances > 200 m (areal density > 25 g/cm^2), while closer to the source the experiment gives slightly greater values as a result of radiation which first interacts in the silo wall and then reaches the detector. This in-silo photon scattering was neglected by the DOT calculations. The 10-group DOT calculations are about 10% lower than the 39-group values -- a result of the simplistic treatment given to the air-ground interface in the 10-group calculations. For the shielded case, the DOT calculations again underpredict the experimental results. This underprediction was a result of using a perfect absorber in place of a proper air-ground interface.

Table 3.1. Normalized skyshine exposures measured by a high-pressure ionization chamber 1 m above grade for the unshielded (open silo) experiment. Data from Ref. [NaS1] have been normalized to indicated units.

Areal Density (g/cm^2)	Normalized Exposure (m^2R/sr)	Areal Density (g/cm^2)	Normalized Exposure (m^2R/sr)	Areal Density (g/cm^2)	Normalized Exposure (m^2R/sr)
5.72	4.78E-17	22.88	7.85E-17	57.20	2.06E-17
5.48	4.86E-17	21.92	7.77E-17	54.80	2.34E-17
11.58	7.44E-17	34.32	5.57E-17	67.44	1.38E-17
11.44	7.45E-17	34.32	5.26E-17	67.44	1.46E-17
11.19	7.98E-17	32.88	5.35E-17	65.76	1.56E-17
10.96	7.74E-17	32.88	5.48E-17	77.77	9.62E-18
10.89	7.45E-17	45.76	3.52E-17	76.72	9.54E-18
10.89	7.31E-17	43.84	3.97E-17		

Table 3.2. Normalized skyshine exposures derived from NaI spectral measurements 2.2 m above grade for the unshielded (open silo) experiment. Data from Ref. [NaS1] have been normalized to the indicated units.

Areal Density (g/cm^2)	Normalized Exposure (m^2R/sr)	Areal Density (g/cm^2)	Normalized Exposure (m^2R/sr)	Areal Density (g/cm^2)	Normalized Exposure (m^2R/sr)
11.38	8.175E-17	33.74	6.043E-17	67.21	1.627E-17
11.34	7.903E-17	46.22	3.903E-17	75.99	1.106E-17
22.00	8.416E-17	58.77	2.236E-17		
33.75	6.156E-17	67.62	1.515E-17		

Table 3.3. Normalized skyshine exposures measured by a high-pressure ionization chamber 1 m above grade for shielded geometry in which concrete slabs of two different thicknesses were placed atop the silo. Data from Ref. [Na81] have been normalized to the indicated units.

Areal Density (g/cm^2)	Normalized Exposure (m^2R/sr)	Areal Density (g/cm^2)	Normalized Exposure (m^2R/sr)	Areal Density (g/cm^2)	Normalized Exposure (m^2R/sr)
A. 21.0 cm Concrete Slab					
3.629	3.238E-18	11.62	5.562E-18	47.64	1.523E-18
3.499	3.094E-18	11.08	5.442E-18	46.08	1.611E-18
3.360	2.990E-18	17.94	5.386E-18	44.64	1.859E-18
6.025	4.649E-18	17.42	5.434E-18	59.31	7.670E-19
5.831	4.657E-18	16.86	5.426E-18	57.20	8.416E-19
5.581	4.280E-18	23.92	4.617E-18	55.63	9.217E-19
8.404	5.394E-18	23.14	4.641E-18	71.13	4.144E-19
8.404	5.082E-18	22.24	4.657E-18	69.15	4.304E-19
8.103	5.009E-18	35.74	2.749E-18	66.51	4.801E-19
7.786	4.793E-18	35.74	2.829E-18	80.35	2.501E-19
12.13	6.131E-18	34.57	2.950E-18	78.14	2.493E-19
12.13	5.819E-18	33.49	2.917E-18		
B. 42.8-cm Concrete Slab					
3.380	2.581E-19	7.772	3.911E-19	22.35	3.711E-19
3.378	2.533E-19	11.42	4.480E-19	22.19	3.775E-19
3.343	2.541E-19	11.18	4.448E-19	34.61	2.020E-19
5.653	3.751E-19	11.10	4.657E-19	33.64	2.068E-19
5.611	3.799E-19	17.20	4.617E-19	33.29	2.196E-19
5.572	3.823E-19	16.76	4.536E-19	46.15	1.026E-19
7.791	4.120E-19	16.65	4.577E-19	44.83	1.178E-19
7.828	4.152E-19	23.01	3.743E-19	44.52	1.274E-19

Table 3.4. Normalized skyshine exposures derived from NaI spectral measurements 2.2 m above grade for shielded geometry in which concrete slabs of two thicknesses were placed atop the silo. Data from Ref. [Na81] have been normalized to the indicated units.

Areal Density (g/cm^2)	Normalized Exposure (m^2R/sr)	Areal Density (g/cm^2)	Normalized Exposure (m^2R/sr)	Areal Density (g/cm^2)	Normalized Exposure (m^2R/sr)
A. 21.0-cm Concrete Slab					
11.46	6.348E-18	35.08	2.990E-18	57.67	1.010E-18
11.57	6.612E-18	34.88	2.757E-18	68.68	5.602E-19
11.68	6.172E-18	35.28	2.966E-18	68.60	6.083E-19
23.71	4.817E-18	45.73	1.747E-18	78.59	3.783E-19
B. 42.8-cm Concrete Slab					
10.99	5.723E-19	23.67	3.823E-19	56.74	6.260E-20
11.95	5.073E-19	35.09	2.396E-19	56.71	6.172E-20
11.96	5.554E-19	38.83	2.260E-19	57.21	6.212E-20
11.06	5.170E-19	46.34	1.282E-19		

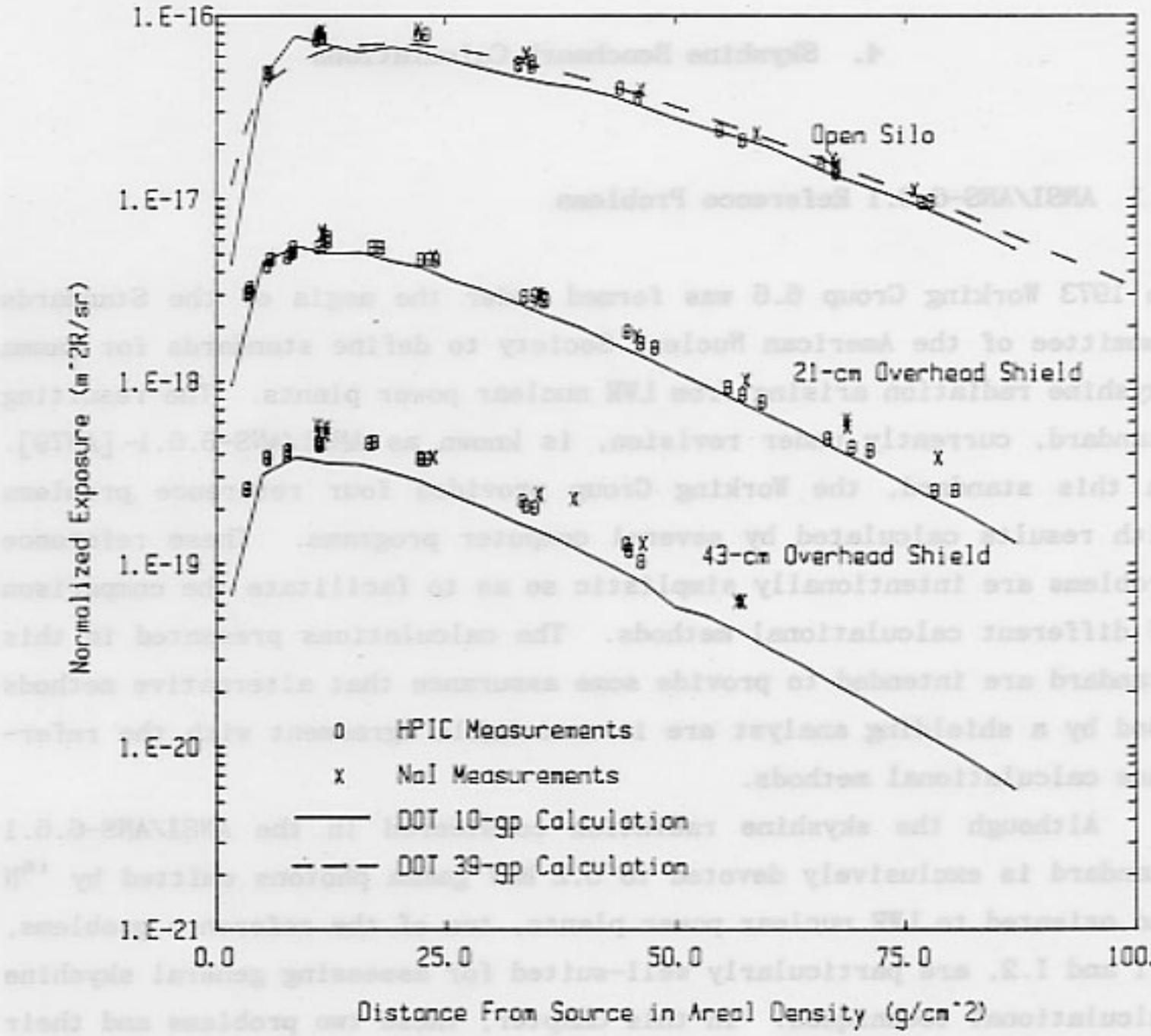

Fig. 3.1 Measurements and DOT calculations for the KSU benchmark skyshine experiments.

4. Skyshine Benchmark Calculations

4.1 ANSI/ANS-6.6.1 Reference Problems

In 1973 Working Group 6.6 was formed under the aegis of the Standards Committee of the American Nuclear Society to define standards for gamma skyshine radiation arising from LWR nuclear power plants. The resulting standard, currently under revision, is known as ANSI/ANS-6.6.1 [AN79]. In this standard, the Working Group provided four reference problems with results calculated by several computer programs. These reference problems are intentionally simplistic so as to facilitate the comparison of different calculational methods. The calculations presented in this standard are intended to provide some assurance that alternative methods used by a shielding analyst are in reasonable agreement with the reference calculational methods.

Although the skyshine radiation considered in the ANSI/ANS-6.6.1 Standard is exclusively devoted to 6.2 MeV gamma photons emitted by ^{16}N and oriented to LWR nuclear power plants, two of the reference problems, I.1 and I.2, are particularly well-suited for assessing general skyshine calculational techniques. In this Chapter, these two problems and their reference calculations are summarized. Then in Chapter 6, MicroSkyshine results for these two problems will be presented and compared to the reference calculations.

4.1.1 ANSI/ANS-6.6.1 Reference Problem I.1

The first Reference Problem I.1 is for a bare, point, isotropic

source of ^{16}N gamma photons with energies of 6.2 MeV. The source, which has a strength of 1 photon per second, is positioned 60 ft (18.3 m) in air above a horizontal air-ground interface. Detectors are placed at distances from 200 ft (61 m) to 5000 ft (1,500 m) from the normal through the source to the ground-interface and at a height of 3 ft (0.91 m) above grade. The problem geometry is shown in Fig. 4.1. The detector response is to be calculated for the total dose rate (in units of rads(air)/yr) as well as for the skyshine component alone.

4.1.2 ANSI/ANS-6.6.1 Reference Problem I.2

The second Reference Problem places the source of Problem I.1 on the vertical axis of a rectangular roofless building having 4 ft (1.22 m) thick concrete walls on all four sides. The source is 60 ft (18.3 m) above grade and the building sides at 62 ft (18.9 m) high. The detectors are located as in Problem I.1. The inside dimensions of the enclosure are 100 ft (30.5 m) by 150 ft (45.7 m) and the building is oriented so that the long walls are perpendicular to the line of detectors. The geometry for this problem is shown in Fig. 4.2. Again the detector response is to be calculated for the total dose rate (in rads (air) per year) and for only the skyshine component.

4.1.3 Material Compositions for Reference Problems

In all the reference calculations the air density is to be taken as 1.22 mg/cm^3 with a number density of 1.07×10^{19} $atoms/cm^3$ of oxygen and 4.02×10^{19} $atoms/cm^3$ of nitrogen. The density of concrete is to be taken as 2.34 g/cm^3 with the following composition:

Concrete Composition

Element	Atoms/cm^3	Element	Atoms/cm^3	Element	Atoms/cm^3
H	7.86×10^{21}	Mg	1.40×10^{20}	K	6.90×10^{20}
O	4.38×10^{22}	Al	2.39×10^{21}	Ca	2.92×10^{21}
Na	1.05×10^{21}	Si	1.58×10^{22}	Fe	3.10×10^{20}

If the ground can be treated by the analysis code, the soil density is to be taken as 1.7 g/cm^3 with the following composition:

Ground Composition

Element	Atoms/cm^3	Element	Atoms/cm^3
H	9.77×10^{21}	Al	4.88×10^{21}
O	3.48×10^{22}	Si	1.16×10^{22}

4.2 Methods Used for Reference Calculations

The ANSI/ANS-6.6.1 Reference Problems were solved by several codes using a variety of radiation transport techniques. Specifically, the following codes were used:

(a) DOT II [My73]: This a two-dimensional, discrete ordinates, general-purpose transport code that uses an energy multigroup approximation and allows for anisotropic scattering.

(b) OGRE [Pe65]: This is a Monte Carlo code specifically designed for gamma transport problems.

(c) COHORT II [So75]: This is a specialized Monte Carlo code designed for shielding calculations.

(d) QADMOD [Pr74]: This is a three-dimensional point-kernel code based on the single scatter approximation.

(e) SKREEN [Ro73]: This is a point-kernel shielding code.

(f) G^3 [Ma73]: This a three-dimensional, single-scatter (point kernel) code especially suitable for photon skyshine calculations.

(g) SKYSHINE [Pr76]: This code numerically integrates empirically derived beam response functions (based on Monte Carlo results) to find skyshine dose rates.

The results obtained with these codes were based on a variety of different assumptions and simplifications to the reference problems. For example, several calculations ignored the presence of the ground by simply replacing it by an infinite air medium. Moreover, different energy-group structures and different cross-section libraries were used. Yet despite these differences and approximations, the reported results are all in reasonable agreement and serve as excellent standards against which to compare other calculational schemes. (The ANSI/ANS Reference Calculations are shown later in Figs. 6.6 and 6.7. along with the Micro-Skyshine results.)

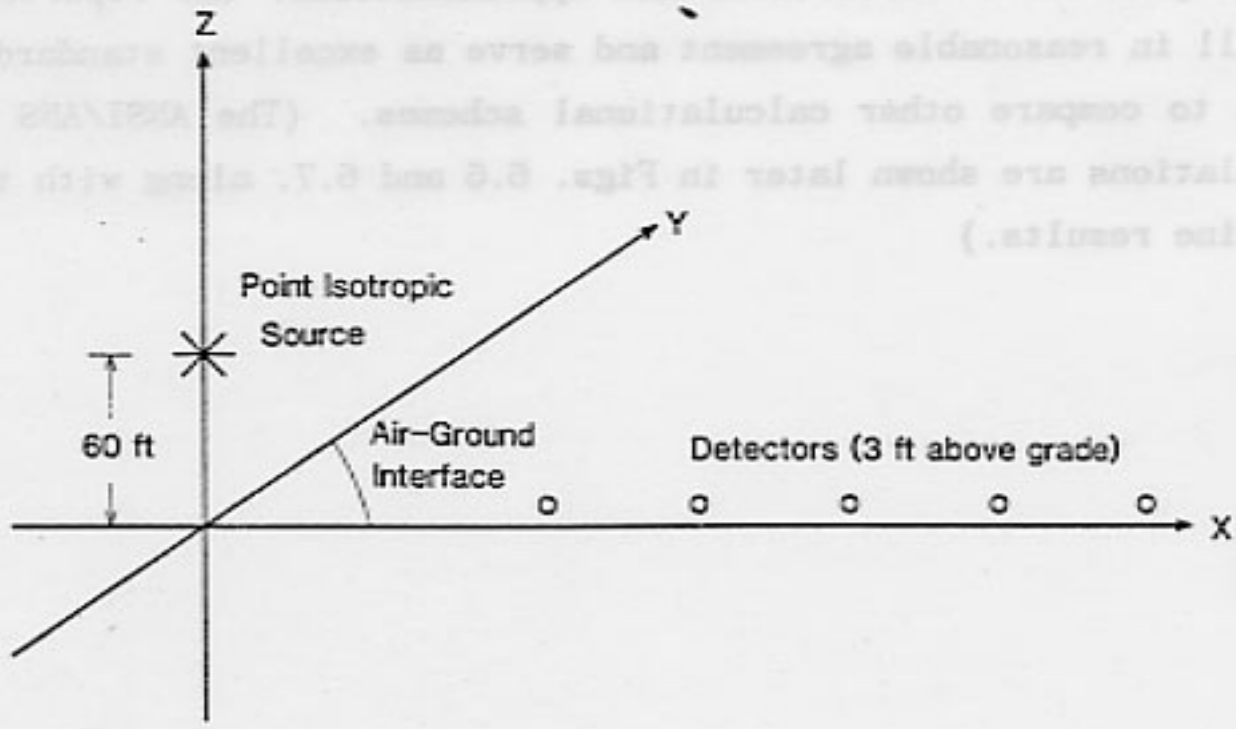

Fig. 4.1. Geometry for ANSI/ANS-6.6.1 Reference Problem I.1.

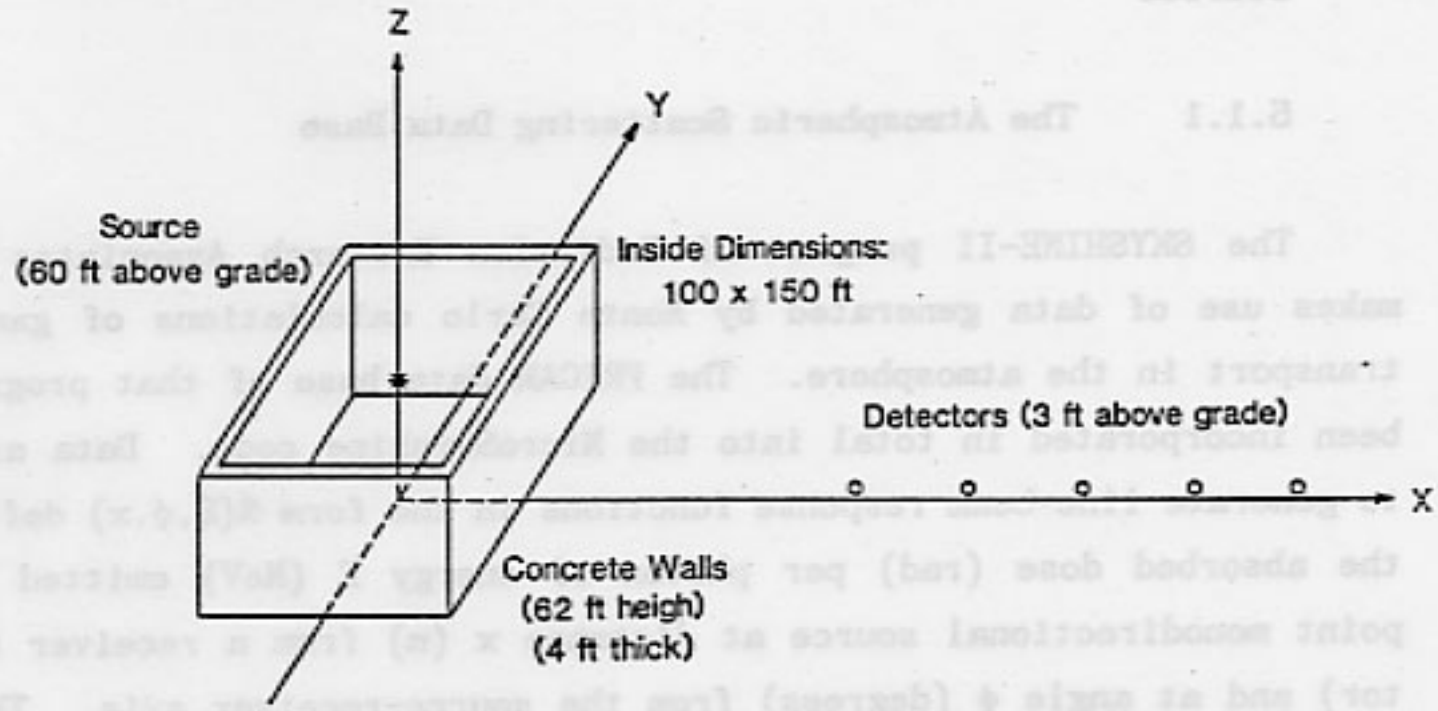

Fig. 4.2. Geometry for ANSI/ANS-6.6.1 Reference Problem I.2.

5. The MicroSkyshine Method

5.1 Atmospheric Transport of Gamma Rays from Point Monodirectional Sources

5.1.1 The Atmospheric Scattering Data Base

The SKYSHINE-II program of Radiation Research Associates [La79] makes use of data generated by Monte Carlo calculations of gamma ray transport in the atmosphere. The PRIGAM data base of that program has been incorporated in total into the MicroSkyshine code. Data are used to generate line-beam response functions in the form $\mathcal{R}(E,\phi,x)$ defined as the absorbed dose (rad) per photon of energy E (MeV) emitted from a point monodirectional source at distance x (m) from a receiver (detector) and at angle ϕ (degrees) from the source-receiver axis. The data base provides three constants a_{ij}, b_{ij}, and c_{ij}, used as follows:

$$\mathcal{R}(E,\phi,x) = E\,\mathcal{F}(E,\phi,x), \tag{5.1}$$

where

$$\mathcal{F}(E,\phi,x) = k(\rho/\rho_o)^2[x(\rho/\rho_o)]^{b_{ij}}\exp[a_{ij}-c_{ij}x(\rho/\rho_o)], \tag{5.2}$$

in which the conversion factor k is 1.3078×10^{-11} m^3rad/MeV and ρ is the air density in the same units as the reference density $\rho_o = 0.001225$ g/cm^3. Indices for the constants are determined by $E_{i+1} \le E < E_i$ and $\phi_j \le \phi < \phi_{j+1}$. As described in Tables 5.1 and 5.2, E varies from 0.01 to 10 MeV in 12 intervals (energy groups) and ϕ varies from 0 to 180 degrees in 19 intervals (angle groups).

5.1.2 Response Function Variation with Energy

In the SKYSHINE-II code, a strict multi-group approach for both energy and angle is used to evaluate response functions. However, in the MicroSkyshine code, an interpolation procedure is used to render the response function continuously variable in energy. Let median group energies be symbolized by $\langle E_i \rangle \equiv (E_i+E_{i+1})/2$ $(i = 1,2,\ldots,12)$, and the tabulated response functions at these median energies, $\mathcal{F}(\langle E_i \rangle,\phi,x)$, by $\mathcal{F}_i(\phi,x)$. Then, MicroSkyshine calculates the response functions as

$$\mathcal{F}(E,\phi,x) = \mathcal{F}_1(\phi,x)(E-8.5) + \mathcal{F}_2(\phi,x)(9.5-E), \quad 9.5 < E \leq 10 \text{ MeV}, \tag{5.3}$$

$$\mathcal{F}(E,\phi,x) = \mathcal{F}_{12}(\phi,x), \quad 0.01 \leq E < 0.055 \text{ MeV}, \tag{5.4}$$

and, for $0.055 \leq \langle E_{i+1} \rangle \leq E \leq \langle E_i \rangle \leq 9.5$ MeV,

$$\mathcal{F}(E,\phi,x) = \mathcal{F}_{i+1}(\phi,x)\,\frac{\langle E_i \rangle - E}{\langle E_i \rangle - \langle E_{i+1} \rangle} + \mathcal{F}_i(\phi,x)\,\frac{E - \langle E_{i+1} \rangle}{\langle E_i \rangle - \langle E_{i+1} \rangle}. \tag{5.5}$$

5.1.3 Representative Results

Figure 5.1 illustrates the variation of $\mathcal{F}(E,\phi,x)$ with angle of photon emission ϕ at fixed source-detector distance x for three photon energies. At emission angles greater than 90 degrees, the response function varies only slightly with angle. In the MicroSkyshine methodology, which treats only isotropic sources, integrations are performed over the permissible range of emission angles. For this reason, no attempt has been made to smooth or otherwise modify the angular dependence of the response function.

Figure 5.2 illustrates the variation of $\mathcal{F}(E,\phi,x)$ with energy E at fixed ϕ for several values of x. The MicroSkyshine calculations deal most generally with sources emitting photons with one or more discrete

energies. For this reason, the interpolation technique described above has been used to smooth the energy dependence of the response function.

5.1.4 Comparison with Other Calculations

Response functions for point monodirectional sources have been computed by Lynch et al. [Ly58] use Monte Carlo methods. Results are in terms of tissue dose rather than air dose and are limited to source-detector distances from 5 to 100 ft (1.52 to 30.5 m) in air of density 0.001225 g/cm^3. Results are also for discrete energies between 0.6 and 12 MeV and discrete emission angles between 1 and 180 degrees. Trubey [Tr60] calculated approximate response functions for the same cases examined by Lynch et al., but included in the response only singly scattered photons with no allowance for attenuation or buildup of multiply scattered photons. Trubey's calculations confirmed that, for the cases considered, singly scattered photons are the dominant contributors to the response. Kitazume [Ki68] extended Trubey's calculations to include attenuation and buildup and found closer agreement with the results of Lynch et al. Kitazume observed that agreement was better for smaller angles of emission and source-detector distances and that, for the entire scope of calculations, agreement was within ± 20 percent.

Comparison of response functions calculated by Lynch et al. with those based on the PRIGAM data is not as straightforward as would be desired. The responses are different — air dose vs. tissue dose — and the PRIGAM data are for energy and angle groups rather than at discrete energies and angles. Tissue dose exceeds air dose by about 10 percent for photons with energies between 0.1 and 10 MeV. Also, the angles at which Lynch et al. calculated response functions generally fall at the break points within the PRIGAM angle-group structure. Reference to Fig. 5.1 suggests that in such circumstance the logarithmic average of the response functions for adjoining angular groups would best represent the response function at the break point. Furthermore, the response function for the 0-1 degree PRIGAM angular group is heavily biased by the

much greater response due to photons emitted almost directly towards the detector. For this reason, the Lynch et al. response function for emission angle of 1 degree would no doubt agree more closely with the PRIGAM response function for the 1-2 degree angular group than with that for the 0-1 degree group. Likewise, it is not reasonable to compare the Lynch et al. response function for a single angle of emission of 180 degrees with the PRIGAM response function for the entire 160-180 degree angular group. At any rate, in the MicroSkyshine calculations, emission angles near 180 degrees are of negligible significance and those near 0 degrees are largely precluded either because of the presence of a direct line-of-sight response component or because of structure-imposed collimation. Table 5.3 and the accompanying Fig. 5.3 compare the Lynch et al. response functions with PRIGAM generated response functions as a function of source-detector distance at a fixed energy of 2 MeV and at selected angles of emission. This comparison was chosen to illustrate angle and distance effects and is representative of similar comparisons at other source energies.

5.2 The Point Source in a Cylindrical Silo

5.2.1 Formulation of the Problem

The geometry for this problem is illustrated in Fig. 5.4. A point monoenergetic source isotropically emitting photons of energy E is located on the vertical axis of a cylindrical-shell shield (silo) of inner radius r. The source is distance y below the horizontal top of the silo which collimates the emergent radiation into a cone with a polar angle θ_{max} measured from the vertical axis and defined by

$$\omega_o \equiv \cos\theta_{max} = (1+r^2/y^2)^{1/2}. \qquad (5.6)$$

A detector (receiver or dose point) is located in air of density ρ at radial distance x from the silo axis and at distance h below the hori-

zontal plane of the silo top. If either y or h is above the plane, the distance is taken to be negative in sign. Above the source, and generally within the confines of or atop the silo, shielding is permitted in the form of a horizontal slab of material with thickness equivalent to λ mean free paths at photon energy E. The distance from the source to the detector is

$$d = [x^2+(y-h)^2]^{1/2} \tag{5.7}$$

and the angle α between the horizontal and the source detector axis is

$$\alpha = \cos^{-1}(x/d). \tag{5.8}$$

Consider a ray from the source at polar angle θ (measured from the silo axis) and at azimuthal angle ψ (measured from the vertical plane through the source and detector). The cosine of the angle of emission ϕ between the photon direction and the source-detector axis is the dot product of the (unit) vector in the emission direction and a unit vector along the source-detector axis, namely,

$$\cos\phi = \sin\theta\cos\psi\cos\alpha - \cos\theta\sin\alpha. \tag{5.9}$$

Two cases are now considered in evaluation of the detector response.

5.2.2 The Open-Silo Case

In this case, the PRIGAM point-monodirectional response functions may be integrated directly over all angles of photon emission permitted by the collimation to obtain the detector response. That response, in units of rad (air) per photon emitted (isotropically), is given by

$$R = \frac{1}{4\pi}\int_0^{2\pi} d\psi \int_0^{\theta_{max}} d\theta\, \sin\theta\, \mathfrak{R}(E,\phi,d), \tag{5.10}$$

where $\mathfrak{K}$ is a function of E, r, x, y, and h, and the functional dependencies of θ_{max}, ϕ, and d are as given in Eqs. (5.6)-(5.9). In the MicroSkyshine calculations, advantage is taken of the symmetry about the azimuthal reference plane, and the θ variable of integration is changed to $\omega \equiv \cos\theta$, with the result that

$$R = \frac{1}{2\pi} \int_0^{\pi} d\psi \int_{\omega_o}^{1} d\omega \, \mathfrak{K}(E,\phi,d). \qquad (5.11)$$

The above result is evaluated in the MicroSkyshine code by using double Gaussian quadrature (see Section 5.5). The user has the choice of order 4, 8, 16, or 32, with the 8th order being the recommended choice for routine calculations.

Inherent in this approach to estimation of the detector response are minor approximations which are common with those of the SKYSHINE-II approach. The silo defines the angle of source collimation but does not otherwise influence the dose estimate. The response is thus under-estimated because of the neglect of contributions from photons which suffer their first scatter with the silo wall before escaping the confines of the silo. These photons would have to scatter at least one additional time in the atmosphere before reaching the detector. This under-estimate is more than balanced by the neglect of the shielding provided by the silo walls against photons which have scattered in air within the confines of the silo before proceeding in a direction toward the detector. Thus, in order that estimates of detector response not be unduly conservative, it is recommended that the MicroSkyshine method be applied to cases for which r and y are both substantially less than the mean-free-path length (in air) for the source photon. A very rough estimate has been made of the degree to which skyshine dose rates may be over-estimated if these conditions on r and y cannot be met. Consider a ray from the source on the azimuth toward the detector, but just clearing the top of the shield wall. Let θ be the angle from the vertical to

this ray and d be the (inside-leg) distance from the source to the top of the wall along the ray. Now let d and the source-to-detector distance x be measured in mean-free-path lengths as given in the following table for air of density 0.00123 g/cm^3.

Photon Energy (MeV)	Mean-Free-Path Length (m)
0.1	55
0.3	77
0.5	94
0.8	115
1.0	128
3.0	228
5.0	296
10.0	401

Two cases for θ are examined, 45 and 67.5 degrees. The following table gives maximum values of d for which the skyshine dose rate is likely to be over-estimated by less than 10 percent and by less than 50 percent.

Source-to-Detector Distance (mfp)	Maximum Value of Inside-Leg Distance d (mfp)			
	For Over-Estimate < 10%		For Over-Estimate <50%	
	θ = 45°	θ = 67.5°	θ = 45°	θ = 67.5°
1	0.14	0.31	0.59	0.82
2	0.20	0.51	0.92	1.4
3	0.24	0.65	1.2	2.0
5	0.28	0.84	1.5	2.9
8	0.30	0.99	1.7	3.9
10	0.32	1.1	1.9	4.9

For example, for 5-MeV photons, a source-detector distance of 592 m (2 mfp), and θ = 45°, the distance from the source to the top of the shield wall should be less than 0.2 mfp (59 m) to assure that the skyshine dose

rate is not over-estimated by more than 10 percent. For 0.1-MeV photons, an inside leg distance of 7.7 m (0.14 mfp), and $\theta = 45^{o}$, skyshine dose rate may be over-estimated by more than 10 percent for source-detector distances less than 1 mfp (55 m).

5.2.3 The Shielded-Silo Case

One major approximation is made in the treatment of this case. The verification of the suitability of this approximation is a major theme of this report. It is assumed that the effect of overhead shielding in the vicinity of the source may be accounted for by modifying the response functions to account for both exponential attenuation and buildup of secondary photons along the slant path through the shielding.

If t (cm) is the thickness of a horizontal shielding slab, ρ_s (g/cm^3) is its density, and μ/ρ (cm^2/g) is the total mass interaction coefficient in the shield material for photons of energy E, then the slab thickness in units of mean free paths is given by

$$\lambda = t\ \rho_s\ (\mu/\rho). \tag{5.12}$$

For a ray at polar angle θ, the slant path through the shield, in units of mean free paths is given by $\lambda \sec\theta = \lambda/\omega$.

In the MicroSkyshine program, mass interaction coefficients are determined from data given by Storm and Israel [St67] for air, water, concrete, iron, lead, zirconium, and uranium dioxide. Interpolation in the data is logarithmic for both E and μ/ρ. For laminate shields, the number of mean free path lengths is cumulative. For mixtures of materials identified by subscript i, the number of mean free paths is given by

$$\lambda = t \sum_i \rho_i\ (\mu/\rho)_i, \tag{5.13}$$

in which ρ_i is the partial density of material i.

Buildup in the shielding slab is accounted for by application of the air-kerma (absorbed-dose) buildup factor calculated using the Berger approximation, namely,

$$B = 1 + a\,(\lambda/\omega)\; e^{+b\lambda/\omega}, \qquad (5.14)$$

in which the parameters a and b depend on the nature of the shield and the photon energy. In the MicroSkyshine code, the parameters are determined from data of Chilton, Eisenhauer and Simmons [Ch84] and users may select from among water, concrete, iron, and lead to best represent the shielding material. If air is chosen as the shield material, the buildup factor is taken as unity since air buildup is already included in the line-beam response functions. The buildup factors so determined are applicable for energies from 0.015 to 15 MeV and for up to 40 mean free paths of shielding material. Interpolation is linear in a or b and logarithmic in E.

For the shielded-silo case, the total detector response (rad/photon) is given by

$$R = \frac{1}{2\pi}\int_0^{\pi} d\psi \int_{\omega_o}^{1} d\omega\; \mathfrak{R}(E,\phi,d)\; e^{-\lambda/\omega}\,[1+a\,(\lambda/\omega)\; e^{+b\lambda/\omega}], \qquad (5.15)$$

where R now depends on the nature and thickness of the overhead shielding material as well as E, r, x, y, and h.

5.3 The Point Source Behind an Infinite Wall

5.3.1 Formulation of the Problem

The geometry for this problem is illustrated in Fig. 5.5. A point monoenergetic source isotropically emitting photons of energy E is located perpendicular distance r from a vertical shield wall. The source is distance y beneath the horizontal plane through the top of the

wall. A detector (receiver or dose point) is located in air of density ρ at coordinates x and z in a horizontal plane, with x measured from the source along a normal to the wall and z offset from the normal. The detector is at distance h beneath the horizontal plane through the top of the wall. If either source or detector are above the plane, h or y are taken to be negative in sign. Above the source and generally within the confines of or atop the wall is permitted a horizontal slab of shielding material of thickness equivalent to λ mean free paths at the source-photon energy.

Consider now a photon ray from the source emitted at polar angle θ measured from a vertical line through the source and at azimuthal angle ψ measured from a vertical reference plane through the source and detector. The angle ξ between the wall and the reference plane is given by

$$\xi = \tan^{-1}(z/x), \tag{5.16}$$

and the distance along the source-detector axis is given by

$$d = [x^2 + z^2 + (y-h)^2]^{1/2}. \tag{5.17}$$

The angle α between the horizontal and the source-detector axis is given by

$$\alpha = \cos^{-1}[(x^2 + z^2)^{1/2}/d], \tag{5.18}$$

and the angle ϕ between the direction of emission and the source-detector axis is given by Eq. (5.9).

Two cases are now considered in estimating the detector response.

5.3.2 Source Behind a Wall Without Overhead Shielding

Application of the PRIGAM response functions in this case is more

complicated that it is for the point source in a silo. Now the maximum polar angle θ_{max} (or the minimum ω_o) limits photon rays which clear the shield wall depends on the azimuthal angle ψ. The detector response, in units of rad per photon, is given by

$$R = \frac{1}{4\pi} \int_0^{2\pi} d\psi \int_{\omega_o(\psi)}^{1} d\omega \, \mathfrak{R}(E,\phi,d), \tag{5.19}$$

in which $\omega_o(\psi) = \cos[\theta_{max}(\psi)]$, and

$$\theta_{max}(\psi) = \tan^{-1}\left[\frac{r}{y\cos(\psi-\xi)}\right], \qquad 0 \le \psi \le \pi/2+\xi, \tag{5.20}$$

$$= \pi/2, \qquad \pi/2+\xi \le \psi \le 3\pi/2+\xi,$$

$$= \tan^{-1}\left[\frac{r}{y\cos(\psi-\xi)}\right], \qquad 3\pi/2+\xi \le \psi \le 2\pi.$$

5.3.3 Source Behind a Wall With Overhead Shielding

Treatment of overhead shielding in this case is identical with that for the shielded-silo case. The detector response, in units of rad per photon is given by

$$R = \frac{1}{4\pi} \int_0^{2\pi} d\psi \int_{\omega_o(\psi)}^{1} d\omega \, \mathfrak{R}(E,\phi,d) \; e^{-\lambda/\omega} \left[1+a(\lambda/\omega)e^{+b\lambda/\omega}\right], \tag{5.21}$$

in which R now depends on the nature and thickness of the overhead shield as well as the parameters E, r, x, y, z, and h.

5.4 Representative Results

5.4.1 The Silo-Geometry Case

Effects of collimation angle, source energy, and overhead shielding on the skyshine dose are illustrated in a series of tables and corresponding figures presented in this section.

Table 5.4 and Fig. 5.6 illustrate the effect of collimation angle for two photon energies and selected source-detector distances. The independent variable is $\omega_o \equiv \cos\theta_{max}$, as illustrated in Fig. 5.4. The limiting case of "2π geometry," i.e., y = h = 0, corresponds to θ_{max} = 90 degrees or $\omega_o = 0$.

Effects of source energy are illustrated in Table 5.5 and Figs. 5.7a-5.7c for selected source-detector distances and angles of collimation. The source and detector depths, y and h, are equal for the cases presented. The MicroSkyshine results are shown as data points in the figures. For comparison purposes, and shown as solid lines, are results of K-Shine calculations as discussed in § 6.4.2.

Table 5.6 and Figs. 5.8a and 5.8b illustrate the effects of concrete overhead-shield thickness at selected energies, source-detector distances, and angles of collimation. The source and detector depths, y and h, are again equal for the cases presented. The dotted lines in the figures are the results of K-Shine calculations.

5.4.2 The Wall-Geometry Case

Effects of source energy, source-detector lateral displacement, and overhead shielding on the skyshine dose are illustrated in a series of tables and figures presented in this section.

Table 5.7 and Fig. 5.9 illustrate the effects of source energy at selected source-detector distances (x) for the case of y = h = r = 3 m, and z = 0.

Effects of lateral displacement are illustrated in Table 5.8 for selected photon energies. Here, y, r, and h are fixed at 3 m. Lateral

displacement z varies from 0 to 275 m while x is adjusted so the true (direct) source-detector distance remains fixed at 300 meters.

Overhead shielding effects are illustrated in Table 5.9 and Figs 5.10a and 5.10b for selected energies and source-detector distances. In these results, y, r, and h are fixed at 3 m and z is fixed at 0.

5.5 Numerical Integration and Gauss Quadrature

The evaluation of the skyshine dose from Eqs. (5.11), (5.15), (5.19) or (5.21) requires the numerical evaluation of a double integral of the form

$$R = \int_a^b \int_c^d f(x,y)\, dy\, dx \ . \qquad (5.22)$$

Such a double integral can be approximated using numerical quadrature of order N as

$$R \simeq \sum_{i=1}^{N} w_i \sum_{j=1}^{N} w_j\, f(x_i, y_j) \qquad (5.23)$$

where the x_i and y_j are the quadrature ordinates and w_i and w_j are the corresponding weights for the integration ranges (a,b) and (c,d), respectively. Many possible choices for the quadrature ordinates and weights can be made. However, unless there are special properties of the integrands (e.g., known singularities), Gauss quadrature is usually selected since this quadrature set, for order N, can integrate exactly an arbitrary polynomial of degree (2N-1), a higher degree than can be integrated exactly by any other quadrature set of the same order.

The ordinates and weights of the Gaussian quadrature set for the x-integral in Eq. (5.22) are given by

$$x_i = \frac{(b-a)}{2} z_i + \frac{(b+a)}{2} \qquad (5.24)$$

$$w_i = \frac{(b-a)}{2}\,\omega_i \qquad (5.25)$$

where z_i are the zeros of the Legendre polynomial $P_{N+1}(z)$ and ω_i are given by

$$\omega_i = \frac{2(1-z_i^2)}{(N+1)^2[P_{N+1}(z_i)]^2} \qquad (5.26)$$

The y-integral in Eq. (5.22) can be treated similarly (although with the appropriate y_j and w_j constructed for the integration range (c,d)). Gauss quadrature ordinates and weights (z_i,ω_i) are provided in the Micro Skyshine code for orders 4, 8, 16, and 32. Results given in this report were calulated using 16th order quadrature.

Table 5.1

Energy group structure used in the definition of the line-beam response functions.

i	E_i (MeV)
1	10.0
2	9.0
3	8.0
4	7.0
5	6.0
6	5.0
7	4.0
8	3.0
9	2.00
10	1.00
11	0.50
12	0.10
13	0.01

Table 5.2

Angle group structure used in the definition of the line-beam response functions.

j	ϕ_j (deg)
1	0
2	1
3	2
4	3
5	5
6	7
7	10
8	15
9	20
10	30
11	40
12	50
13	60
14	70
15	80
16	90
17	100
18	120
19	140
20	160
21	180

Table 5.3. Comparison of $\mathfrak{R}(E,\phi,x)$ based on PRIGAM data with results of Lynch et al.[a] for 2 MeV photons. See Fig. 5.3.

ϕ (deg)	x (ft)	$\mathfrak{R}(E,\phi,x)$ (rad/photon) PRIGAM[b]	$\mathfrak{R}(E,\phi,x)$ (rad/photon) Lynch et al.[c]
1	5	3.272E-14[d]	9.6E-15
	10	1.067E-14	2.4E-15
	20	3.463E-15	1.2E-15
	40	1.112E-15	5.3E-16
	65	4.960E-16	3.1E-16
	100	2.387E-16	1.9E-16
15	5	9.892E-17	1.6E-16
	10	5.199E-17	8.1E-17
	20	2.729E-17	3.6E-17
	40	1.421E-17	2.0E-17
	65	8.893E-18	1.2E-17
	100	5.770E-18	7.1E-18
30	5	3.924E-17	3.5E-17
	10	2.006E-17	1.9E-17
	20	1.019E-17	9.2E-18
	40	5.102E-18	4.3E-18
	65	3.089E-18	2.3E-18
	100	1.939E-18	1.7E-18
60	5	4.408E-18	6.8E-18
	10	2.494E-18	3.5E-18
	20	1.422E-18	1.8E-18
	40	8.121E-19	8.5E-19
	65	5.421E-19	5.8E-19
	100	3.709E-19	3.8E-19
90	5	2.226E-18	2.9E-18
	10	1.249E-18	1.6E-18
	20	7.018E-19	7.8E-19
	40	3.900E-19	3.7E-19
	65	2.534E-19	2.5E-19
	100	1.682E-19	1.6E-19

Table 5.3. (continued).

ϕ (deg)	x (ft)	$\mathfrak{R}(E,\phi,x)$ (rad/photon) PRIGAM[b]	Lynch et al.[c]
135	5	1.852E-18	1.8E-18
	10	9.084E-19	8.5E-19
	20	4.561E-19	3.5E-19
	40	2.319E-19	2.4E-19
	65	1.432E-19	1.2E-19
	100	9.120E-20	8.1E-20

(a) Source: Reference Ly(58). Data scaled from graph.
(b) Units: rad (air)
(c) Units: rad (tissue)
(d) PRIGAM data for 1-2 degree subinterval.

Table 5.4. Effect of collimation angle on results of MicroSkyshine calculations for a point source in a silo without overhead shielding. Air density 0.001225 g/cm^3. Quadrature order 16. See Fig. 5.6.

		Absorbed Dose in Air (rad) per photon			
Source-Detector Distance (m)		30	100	300	1000
E (MeV)	$\cos\theta_{max}$				
1.25	0.05	2.727E-19	6.297E-20	6.021E-21	2.063E-23
	0.1	2.176E-19	5.311E-20	5.159E-21	1.651E-23
	0.2	1.655E-19	4.081E-20	3.876E-21	1.085E-23
	0.3	1.279E-19	3.116E-20	2.819E-21	6.624E-24
	0.4	1.001E-19	2.388E-20	2.039E-21	4.032E-24
	0.5	7.553E-20	1.780E-20	1.444E-21	2.354E-24
	0.6	5.430E-20	1.275E-20	9.999E-22	1.379E-24
	0.7	3.647E-20	8.760E-21	6.689E-22	7.242E-25
	0.8	2.219E-20	5.427E-21	4.030E-22	3.404E-25
	0.9	1.055E-20	2.451E-21	1.734E-22	1.526E-25
	0.95	5.152E-21	1.152E-21	7.961E-23	7.772E-26
6.13	0.05	2.826E-19	5.751E-20	8.803E-21	2.910E-22
	0.1	1.945E-19	4.329E-20	6.723E-21	1.865E-22
	0.2	1.384E-19	3.025E-20	4.159E-21	9.442E-23
	0.3	9.682E-20	2.116E-20	2.702E-21	4.590E-23
	0.4	7.095E-20	1.526E-20	1.808E-21	2.315E-23
	0.5	5.122E-20	1.089E-20	1.198E-21	1.090E-23
	0.6	3.650E-20	7.677E-21	7.922E-22	5.070E-24
	0.7	2.468E-20	5.216E-21	5.078E-22	2.221E-24
	0.8	1.460E-20	3.208E-21	3.008E-22	8.504E-25
	0.9	6.125E-21	1.442E-21	1.336E-22	2.550E-25
	0.95	2.803E-21	6.806E-22	6.294E-23	1.063E-25

Table 5.5. Effect of source energy on results of MicroSkyshine calculations for the point source in a silo without overhead shielding. Air density 0.001225 g/cm^3. Quadrature order 16. See Figs. 5.7a through 5.7c.

		Absorbed Dose in Air (rad) per photon			
Source-Detector Distance (m)		30	100	300	1000
θ_{max} (deg)	E (MeV)				
30	0.100	2.132E-20	1.457E-21	1.719E-23	1.163E-27
	0.215	2.718E-20	2.666E-21	6.906E-23	8.262E-27
	0.464	2.181E-20	3.983E-21	1.763E-22	3.213E-26
	1.000	1.490E-20	3.657E-21	2.417E-22	1.244E-25
	2.15	1.212E-20	2.756E-21	2.225E-22	2.977E-25
	4.64	6.494E-21	1.847E-21	1.987E-22	4.006E-25
	10.0	1.375E-20	2.614E-21	2.177E-22	3.737E-25
60	0.100	9.171E-20	6.426E-21	8.562E-23	4.782E-27
	0.215	1.197E-19	1.241E-20	3.405E-22	3.345E-26
	0.464	1.022E-19	1.951E-20	9.053E-22	2.509E-25
	1.000	7.521E-20	1.842E-20	1.403E-21	1.478E-24
	2.15	6.734E-20	1.502E-20	1.434E-21	5.771E-24
	4.64	4.025E-20	1.043E-20	1.294E-21	9.683E-24
	10.0	7.717E-20	1.318E-20	1.255E-21	8.479E-24
90	0.100	2.720E-19	1.806E-20	2.524E-22	2.682E-26
	0.215	3.696E-19	3.572E-20	1.018E-21	1.849E-25
	0.464	3.547E-19	6.002E-20	3.070E-21	1.558E-24
	1.000	3.338E-19	7.206E-20	6.382E-21	1.395E-23
	2.15	4.230E-19	8.221E-20	9.463E-21	9.303E-23
	4.64	3.451E-19	7.693E-20	1.260E-20	3.213E-22
	10.0	4.717E-19	8.602E-20	1.349E-20	6.379E-22

Table 5.6. Effect of overhead concrete thickness on results of MicroSkyshine calculations for the point source in a silo. Air density 0.001225 g/cm^3. Quadrature order 16. Concrete density = 2.35 g/cm^3. See Figs. 5.8a and 5.8b.

			Absorbed Dose in Air (rad) per Photon			
Source-Detector Distance (m)			30	100	300	1000
E (MeV)	zmax (deg)	t (m)				
1.25	30	0	1.424E-20	3.388E-21	2.430E-22	2.005E-25
		.1	9.114E-21	2.164E-21	1.551E-22	1.286E-25
		.2	3.647E-21	8.635E-22	6.177E-23	5.161E-26
		.4	3.985E-22	9.381E-23	6.688E-24	5.680E-27
		.8	2.972E-24	6.918E-25	4.900E-26	4.290E-29
		1.0	2.357E-25	5.459E-26	3.855E-27	3.421E-30
	60	0	7.553E-20	1.780E-20	1.444E-21	2.354E-24
		.1	3.625E-20	8.576E-21	6.846E-22	1.023E-24
		.2	1.035E-20	2.461E-21	1.921E-22	2.529E-25
		.4	7.229E-22	1.726E-22	1.300E-23	1.385E-26
		.8	3.702E-24	8.747E-25	6.349E-26	5.786E-29
		1.0	2.706E-25	6.346E-26	4.560E-27	4.096E-30
6.13	30	0	8.574E-21	1.993E-21	1.850E-22	3.736E-25
		.1	5.667E-21	1.318E-21	1.223E-22	2.465E-25
		.2	3.549E-21	8.262E-22	7.665E-23	1.540E-25
		.4	1.266E-21	2.953E-22	2.739E-23	5.465E-26
		.8	1.330E-22	3.114E-23	2.887E-24	5.677E-27
		1.0	4.098E-23	9.613E-24	8.913E-25	1.739E-27
	60	0	5.122E-20	1.089E-20	1.198E-21	1.090E-23
		.1	2.889E-20	6.128E-21	6.651E-22	5.667E-24
		.2	1.523E-20	3.225E-21	3.446E-22	2.697E-24
		.4	3.969E-21	8.402E-22	8.702E-23	5.584E-25
		.8	2.681E-22	5.734E-23	5.691E-24	2.439E-26
		1.0	7.143E-23	1.538E-23	1.511E-24	5.486E-27

Table 5.7. Effect of source energy on results of MicroSkyshine calculations for the point source behind a wall. Air density 0.0012 g/cm^3. Quadrature order 16. y = h = r = 3 m. See Fig. 5.9.

	Absorbed Dose in Air (rad) per Photon			
Source-Detector Distance (m)	30	100	300	1000
E (MeV)				
0.12	1.247E-19	8.907E-21	1.265E-22	1.117E-26
0.25	1.329E-19	1.522E-20	4.746E-22	6.794E-26
0.50	1.153E-19	2.074E-20	9.498E-22	2.360E-25
1.0	7.936E-20	1.875E-20	1.245E-21	8.464E-25
2.5	5.426E-20	1.288E-20	1.052E-21	2.390E-24
5.0	3.359E-20	9.680E-21	1.038E-21	3.304E-24
8.0	3.928E-20	9.922E-21	1.015E-21	3.431E-24

Table 5.8. Effect of lateral displacement (z) on results of MicroSkyshine calculations for the point source behind a wall. Air density 0.0012 g/cm^3. Quadrature order 16. y = h = r = 3 m. True source-detector distance = 300 m.

E (MeV)	z (m)	x (m)	Air Dose (rad) per Photon
1.25	0	300.0	1.244E-21
	50	295.8	1.287E-21
	100	282.8	1.369E-21
	150	259.8	1.493E-21
	200	223.6	1.740E-21
	250	165.8	2.284E-21
	275	119.9	2.905E-21
6.13	0	300.0	9.573E-22
	50	295.8	9.902E-22
	100	282.8	1.056E-21
	150	259.8	1.176E-21
	200	223.6	1.422E-21
	250	165.8	2.035E-21
	275	119.9	2.811E-21

Table 5.9. Effect of overhead concrete thickness on results of MicroSkyshine calculations for the point source behind a wall. Air density 0.0012 g/cm^3. y = h = 3 m, z = 0. Quadrature order 16. Concrete density 2.35 g/cm^3. See Figs. 5.10a and 5.10b.

		Absorbed Dose in Air (rad) per Photon			
Source-Detector Distance (m)		30	100	300	1000
E (MeV)	t (m)				
1.25	0.0	7.591E-20	1.738E-20	1.244E-21	1.321E-24
	0.1	3.024E-20	7.155E-21	5.402E-22	6.163E-25
	0.2	9.007E-21	2.151E-21	1.638E-22	1.838E-25
	0.4	6.871E-22	1.646E-22	1.245E-23	1.317E-26
	0.8	3.668E-24	8.675E-25	6.400E-26	6.358E-29
	1.0	2.687E-25	6.306E-26	4.608E-27	4.550E-30
6.13	0.0	4.478E-20	1.009E-20	9.573E-22	3.509E-24
	0.1	2.256E-20	4.974E-21	4.826E-22	1.966E-24
	0.2	1.191E-20	2.607E-21	2.553E-22	1.060E-24
	0.4	3.281E-21	7.190E-22	7.074E-23	2.856E-25
	0.8	2.433E-22	5.437E-23	5.319E-24	1.873E-26
	1.0	6.634E-23	1.499E-23	1.460E-24	4.764E-27

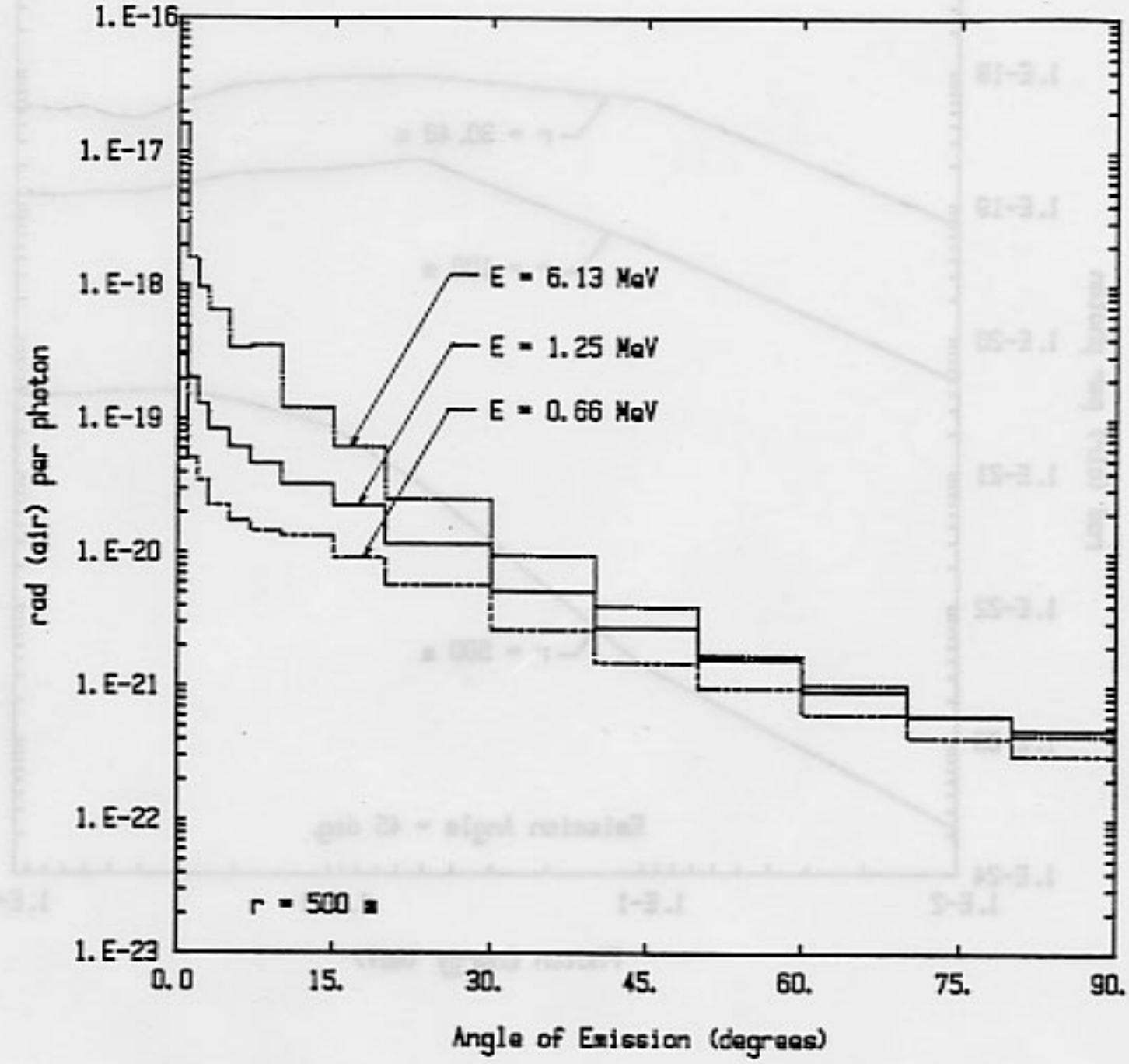

Fig. 5.1 Variation of the PRIGAM atmospheric scattering response function $R(E,\phi,x)$ with angle of photon emission ϕ at fixed source-detector distance x and at selected photon energies.

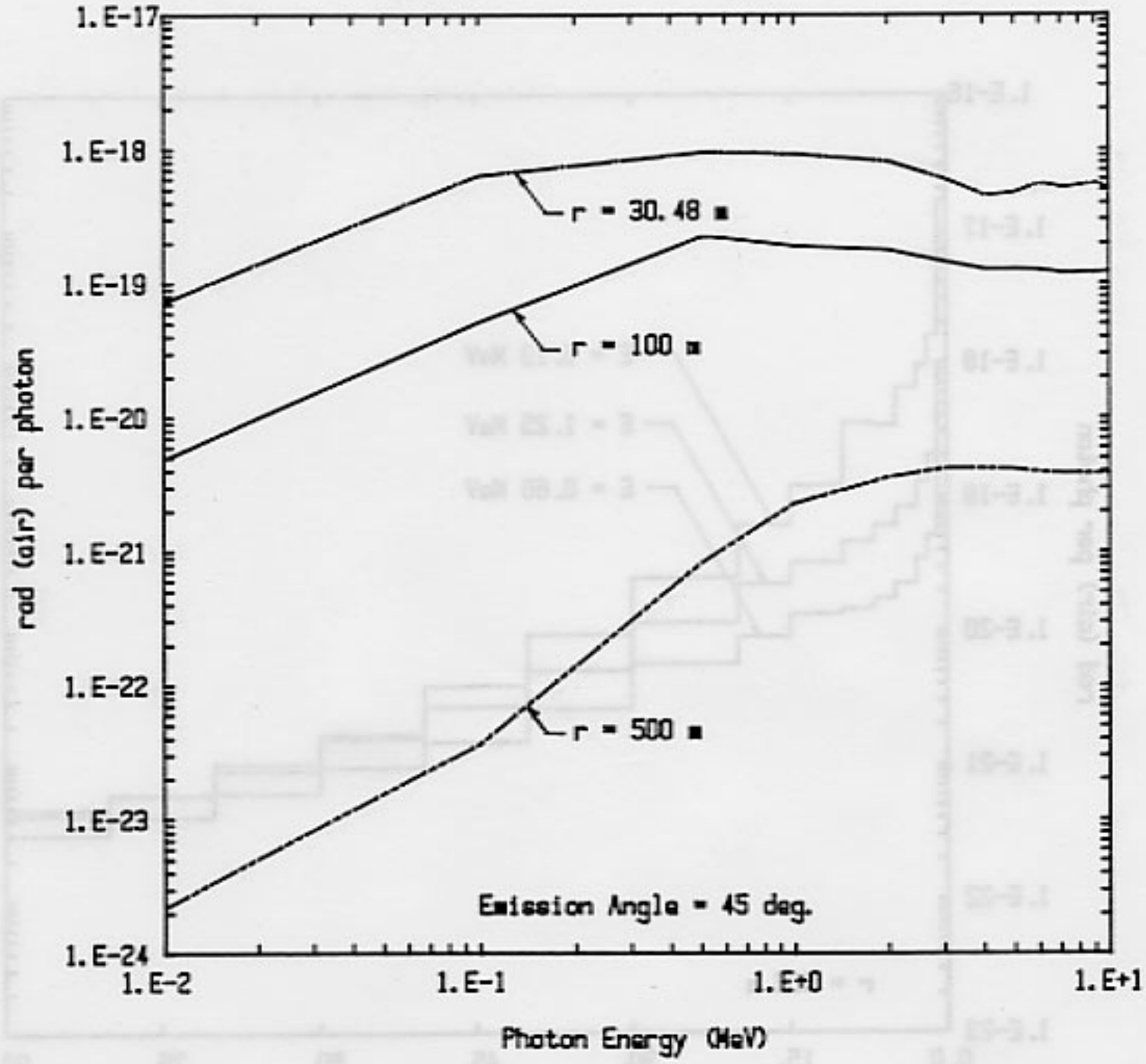

Fig. 5.2 Variation of the PRIGAM atmospheric scattering response function $R(E,\phi,x)$ with photon energy E at fixed angle of emission ϕ and at selected source-detector distances.

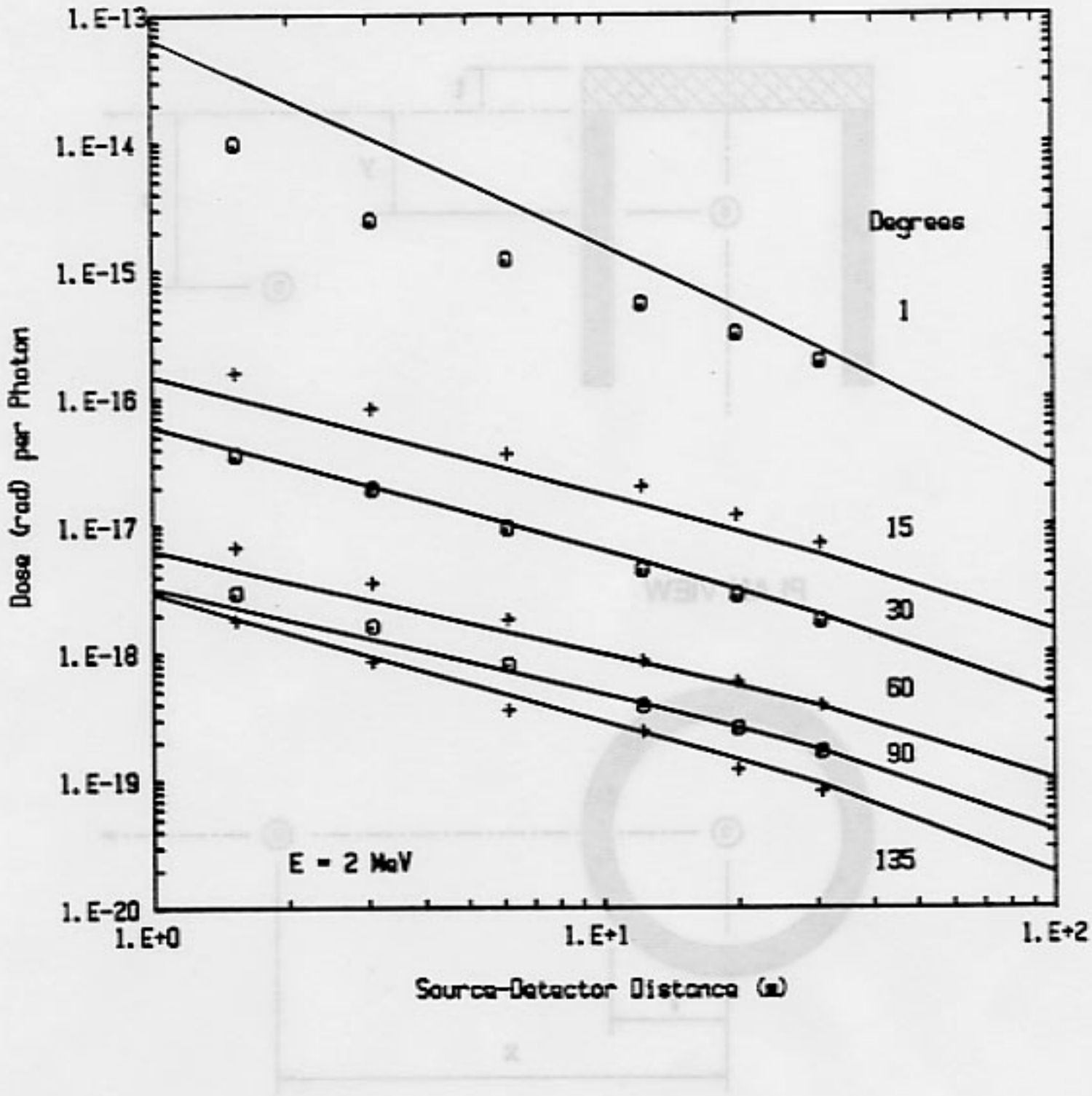

Fig. 5.3 Comparison of PRIGAM atmospheric scattering response functions (solid lines) with response functions calculated by Lynch, et al. [Ly58] for 2-MeV photons at selected angles of emission.

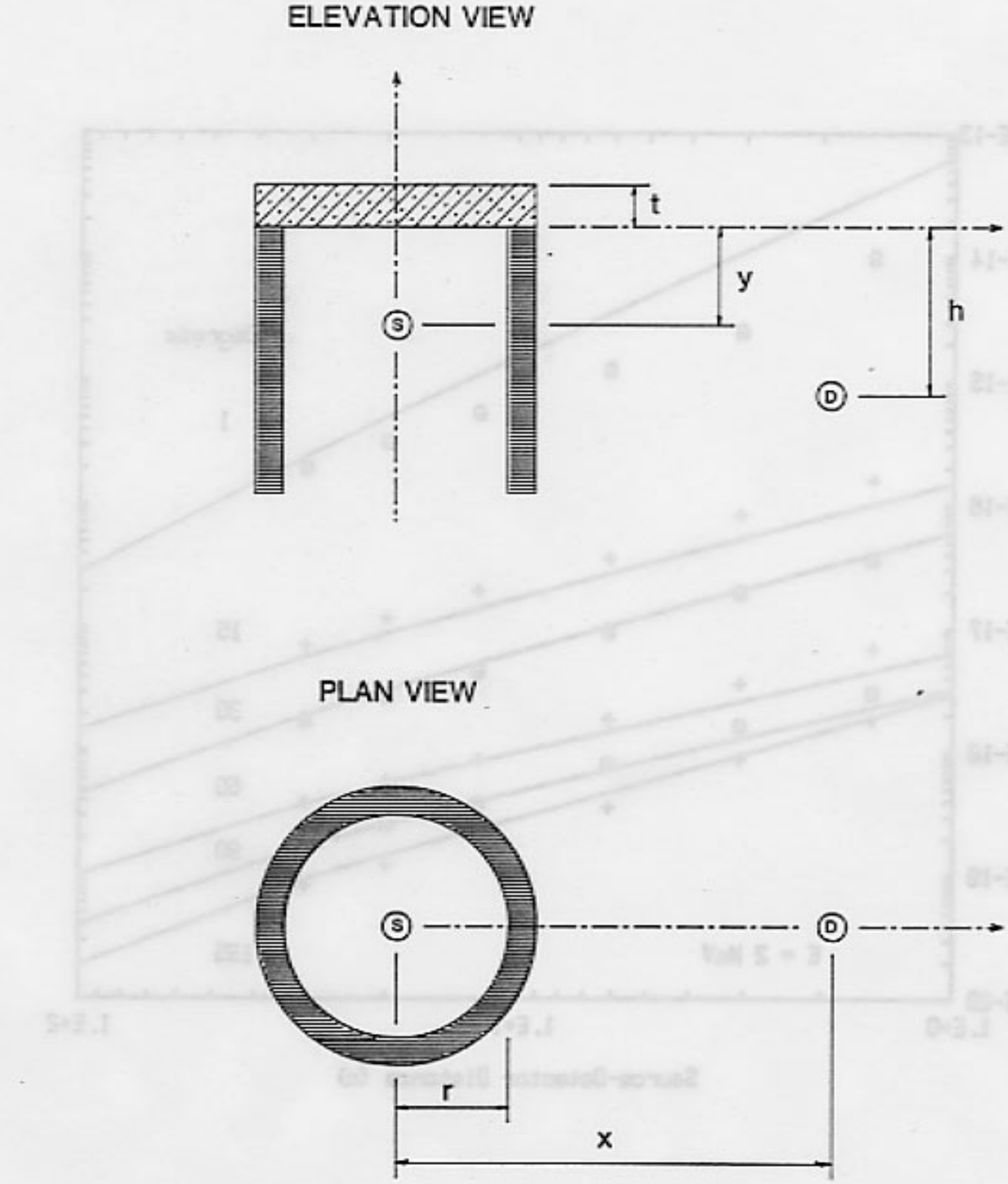

Fig. 5.4 Geometry for the problem of the point source in a cylindrical silo.

ELEVATION VIEW

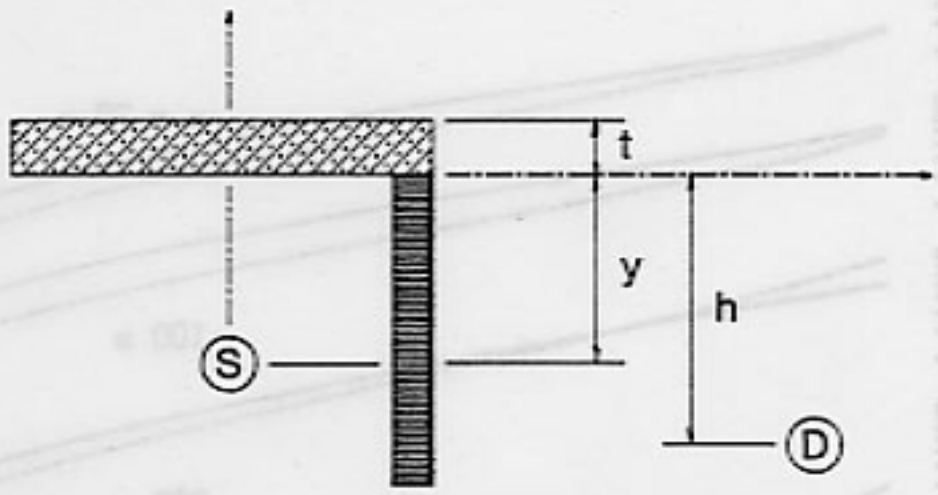

PLAN VIEW

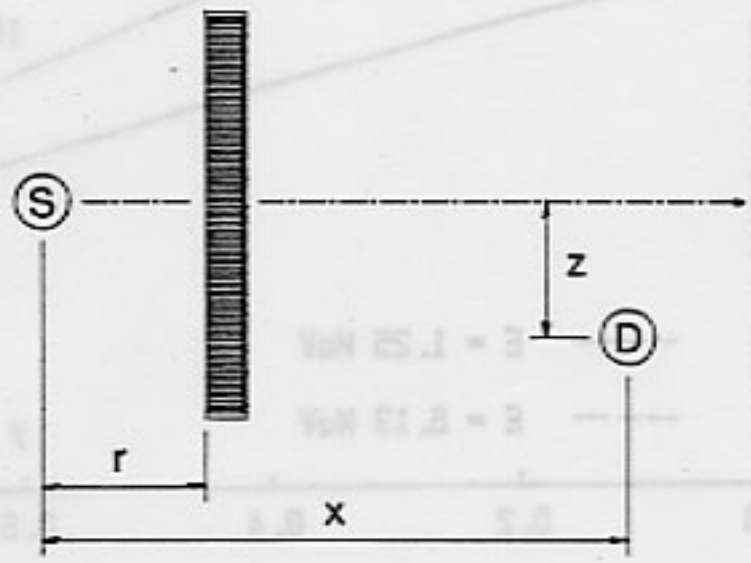

Fig. 5.5 Geometry for the problem of the point source behind an infinite wall.

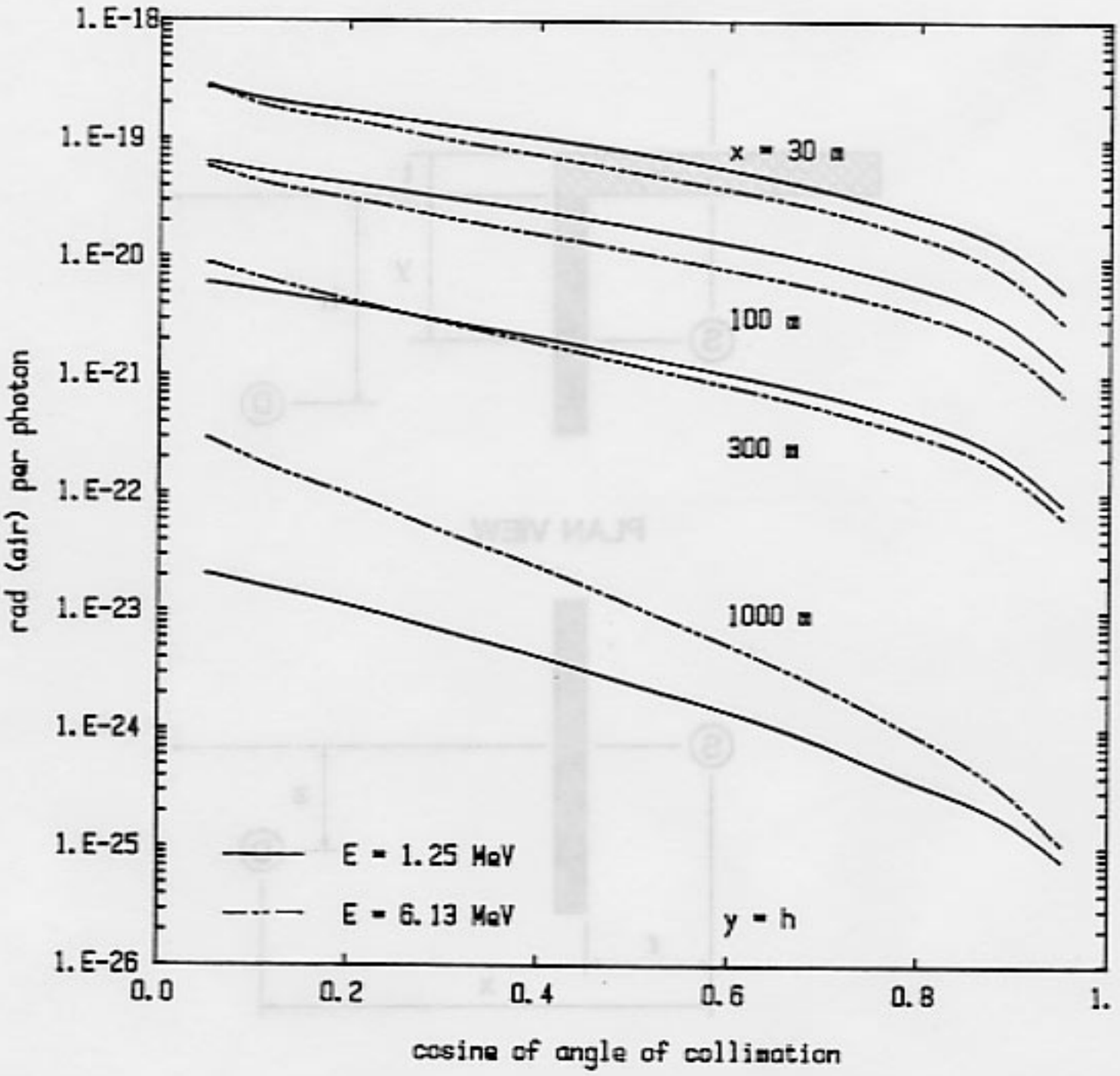

Fig. 5.6 Effect of collimation angle on the dose from a point source in an unshielded silo. Solid lines are the results of MicroSkyshine calculations. Broken lines, shown for comparison, are the results of K-Shine calculations.

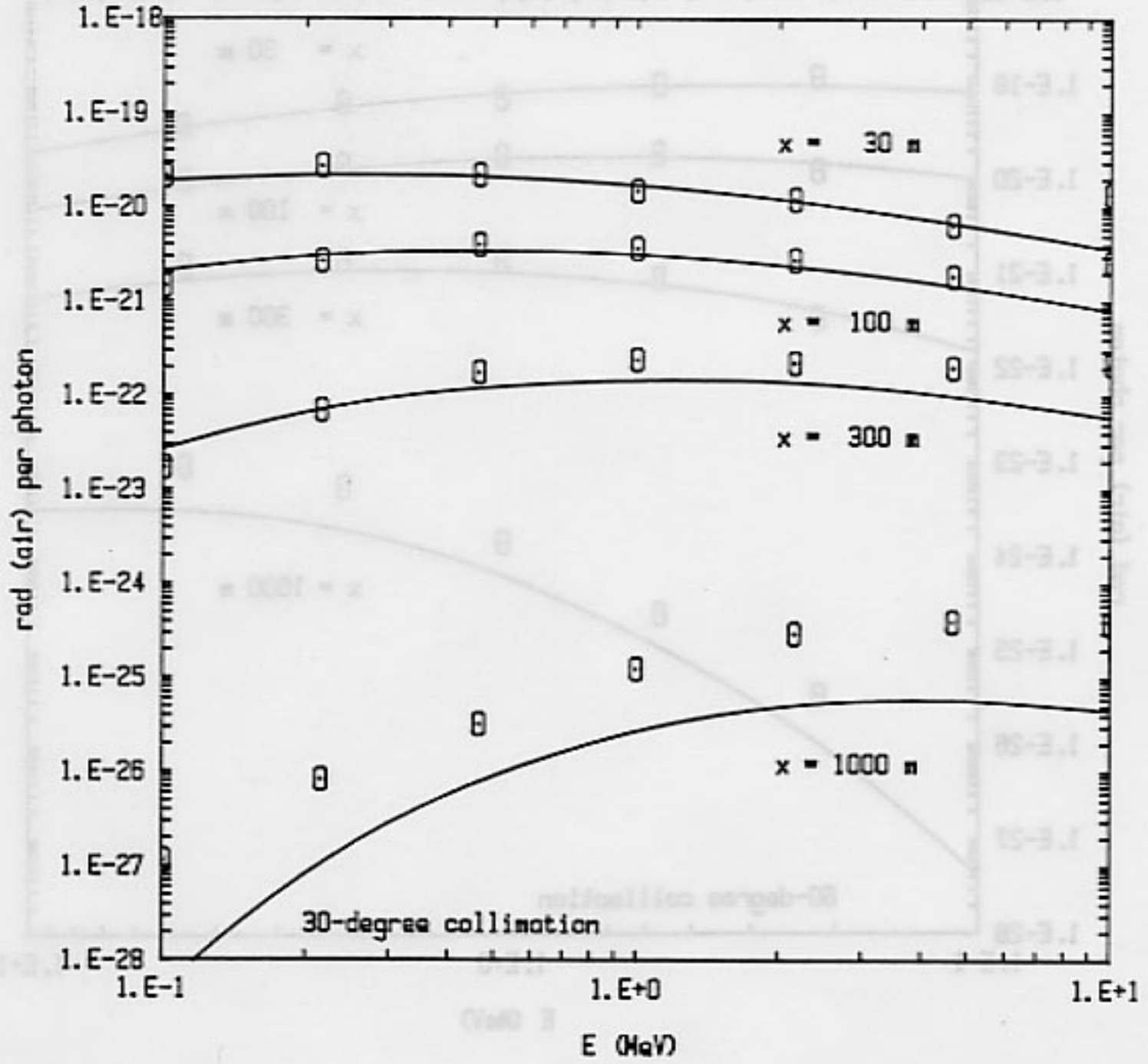

Fig. 5.7a Effect of source energy on the dose from a point source in an unshielded silo. Data points are the results of MicroSkyshine calculations. Solid lines, shown for comparison, are results of K-Shine calculations. (a) 30-degree collimation.

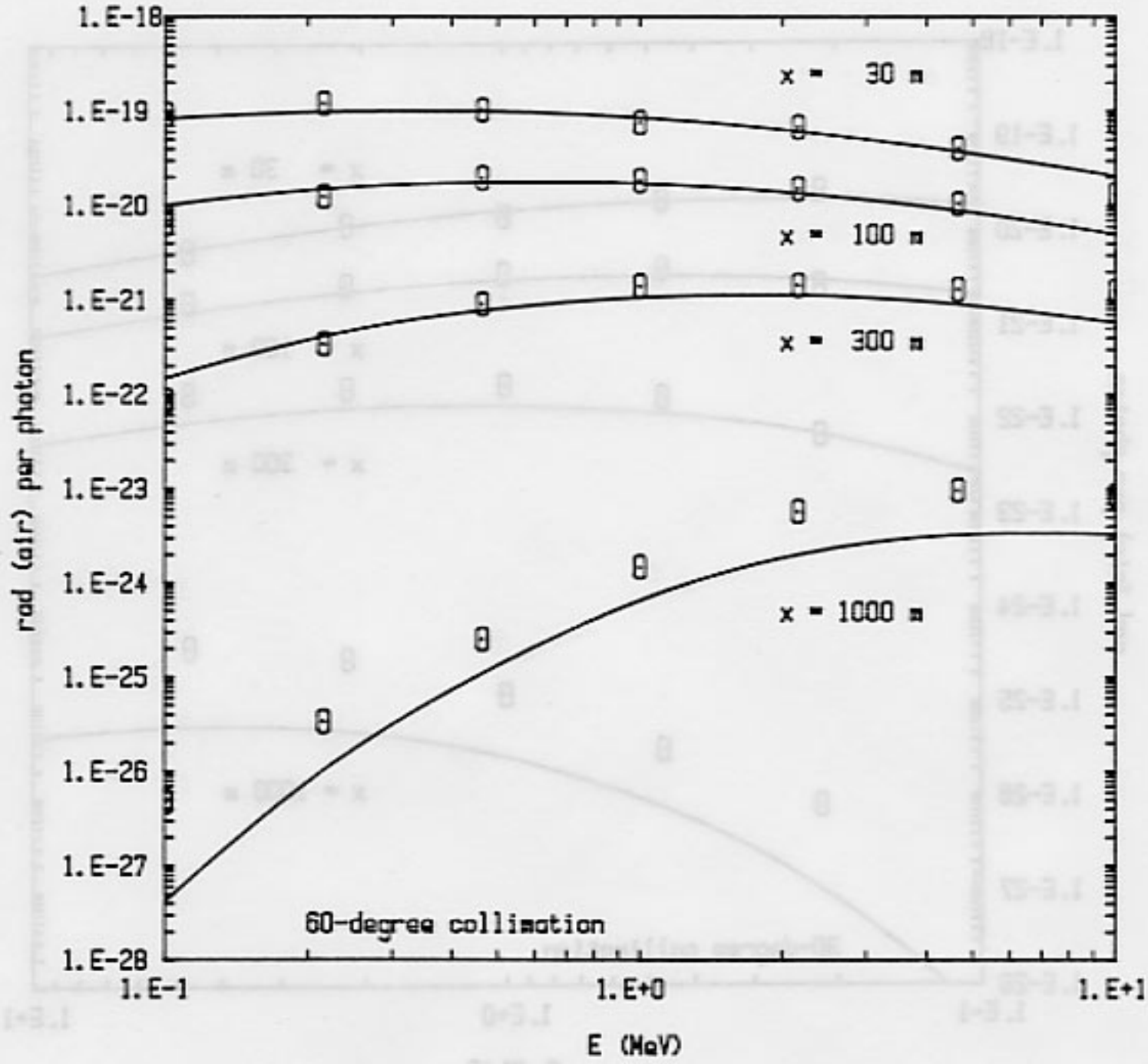

Fig. 5.7b Effect of source energy on the dose from a point source in an unshielded silo. Data points are the results of MicroSkyshine calculations. Solid lines, shown for comparison, are results of K-Shine calculations. (b) 60-degree collimation.

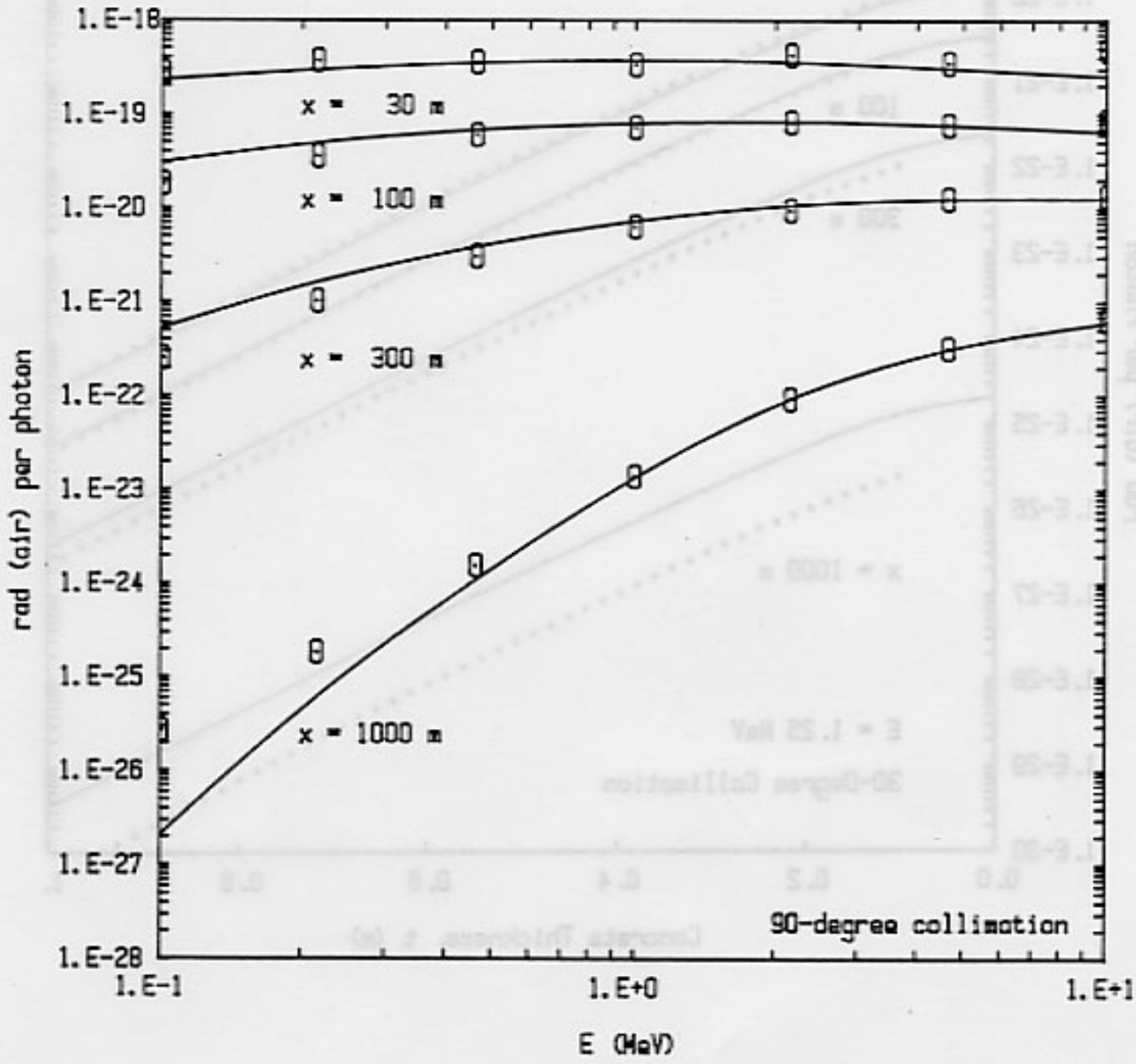

Fig. 5.7c Effect of source energy on the dose from a point source in an unshielded silo. Data points are the results of MicroSkyshine calculations. Solid lines, shown for comparison, are results of K-Shine calculations. (c) 90-degree collimation.

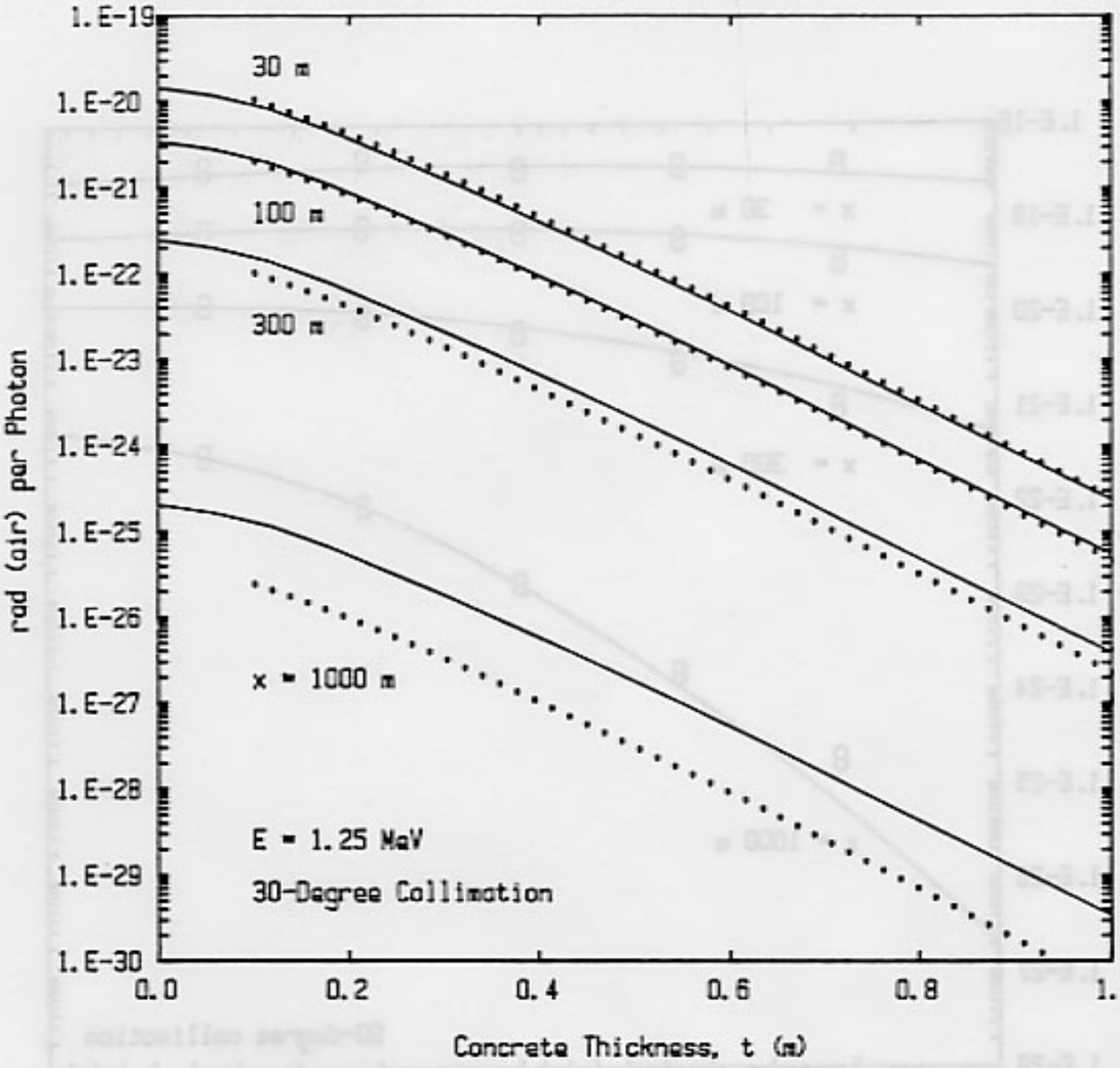

Fig. 5.8a Effect of concrete thickness on the dose from a point source in a silo with overhead concrete shielding. Solid lines are the results of MicroSkyshine calculations. Dotted lines, shown for comparison, are the results of K-Shine calculations. (a) 30-degree collimation, E = 1.25 MeV.

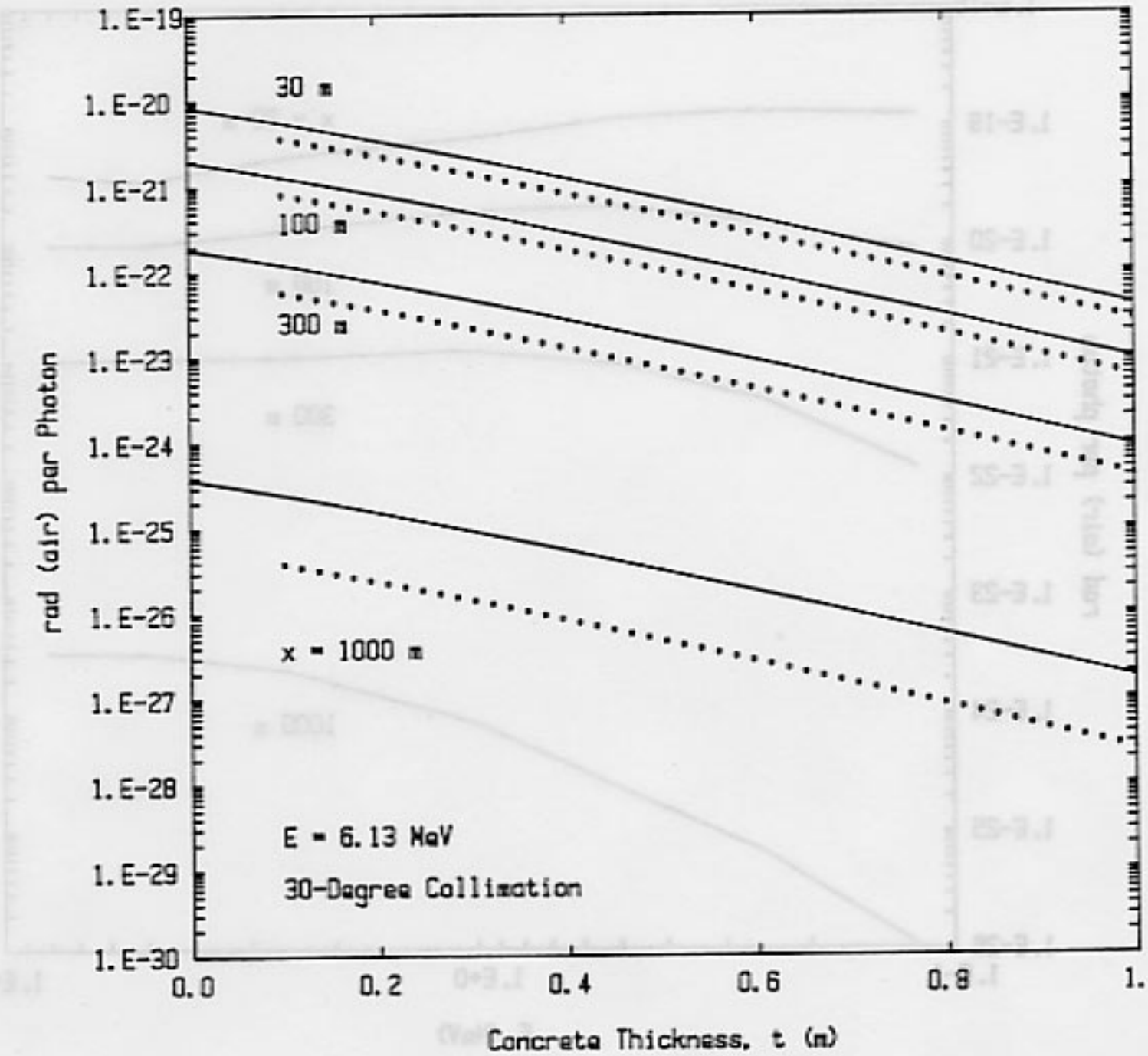

Fig. 5.8b Effect of concrete thickness on the dose from a point source in a silo with overhead concrete shielding. Solid lines are the results of MicroSkyshine calculations. Dotted lines, shown for comparison, are the results of K-Shine calculations. (b) 30-degree collimation, E = 6.13 MeV.

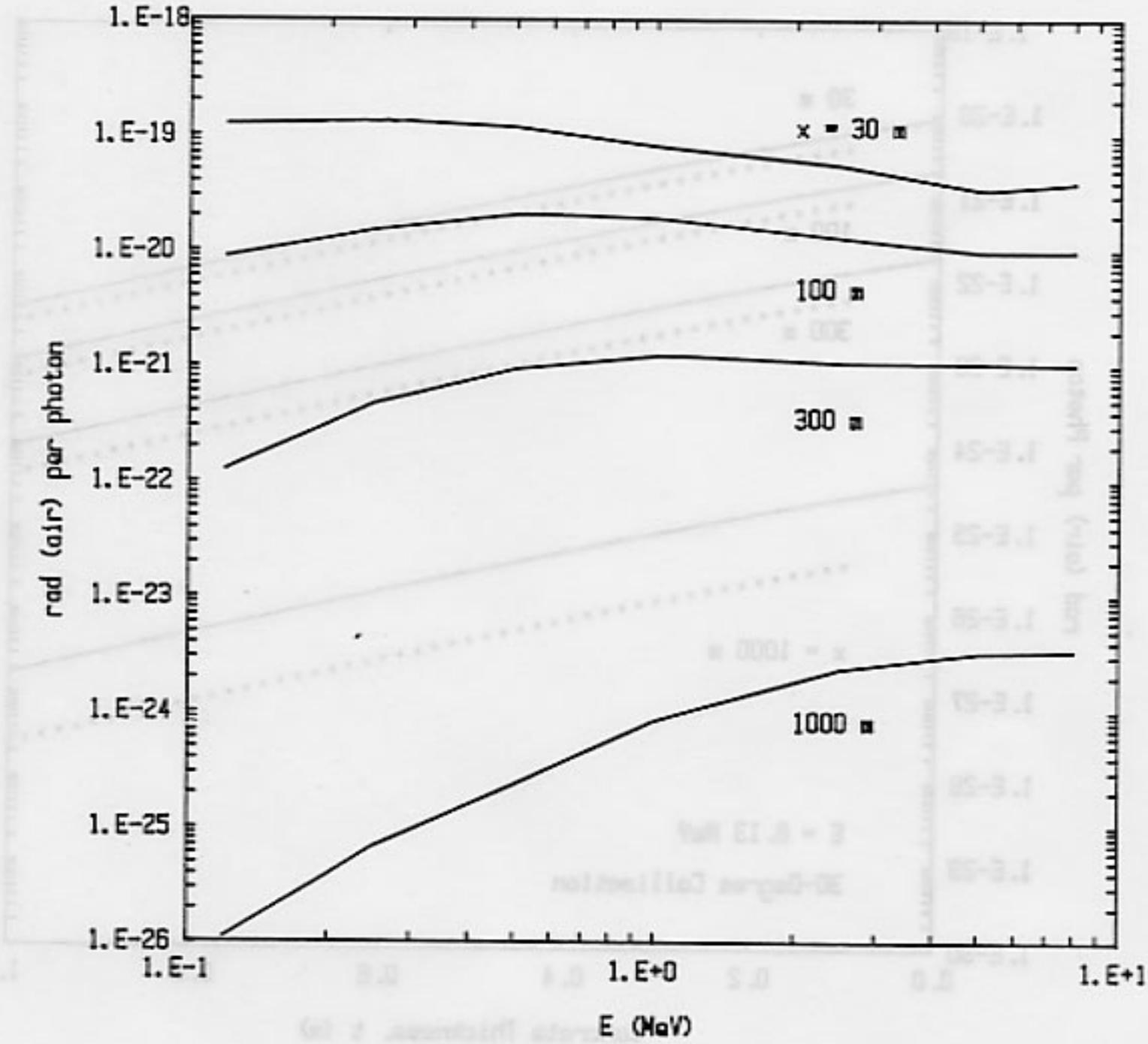

Fig. 5.9 Effect of photon energy on the dose from a point source behind an infinite wall with no overhead shielding. y = h = r = 3 m. z = 0.

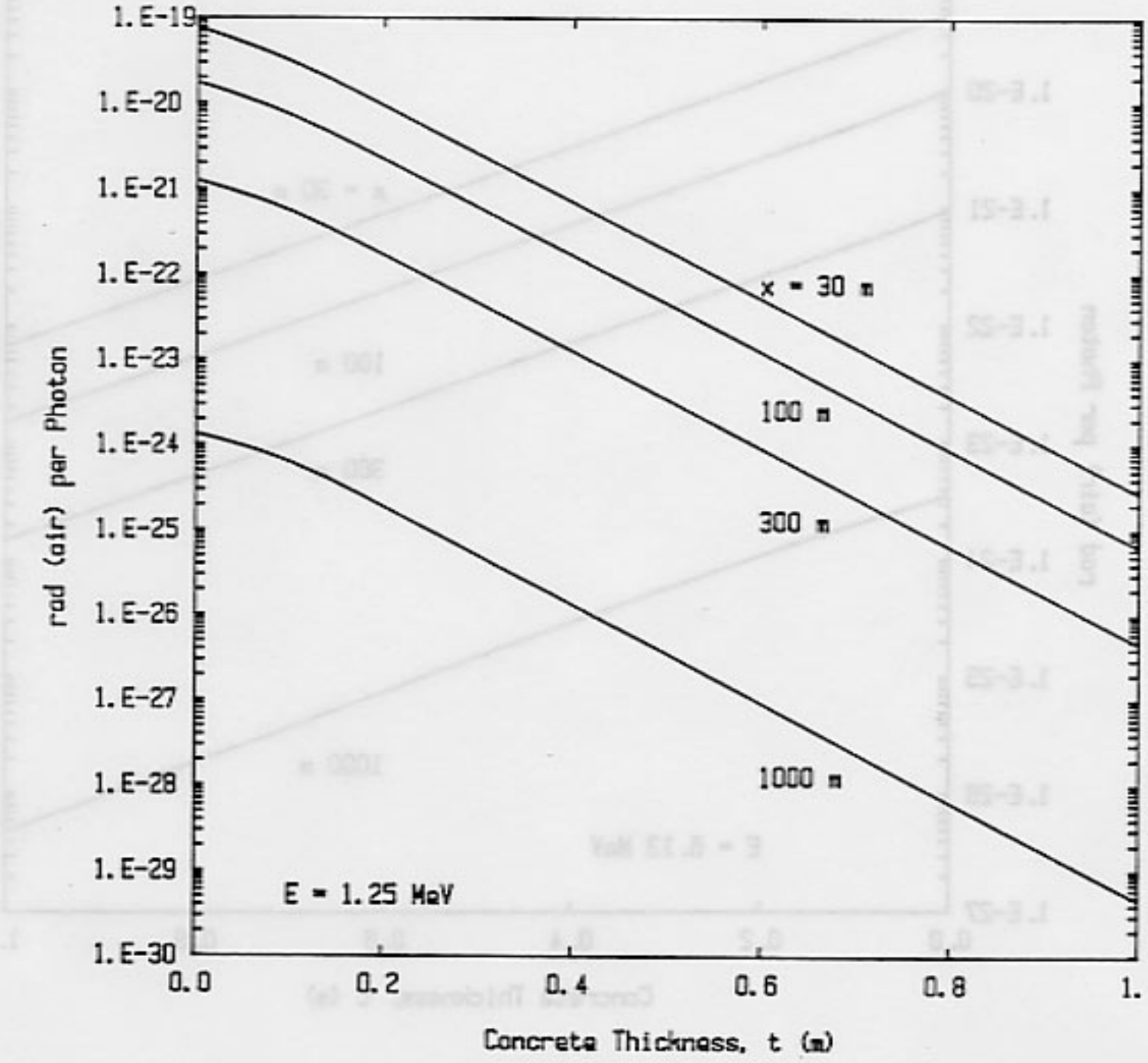

Fig. 5.10a Effect of concrete thickness on the dose from a point source behind an infinite wall with overhead concrete shielding of density 2.35 g/cm^3. y = h = r = 3 m. z = 0. (a) E = 1.25 MeV.

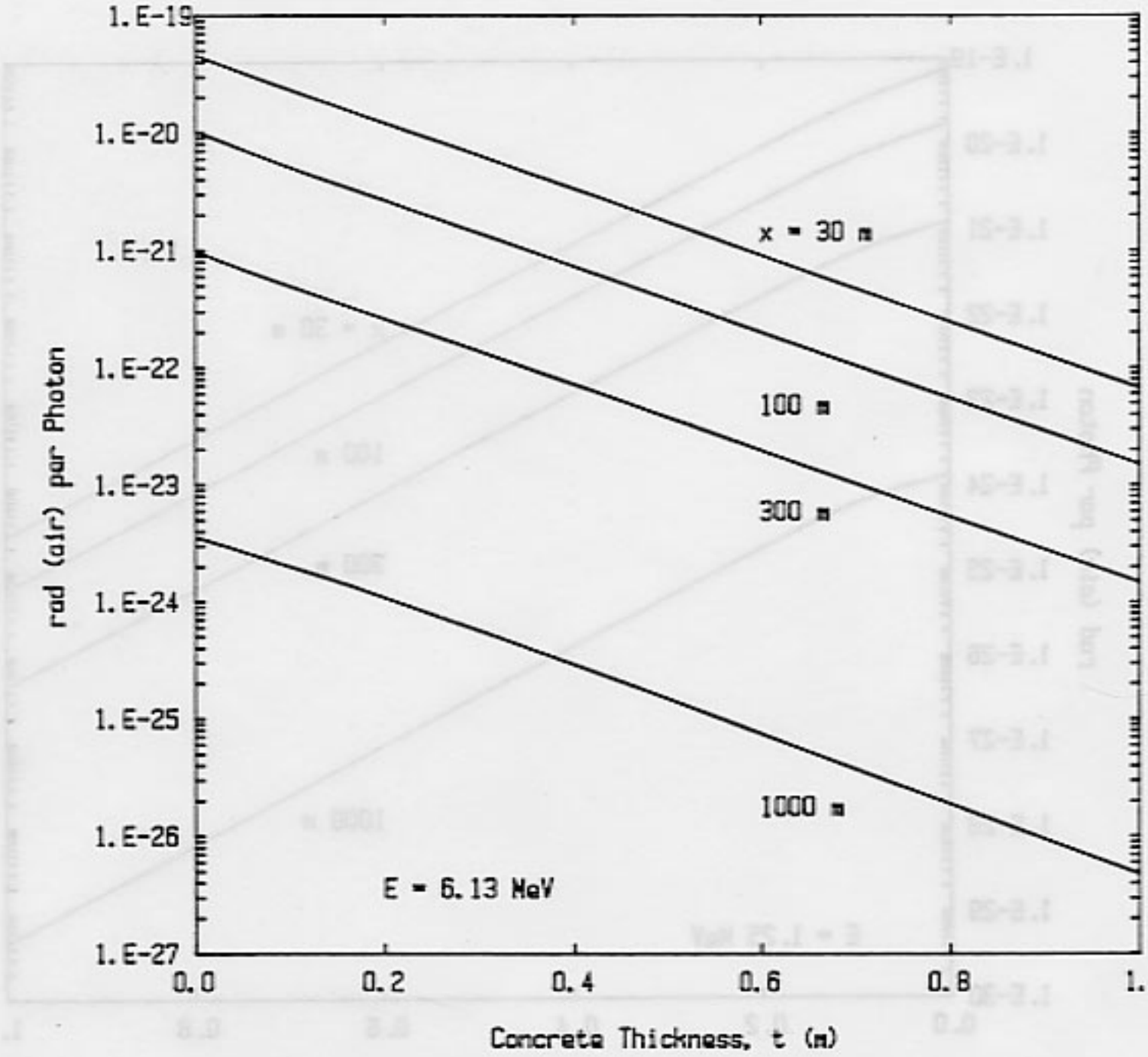

Fig. 5.10b Effect of concrete thickness on the dose from a point source behind an infinite wall with overhead concrete shielding of density 2.35 g/cm^3. y = h = r = 3 m. z = 0. (b) E = 6.13 MeV.

6. Validation of the MicroSkyshine Method

6.1 Comparison with Moments-Method Calculations

A collimation angle of 90 degrees for the point source in a silo represents the limiting case of 2π geometry. For this limiting case, so long as y = h, the detector response from skyshine at a given value of x is equal to half the response at the same source-detector distance resulting from photons originating from a bare point source and subsequently scattering in the atmosphere. It is thus possible to compare results of MicroSkyshine calculations, for this limiting case, with results of moments-method calculations for a point isotropic source in an infinite air medium.

MicroSkyshine calculations for the comparison were performed for y = h = 0, r = 1 m, x ranging from 25 to 2500 m, E ranging from 0.1 to 10 MeV, and an air density of 1.25 mg/cm^3. Infinite medium exposures due to scattered photons were deduced from air-kerma buildup factors computed using the method of moments by Chilton, Eisenhauer, and Simmons [Ch80]. If $R(E)$ is the exposure-rate response function (R m^2), $B(E,x)$ is the buildup factor for photons of energy E at distance x in air of prescribed density, and $\mu(E)$ is the total interaction coefficient for photons of energy E in air of prescribed density, then the response, in units of R/photon, is given by

$$R = \frac{R(E)\ e^{-\mu(E)x}\ [B(E,x)\ -1]}{8\pi x^2}. \qquad (6.1)$$

The comparison is illustrated in Fig. 6.1a for energies 1 MeV and less and distances to 1500 m and in Fig. 6.1b for energies 1 MeV and greater and distances to 2500 m. The solid lines are results of MicroSkyshine calculations and the individual data points are results of the moments-

method calculations. The MicroSkyshine results are listed in Appendix A, Table A6.1. It is apparent from this comparison that, for solid angles of collimation approaching 2π steradians, the MicroSkyshine method may in some cases be used for source-detector distances well beyond the nominal 1500-m limit for the PRIGAM response functions. For gamma-ray energies from 5 to 10 MeV, for example, a 2500-m limit is realistic. As the source energy decreases, however, the maximum distance for which the MicroSkyshine method should be applied directly also decreases. Furthermore, as the solid angle of collimation decreases, it may be expected that, for a given energy, the maximum distance also decreases. The authors recommend that, in either the silo or wall-shield geometries, if the dimension y exceeds the dimension r, then the maximum distances should be further restricted. For gamma-ray energies from 5 to 10 MeV, the recommended limit is 1500 m. For lower energies, lesser distances apply, as is illustrated in the figure.

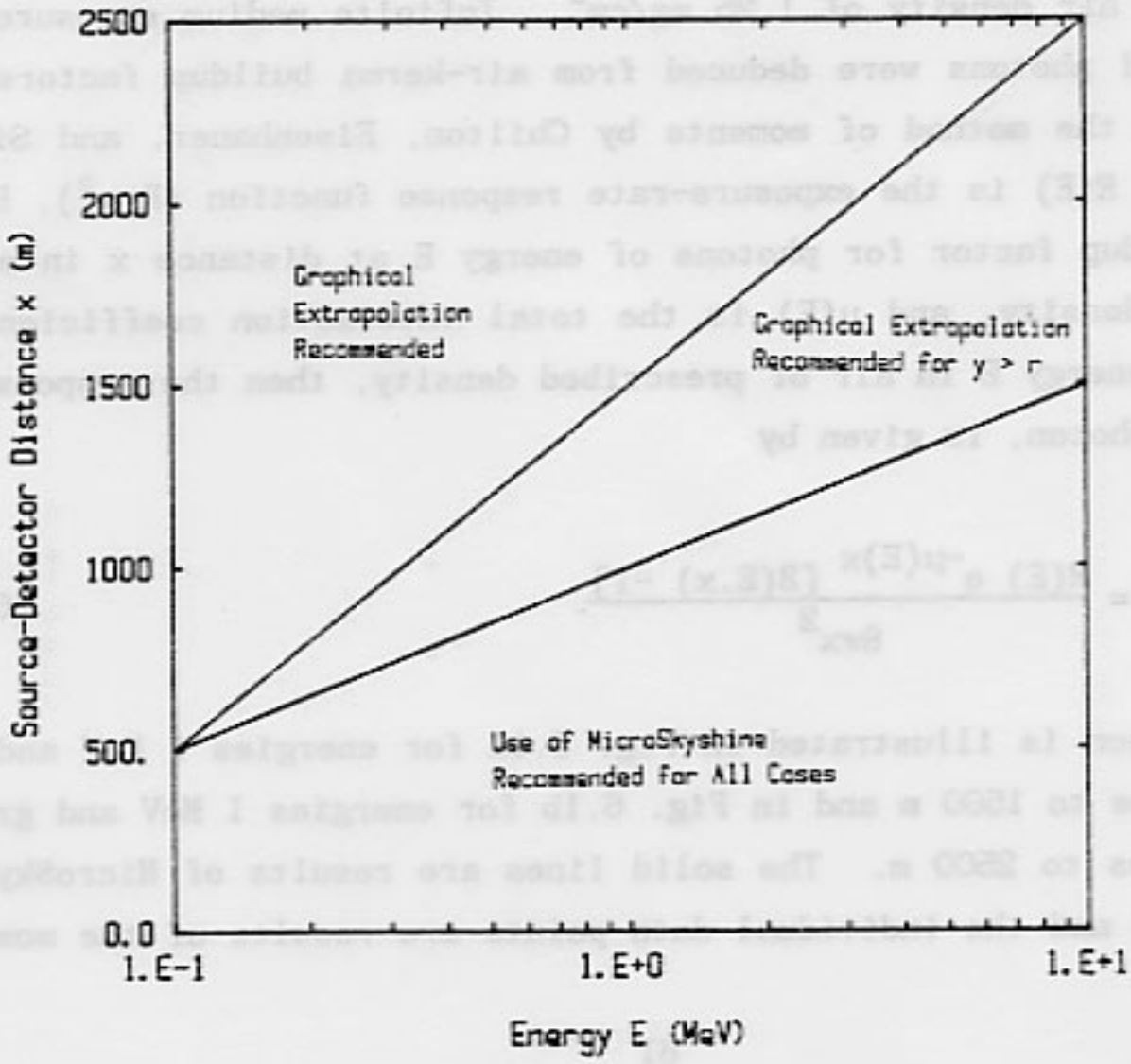

If skyshine dose rates are required at distances exceeding these limits, then the following graphical extrapolation procedure is recommended. Calculate the dose rate for several distances less than the limit. Plot the logarithm of the dose rate versus the distance. On the graph, use straight-line extrapolation to determine the dose rate at the desired distance.

6.2 Comparison with Benchmark Experimental Results

The skyshine experiments described in Chapter 3 serve as benchmarks against which to test the results of MicroSkyshine calculations as well as the results of calculations performed using other codes.

To facilitate the comparison, the results of the MicroSkyshine calculations have been expressed in the same format as those of the experimental data. The independent variable is the areal density separating source and detector, *i.e.*, the product of the air density and the source detector distance. Use of the areal density minimizes effects of day-to day variations in air density experienced during the course of the exper iments. The dependent variable is the exposure per photon multiplied by the square of the source-detector distance and divided by the solid angle of collimation, namely 4.683 sr. In this form, the strong effect of source-detector distance on detector response, through the inverse-square law, is suppressed.

The MicroSkyshine calculations were performed for y = h = 0.31 m, r = 1.18 m, ρ_{air} = 0.00125 g/cm^3, and x in multiples of 32 m to 640 m. For the shielded-silo cases, t = 0.21 or 0.428 m of concrete of density 2.32 g/cm^3. A comparison of MicroSkyshine results with experimental data is shown in Fig. 6.2, a composite figure illustrating both the unshielded and the shielded silo cases. A more detailed comparison is shown in Figs. 6.3 - 6.5. The solid lines are results of MicroSkyshine calculations. The broken lines are results of G^3 calculations (§6.4.1); the dotted lines are results of K-Shine calculations (§6.4.2); and the dashed lines are results of calculations performed using the DOT discrete ordinates transport code. MicroSkyshine results are listed in

Appendix A, Table A6.2. K-Shine results are listed in Appendix D, Table D6.1. G^3 results are summarized in §6.4.1 and output listings are provided in Appendix E.

6.3 Comparison with Benchmark Calculations

The two ANSI/ANS-6.6.1 reference skyshine problems described in Chapter 4 serve as well-studied benchmarks against which MicroSkyshine results can be compared to determine the validity of the MicroSkyshine method. In this section such comparisons are presented.

6.3.1 Unshielded Point Source — Problem I.1

The geometry for ANSI/ANS-6.6.1 Reference Problem I.1 is shown in Fig. 4.1. To adapt MicroSkyshine to this problem, the point N-16 source (E = 6.12 MeV) was placed on the axis of an open silo of 1 m inner radius and with walls 60 ft (18.3 m) high. The source and detector were placed 0.000001 m below this elevation so as to eliminate any direct (unscattered) component. The source-to-detector distance in this MicroSkyshine calculation was then interpreted as the slant distance x between the source and detector in the reference problem. The horizontal range r in the reference problem is related to this slant distance by

$$r = \left[x^2 - (\Delta z)^2 \right]^{1/2} \qquad (6.2)$$

where Δz is the difference in elevation between source and detector in the reference problem (17.4 m).

In Fig. 6.6 the MicroSkyshine results are plotted as a solid line and the results of seven other calculations reported in the ANSI standard are shown as discrete points. (To maintain consistency between this comparison and other results in this report, the scales of the figure have been changed from those in ANSI Standard 6.6.1 so that range is in meters and dose in rad/yr.) It is seen from Fig. 6.6 that the

Microskyshine results are in excellent agreement with the earlier calculations and agree most closely with those produced from SKYSHINE II -- a result to be expected since SKYSHINE II uses the same PRIGAM response functions as MicroSkyshine.

6.3.2 Rectangularly Collimated Point Source — Problem I.2

ANSI/ANS-6.6.1 Reference Problem I.2 collimates a point isotropic source (E = 6.12 MeV) by an open rectangular building. The geometry is shown in Fig. 4.2. To apply MicroSkyshine to this problem, it was first necessary to modify slightly the treatment of the infinite wall geometry so that rays from the source would be limited not only by the front wall (i.e., wall closest to the detectors) but also by the side and rear walls. This additional collimation is readily incorporated into the code by replacing the expression for the maximum polar angle $\theta_{max}(\psi)$ given by Eq. (5.20) by a somewhat more complicated expression which includes the limiting cases resulting from the side and rear walls.

The results of this calculation are shown in Fig. 6.7 along with the four results reported by the ANSI 6.6.1 Standard. In addition, results obtained with SKYSHINE II are also shown [La79], and again it is not surprising that the MicroSkyshine results agree very closely with these results since both codes use the same PRIGAM response functions (although they differ in how the integrals of Eq. (5.19) or (5.21) are evaluated).

Finally, it should be noted that for this reference problem the side and back walls limit the dose almost negligibly. If the problem is approximated by replacing the front wall by an infinitely long wall and ignoring the side and rear walls, the resulting doses at distances greater than 200 m are at most only 2% higher. By contrast, approximating the rectangular structure by a cylindrical silo with equal solid angle of collimation yields doses which are over a factor of two higher at distances greater than 4000 m. This demonstrates the importance of having, with the MicroSkyshine code, the option of analyzing the case of a point source behind a wall shield.

6.4 Comparison with Results of Single-Scatter Calculations

One of the most widely used techniques for calculating gamma doses for fixed source problems is the use of the single-scattering technique. In this method the spatial variation of where source photons make their first scatter is determined and then approximate buildup factors are incorporated to account for the subsequent scattering of photons into the detector. Many codes are based on this technique. Here results from two such codes, which are well-suited to the skyshine problem, are compared to MicroSkyshine calculations. The first code, G^3, is a general-geometry, single-scatter code which has often been used for skyshine calculations. The second code, K-SHINE, is especially designed for the skyshine problems considered in this report.

6.4.1 G^3 Results

The IBM version of the G^3 program [Ma73] was obtained from the Radiation Shielding Information Center (RSIC) and compiled under the FORTRAN-66 option of the FORTVS operating system. G^3 is a general purpose point-kernel shielding code which has been used widely for skyshine calculations [An79].

In order to assure satisfactory operation of the program, two sample problems provided in the RSIC code package [Rs75] were run and yielded results identical to the sample solutions also provided in the code package. Problem 1 deals with air scattering into a collimated detector. Problem 2 deals with air scattering of photons from a collimated source. For details of the sample calculations, the reader is referred to the code description [Ma73,Rs75]. Data input and results are listed in Appendix E, Tables E6.1 through E6.4.

Results from G^3 calculations were also compared with MicroSkyshine results for the point source in a cylindrical silo and the point source behind a shield wall. As described below, G^3 in both cases substantially underpredicts skyshine dose rates when the source has overhead shielding.

G^3 Calculations for the Point Source in a Cylindrical Silo

The G^3 code was run for the conditions of the KSU benchmark skyshine experiments (see §3.1 and §6.2). Figure 6.8 is a vertical section through the source and detector for the point source within a silo shield. Shield regions are denoted by circles, shield boundaries by triangles. Regions 1, 4, and 5 are air with density 0.00125 g/cm^3. Region 2 is concrete of density 2.32 g/cm^3. Region 3 is air for the open-silo case and concrete for the shielded-silo cases. The source location S is the origin of coordinates, and detector locations D are at the same elevation as the source and at radial distance x. Boundaries 1 and 2 are cylinders of radii 1.18 and 2.11 m. Boundaries 3 and 4 are horizontal planes, the former 0.31 m above the source and the latter either 0.52 m for the open-silo and 21-cm shield cases or 0.738 m above the source for the 42.8-cm shield case. Assumed concrete composition, by weight fraction, is as follows: H, 0.0056; O, 0.4983; Na, 0.0171; Mg, 0.0024 (as Al); Al, 0.0456; Si, 0.3158; S, 0.0012 (as Si); K, 0.0192; Ca, 0.0826; and Fe, 0.0122. The scattering geometry is based on a spherical polar coordinate system. Radii are measured from the source location. Polar angles are measured from the vertical axis and are limited to 75.25 degrees (1.3134 radians), consistent with the 150.5-degree full angle of collimation used in the benchmark experiments. Azimuthal angles are measured from the vertical plane through the source and detector. Because of symmetry, the maximum azimuthal angle need be only 180 degrees (π radians).

In order to test convergence, two calculations were performed for the open-silo case. The first calculation, identified as Problem GGG003, treated the ^{60}Co source as emitting both 1.17 and 1.33 MeV photons, with the results averaged for the two. For that calculation, the photon-scattering volumes were defined by the following grid:

GGG003 Azimuthal-Angle Grid (radians)

0.00	0.10	0.20	0.30	0.05	0.70	1.00
1.50	2.00	2.50	3.1416			

GGG003 Polar-Angle Grid (radians)

0.00	0.25	0.50	0.60	0.70	0.80	0.90
1.00	1.10	1.20	1.25	1.30	1.3134	

GGG003 Radial Grid (m)

0.75	1.00	1.50	2.00	2.50	3.00	3.50	4.00	4.50	5.00	6.00
7.00	8.00	9.00	10.0	12.0	14.0	16.0	18.0	20.0	25.0	30.0
35.0	40.0	45.0	50.0	60.0	70.0	80.0	90.0	100.	150.	200.
250.	300.	400.	500.	600.	700.	800.	900.	1000		

The GGG003 grid had relatively coarse azimuthal and polar angle-spacing but relatively fine radial spacing (requiring two-pass computation). The second G^3 calculation, identified as Problem GGG006, had by contrast relatively finer angle spacing and relatively coarser radial spacing, the latter approximating equal logarithmic spacing radially. Furthermore, ^{60}Co was approximated as emitting only 1.25-MeV photons. For the second calculation, the coordinate spacings were as follows:

GGG006 Azimuthal-Angle Spacing (radians)

0.000	0.025	0.050	0.075	0.100	0.150	0.200
0.250	0.300	0.400	0.500	0.600	0.800	1.000
1.200	1.400	1.600	1.800	2.000	2.400	3.1416

GGG006 Polar-Angle Spacing (radians)

0.000	0.100	0.200	0.300	0.400	0.500	0.600
0.700	0.750	0.800	0.850	0.900	0.950	1.000
1.050	1.100	1.125	1.250	1.275	1.300	1.314

GGG006 Radial Spacing (m)

0.550	0.900	1.250	1.500	2.100	3.150	4.650
6.800	10.00	14.70	21.55	31.60	46.40	68.10
100.0	147.6	215.5	316.6	464.0	681.3	1000.

The results of these two calculations are summarized in Table 6.1 and listed in Appendix E, Tables E6.5–E6.8. For reasons explained in §6.2, the results are translated into units of m^2R/sr. Agreement between the two cases is within 4 percent; thus, the scattering-volume grid of Problem GGG006 was used in calculations for the point source in a silo

with 21 cm of overhead concrete shielding (Problem GGG007) and with 42.8 cm of overhead shielding (Problem GGG008). Results of the calculations for the shielded-silo cases are summarized in Table 6.2.

A comparison between G^3 results, experimental data, and results of other calculations is given in Figs. 6.3-6.5. Detailed results are listed in Appendix E, Tables E6.9-E6.12. It will be noted that, while the G^3 results agree reasonable well with other results for the open-silo case, they very substantially underpredict detector response for the shielded-silo cases. This is to be expected because the G^3 program, although accounting for attenuation in overhead shielding, does not account for buildup of secondary photons arising from scattering interactions taking place in the overhead shielding.

G^3 Calculations for the Point Source Behind an Infinite Wall

Two G^3 test problems were run for the wall-shield geometry. The problems differed only in the presence or absence of overhead concrete shielding. Geometry for the problems is illustrated in Fig. 6.9 which is a sectional view in the vertical plane containing the source-detector axis, which axis is perpendicular to the shield wall. Shield regions are indicated by circles, boundaries by triangles. Regions 1-3 are air of density 0.00125 g/cm^3. Region 4 is of effectively infinite density. Region 5 is either air or, in the case of overhead shielding, 30-cm thick concrete of density 2.13 g/cm^3. The location of source S is the origin of coordinates. Boundary 1 is a sphere of radius 1.414 m, while boundaries 2 and 3 are vertical planes 1.0 and 1.1 m from the source. Boundaries 4 and 5 are horizontal planes 0.7 and 1.0 m above the source. The scattering geometry is cylindrical. Azimuthal angles are measured from the vertical plane containing the source-detector axis. Radial distances are measured horizontally from the source. Axial distances are measured vertically upward from the source. Source energy is 6.13 MeV, corresponding to the predominant photon energy in the decay of ^{16}N. The photon scattering volumes were defined by the following grid:

Azimuthal-Angle Grid (radians)

0.000	0.025	0.050	0.075	0.100	0.150	0.200
0.250	0.300	0.400	0.500	0.600	0.800	1.000
1.200	1.400	1.600	1.800	2.000	2.400	3.1416

Radial Grid (m)

0.000	0.500	1.000	1.550	2.100	3.150	4.650
6.800	10.00	14.70	21.55	31.60	46.40	68.10
100.0	146.7	215.5	316.6	464.1	681.3	1000.

Axial Grid (m)

1.000	1.400	2.000	2.800	4.000	5.600	8.000
11.10	16.00	22.00	32.00	45.00	63.00	79.00
125.0	178.0	251.0	355.0	501.0	708.0	1000.

Results of the two G^3 calculations, Problem GGG104 for the wall-shield case without overhead shielding, and Problem GGG103 for the case with 30 cm of overhead concrete shielding are summarized in Table 6.3 along with results of MicroSkyshine results for the same cases. Detailed results of the G^3 calculations are listed in Appendix E, Tables E6.13-E6.16. As in the case of the point source in a silo shield, in comparison to MicroSkyshine results, and as expected, the G^3 program substantially underpredicts detector response in the presence of overhead shielding.

6.4.2 K-SHINE Results

Description of K-Shine Algorithm

K-SHINE is a single-scatter code especially designed for the skyshine problem. Specifically, it is designed for a point, monoenergetic, isotropically emitting source placed on a silo axis or behind a wall, with or without a shielding slab over the source. Since K-SHINE is a recently developed code and not widely known, the silo-geometry case will be briefly reviewed here. The extension to the wall-geometry case is described by George [Ge87].

The K-SHINE code is based on a single-scatter code developed by Roseberry and Shultis [Ro81, Ro82] which in turn is an extension of the

work by Kitazume [Ki68]. Consider gamma radiation from a monoenergetic, isotropic point source (of strength S) that, after streaming a distance c through a slab shield and a distance a through air, scatters in a volume element dV through an angle ($\pi - \beta$) and then travels a distance b to a detector without subsequent air interactions (see Fig. 6.10). The detector response R from these single-scattered photons is

$$R = \int_V \frac{S\,K}{4\pi(a+c)^2 b^2} (\mu_{en}/\rho) N \sigma E' \exp(-\mu a - \mu' b - \mu_s c)\, dV \qquad (6.3)$$

where the volume V is that portion of the air hemisphere within which photons can be scattered into the detector. In this expression E' is the photon energy after scattering through an angle ($\pi-\beta$), N is the electron density in the air, and K is the energy flux density to response conversion factor. The total attenuation coefficients for photons of energy E in air and the slab material are denoted by μ and μ_s, respectively, while for photons of energy E' in air, μ' is used. The energy of the scattered photon, E', is calculated from the Compton formula, and the differential scattering cross section σ is approximated by the free-electron Klein-Nishina result.

To obtain an explicit expression needed for the numerical evaluation of Eq. (6.3), a specific coordinate system must be chosen. Many choices are possible, but that defined by ϵ, θ, and β in Fig. 6.11 has been found to have several advantages [Ro82]. With this system, it is found that

$$b = d \sin\theta \csc\beta \,, \qquad (6.4)$$

$$c = t \sec\epsilon \csc\theta \,, \qquad (6.5)$$

$$a = d(\cos\theta + \sin\theta \cot\beta) - c \,, \qquad (6.6)$$

and

$$dV = (a+c)^2 \, d \sin^2\theta \csc^2\beta \, d\beta \, d\theta \, d\epsilon \,. \qquad (6.7)$$

The above expression for the detector response can be modified to

account approximately for the multiple scattering of photons by using appropriate buildup factors. First, an infinite-medium buildup factor B' is used to correct for multiple scattering in the second air leg (b in Fig. 6.10). For the bare collimated source, neglect of buildup in the first air leg is justified since, by the problem formulation, photons make their first scatter in dV. Although buildup in the first air leg is properly omitted, the effect of a slab shield over the source cannot be be disposed of so cavalierly. Attenuation of source photons in the shield is accompanied by the buildup of scattered photons. Those photons emerging from a thick slab shield over the source are effectively collimated into an upward beam and consist primarily of uncollided photons or those that have made only small-angle scatters and, hence, retain most of their original energy. Those escaping photons that have suffered a significant energy loss are preferentially attenuated (compared to source-energy photons) while traveling to the detector and can therefore be ignored. Thus, to account for the overhead shield, an infinite medium buildup factor B is used, and photons emerging from the shield are assumed to retain their source energy.

With these modifications, the detector response to skyshine radiation, corrected for multiple scattering and expressed in the coordinate system of Fig. 6.11, becomes

$$R = \frac{SK}{2\pi d} \int_0^{\beta_{max}} d\beta \; N\sigma E'(\mu_{en}/\rho) \int_{\theta_{min}}^{\theta_{max}} d\theta \; B' \exp(-\mu a - \mu' b)$$

$$\times \int_0^{\epsilon_{max}} d\epsilon \; B \exp(-\mu_s c) \; . \qquad (6.8)$$

For the case of no overhead shield, $c = 0$ and $B = 1$ so that the ϵ-integral can be performed analytically. The minimum value of θ for this unshielded case is defined by the ray from the source that just grazes the silo wall, namely $\theta_{min} = \arctan(h/r)$. For the shielded case,

there is no well-defined minimum value of θ below which a sharp cutoff of the radiation occurs. Nevertheless, an effective θ_{min} can be defined corresponding to the longest photon path through the shield that significantly contributes to the radiation field at the detector. The upper limit of the θ-integral must be chosen such that θ, β, and d in Fig. 6.11 form a closed triangle, i.e., $\theta = \pi - \beta - \arctan[h/(d-r)]$, and such that θ is not greater than that allowed by the silo collimation, i.e., $\theta \leq (\pi - \theta_{min})$. Thus

$$\theta_{max} = \min\{(\pi - \theta_{min}),\ \pi - \beta - \arctan[h/(d-r)]\} \ . \qquad (6.9)$$

The maximum ϵ corresponds to the minimum θ (see Fig. 6.11) so that

$$\epsilon_{max} = \arccos(\sin\theta_{min}\ \csc\theta). \qquad (6.10)$$

Finally, the angle β is limited by the outer lip of the source collimation (or effective collimation for the shielded-source case) to

$$\beta_{max} = (\pi - \theta_{min}) - \arctan[h/(d-c)]. \qquad (6.11)$$

The numerical evaluation of Eq. (6.8) is accomplished by use of numerical quadrature for each integral. In K-SHINE, adaptive Gaussian quadrature is used wherein the integration interval is automatically subdivided to achieve a specified accuracy. The calculations are greatly simplified if two additional approximations are introduced. As the angle β approaches zero, the lengths of the first and second air legs (a and b) become infinite. In reality only those scattering volumes relatively close to the source contribute significantly to the detector response. Thus a limit L on the total air path can be imposed such that $\mu a + \mu' b \leq L$. This restriction is equivalent to $d(\mu\cot\beta + \mu'\csc\beta) \leq L$, which for a given L can be used to find an effective minimum value of β, β_{min}. For L = 10 mean-free-paths lengths, skyshine dose rates are obtained from Eq. (6.8) within 0.4% of values obtained when β_{min} approaches zero. Similarly for the shielded case, a limit on the path length through the shield can be imposed. If the maximum ray

length in the shield is denoted by $L_s \equiv \mu_s c$, then, from Eq. (6.5) one has the maximum effective value for ϵ of

$$\epsilon_{max} = \arccos[\mu_s t \cos\theta / L_s] \qquad (6.12)$$

which replaces the value given by Eq. (6.10) if the former is smaller. It was found [RoS2] that with L_s = 15 mfp, dose rates were within 0.1% of the values obtained without this added restriction on ϵ_{max}.

Comparison with MicroSkyshine Results

Results of K-SHINE calculations have been invoked throughout Chapters 5 and 6 as independent confirmations of the validity of MicroSkyshine calculations. Specific results which pertain to the KSU benchmark skyshine experiments are tabulated in Appendix D. A direct comparison of the two methods for the conditions of the KSU benchmark experiments is shown in Fig. 6.12

6.5 Comparison with Hybrid ANISN/SKYSHINE-II Calculations

Keck and Herchenroder [Ke82] performed calculations for the conditions of the KSU benchmark experiments, with concrete overhead shielding, using a hybrid technique. They first used the ANISN one-dimensional discrete-ordinates transport code to estimate the energy and angular distributions of the gamma rays emerging from the top surface of the overhead concrete shield. Treating the upper shield surface as a secondary source, they then used the SKYSHINE-II code [La79] to calculate skyshine dose rates. Their results, which agree very well with experimental results, are illustrated in Fig. 6.13 along with MicroSkyshine results for the same conditions. The MicroSkyshine results are in good agreement and are for the most part conservative.

Table 6.1. Comparison of G^3 Problems GGG003 and GGG006 for the conditions of the KSU benchmark experiment with a point source in a silo without overhead shielding.

Areal Density		Normalized Exposure (m^2R/sr)	
x (m)	(g/cm2)	GGG003	GGG006
40	5	6.47E-17	6.21E-17
80	10	1.10E-16	1.06E-16
160	20	1.40E-16	1.35E-16
240	30	1.23E-16	1.19E-16
320	40	9.54E-17	9.19E-17
480	60	4.73E-17	4.55E-17
640	80	1.99E-17	1.91E-17

Table 6.2. G^3 Problems GGG007 and GGG008 for the conditions of the KSU benchmark experiment with a point source in a silo with overhead concrete shielding.

Areal Density		Normalized Exposure (m^2R/sr)	
x (m)	(g/cm2)	GGG003 (21 cm)	GGG006 (42.8 cm)
40	5	6.80E-19	2.09E-20
80	10	1.15E-18	3.39E-20
160	20	1.26E-18	3.49E-20
240	30	9.62E-19	2.53E-20
320	40	6.62E-19	1.65E-20
480	60	2.61E-19	5.89E-21
640	80	8.74E-20	1.77E-21

Table 6.3. Comparison of G^3 and MicroSkyshine Results for the case of a point source of 6.13-MeV photons shielded by an infinite vertical wall.

	Normalized Exposure (R/photon)			
	No Overhead Shielding		30 cm Concrete Shielding	
x (m)	GGG104	MicroSkyshine	GGG103	MicroSkyshine
100	9.43E-21	1.18E-20	8.39E-22	1.91E-21
200	2.38E-21	3.14E-21	2.18E-22	5.16E-22
300	7.71E-22	1.05E-21	7.21E-23	1.78E-22
500	1.05E-22	1.57E-22	1.02E-23	2.80E-23
800	6.54E-24	1.38E-23	6.38E-25	2.59E-24

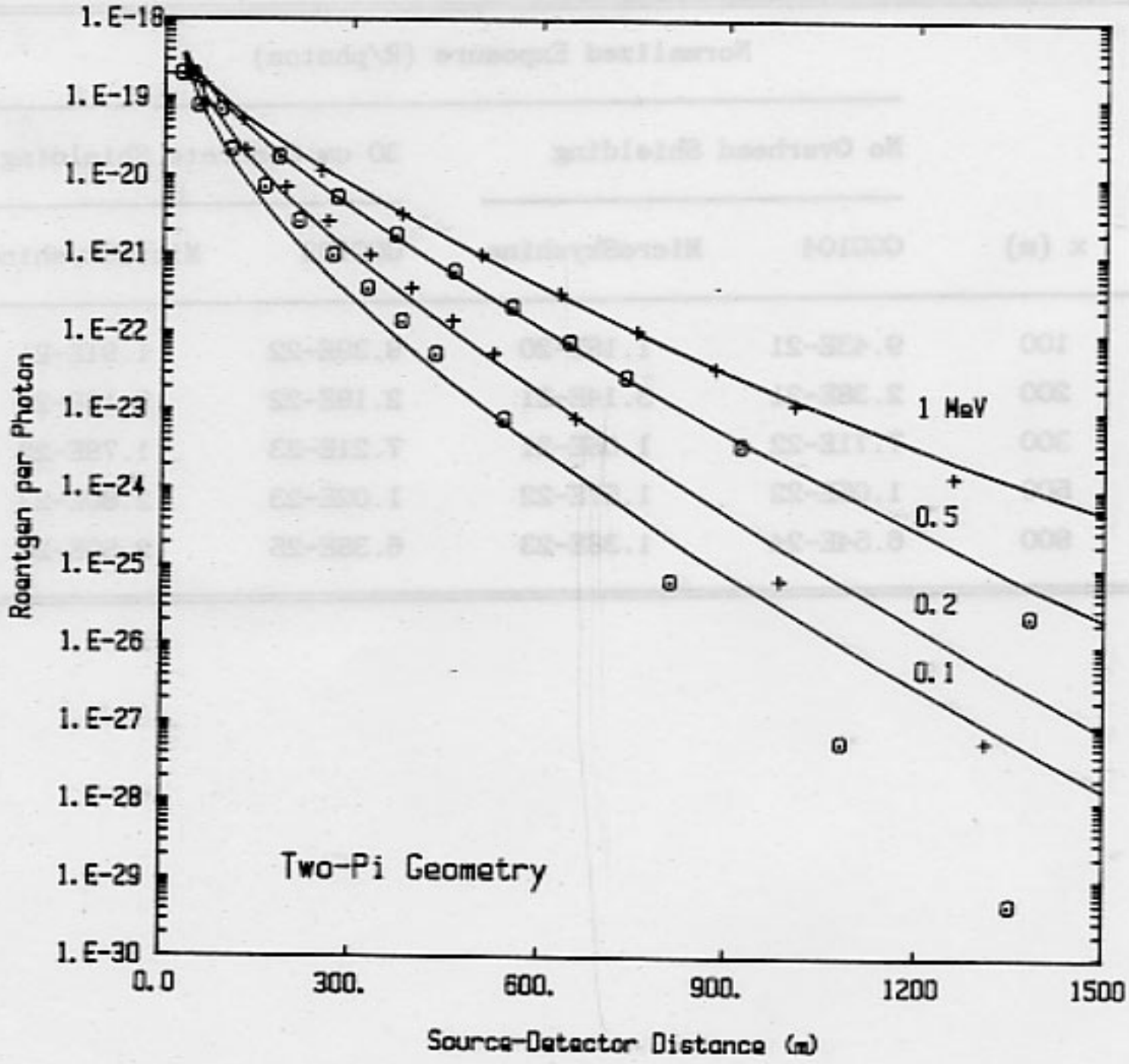

Fig. 6.1a Comparison of MicroSkyshine results (solid lines) with moments-method results (data points) for the scattered-radiation dose arising from a point source emitting photons only in the 2π-steradian upward hemisphere of directions in an infinite atmosphere. Part a: 0.1 - 1 MeV.

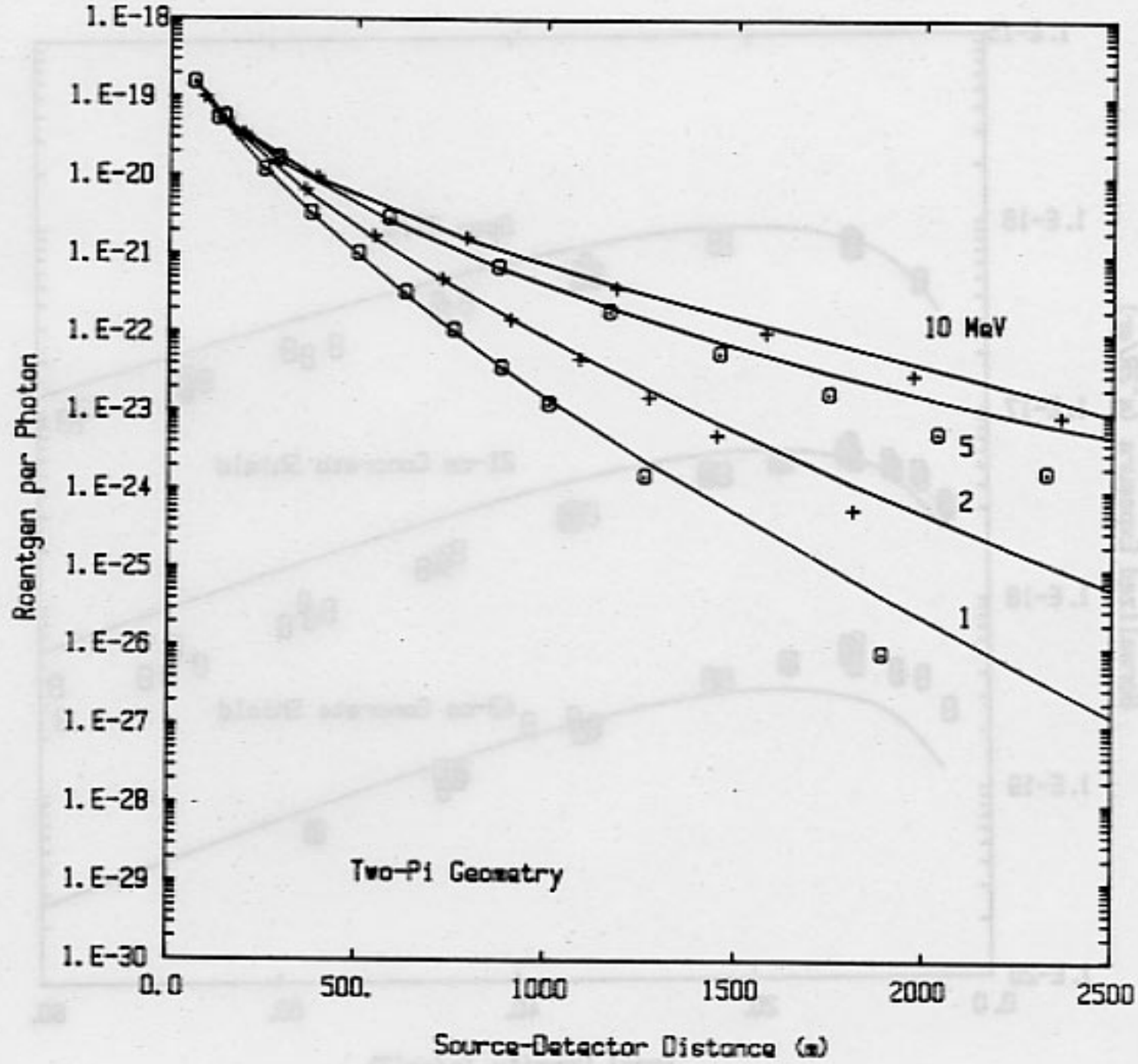

Fig. 6.1b Comparison of MicroSkyshine results (solid lines) with moments-method results (data points) for the scattered-radiation dose arising from a point source emitting photons only in the 2π-steradian upward hemisphere of directions in an infinite atmosphere. Part b: 1 - 10 MeV.

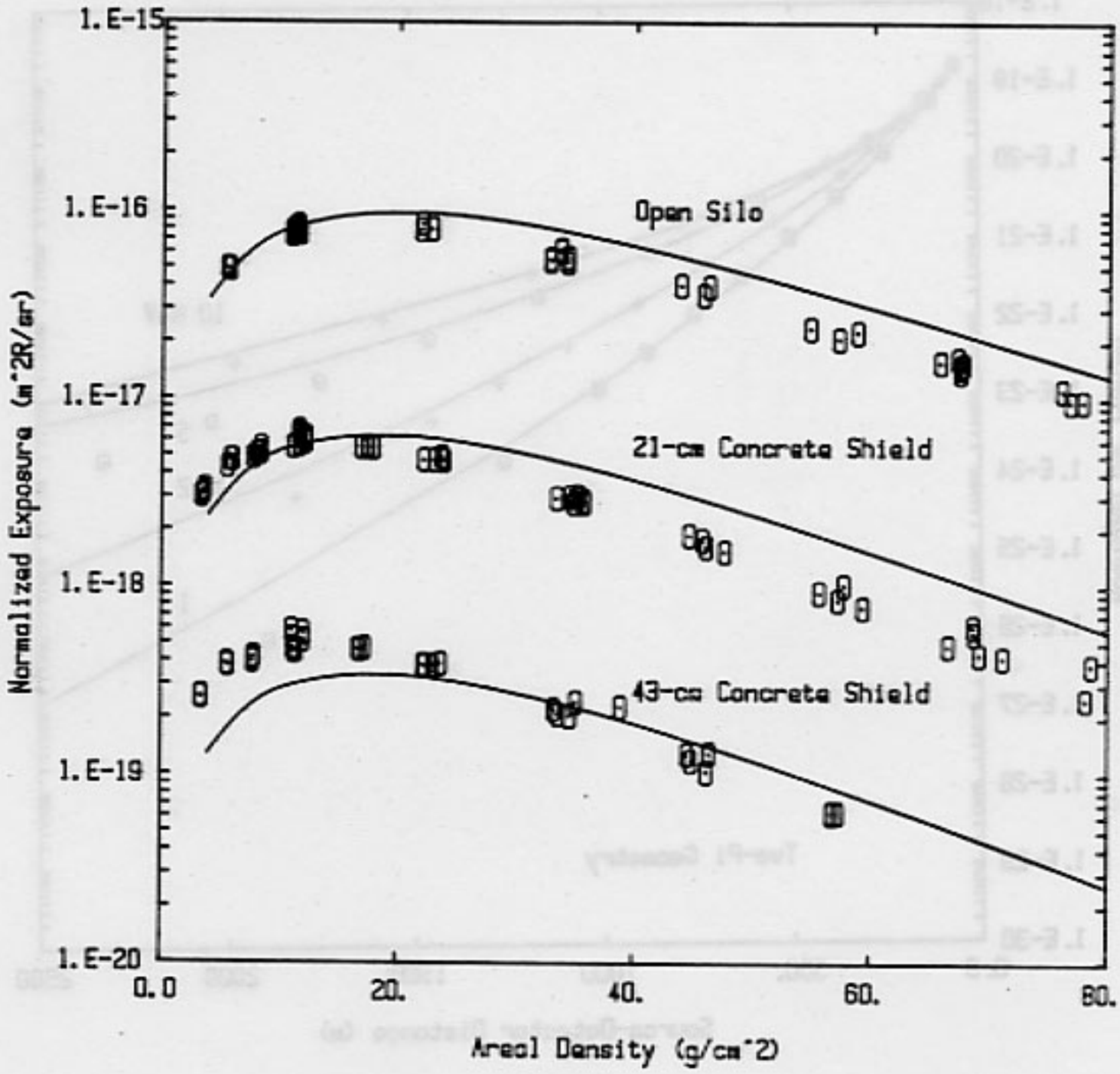

Fig. 6.2 Comparison of MicroSkyshine results (solid lines) with experimental data for the conditions of the KSU benchmark skyshine experiments. A ^{60}Co source is within a cylindrical silo with a 150.5-degree full-angle of collimation. Three cases are shown: (1) no overhead shielding, (2) 21 cm of overhead concrete shielding, and (3) 42.8 cm of overhead concrete shielding of density 2.32.g/cm^3.

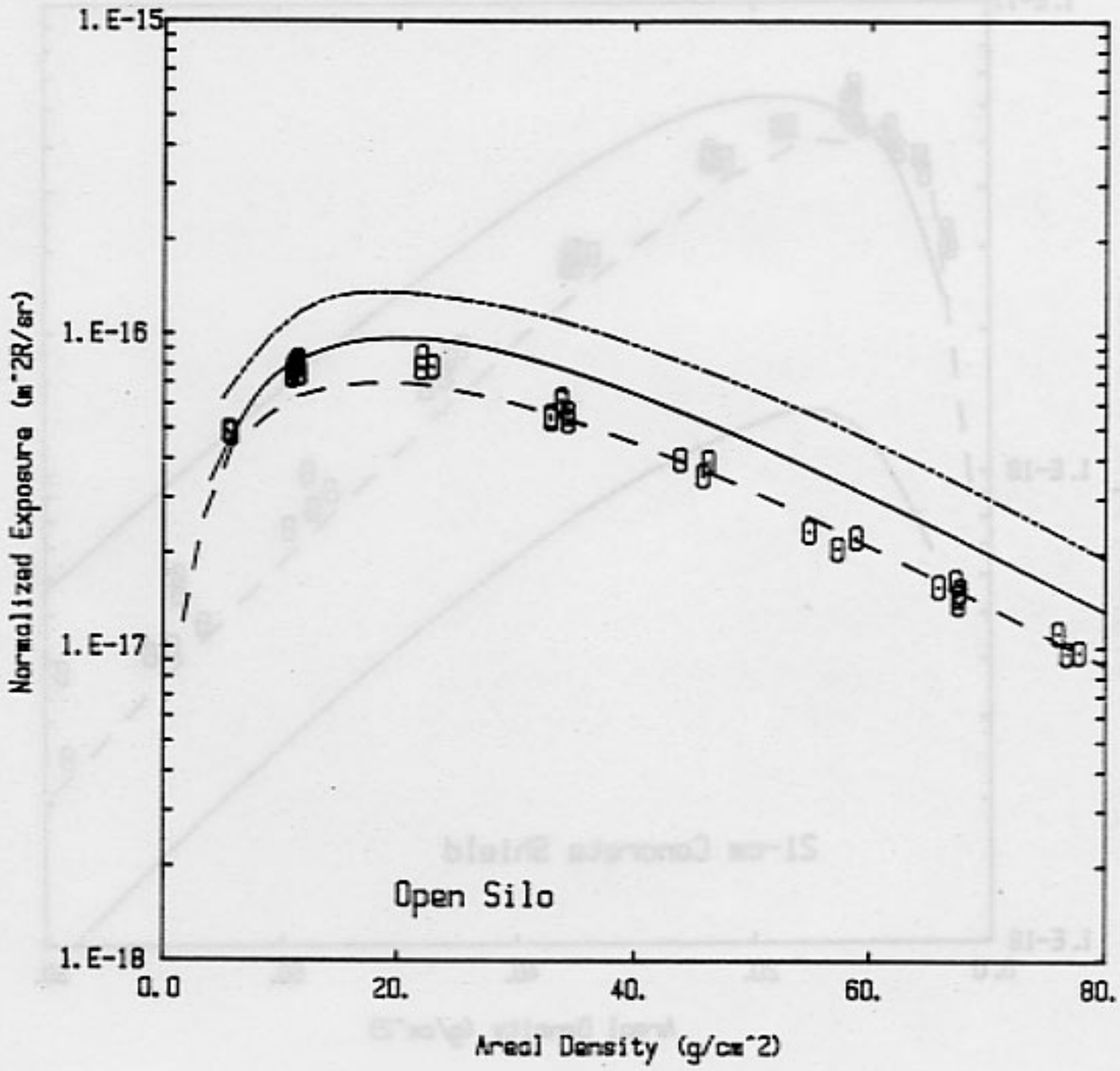

Fig. 6.3 Comparison of MicroSkyshine results with experimental data and results of other calculations for the conditions of the KSU benchmark skyshine experiments. A ^{60}Co source is within a cylindrical silo with a 150.5-degree full-angle of collimation and no overhead shielding. Solid line: MicroSkyshine. Broken line: G^3. Dashed line: 10-group DOT calculations.

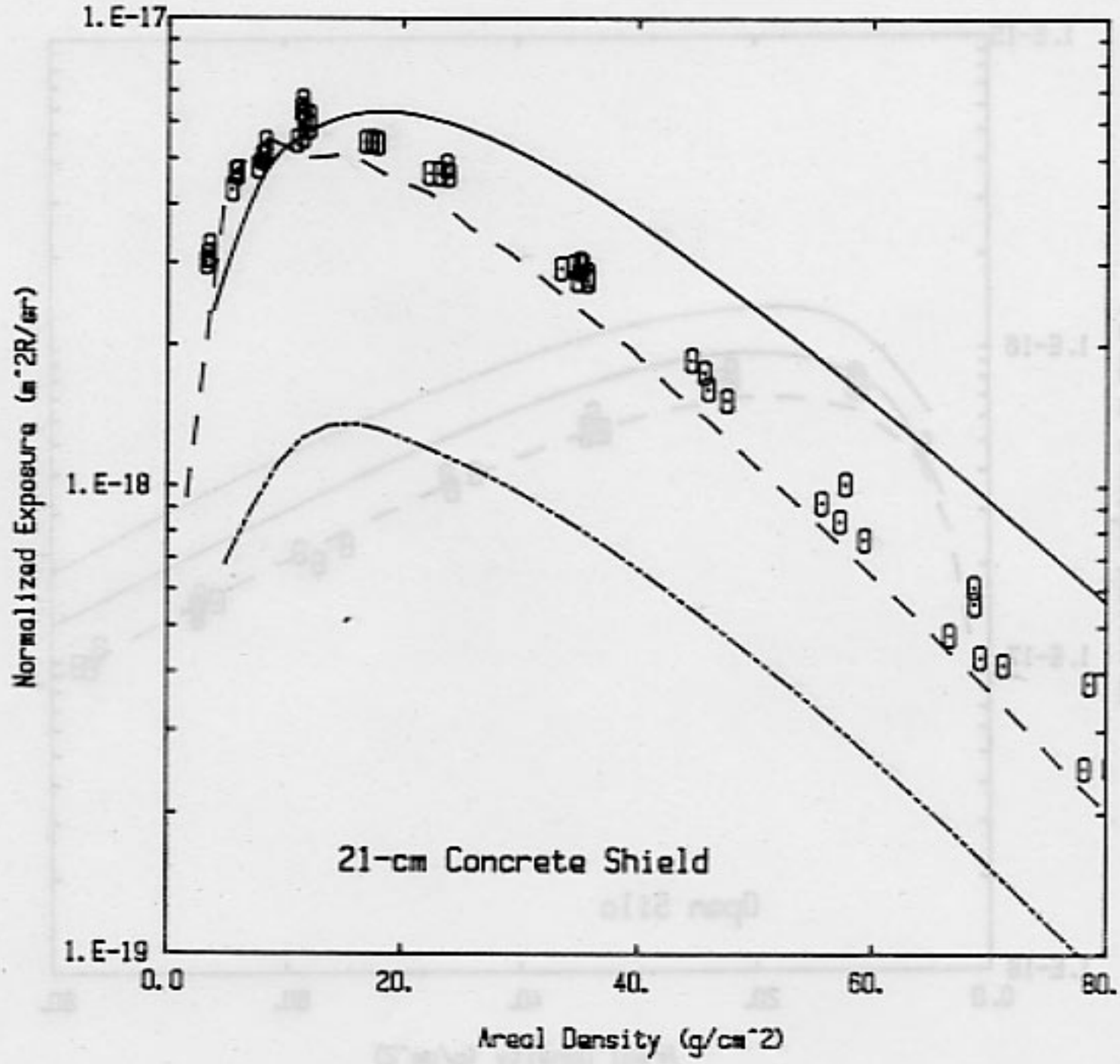

Fig. 6.4 Comparison of MicroSkyshine results with experimental data and results of other calculations for the conditions of the KSU benchmark skyshine experiments. A ^{60}Co source is within a cylindrical silo with a 150.5-degree full-angle of collimation and 21 cm of overhead concrete shielding. Solid line: MicroSkyshine. Broken line: G^3. Dashed line: 10-group DOT calculations.

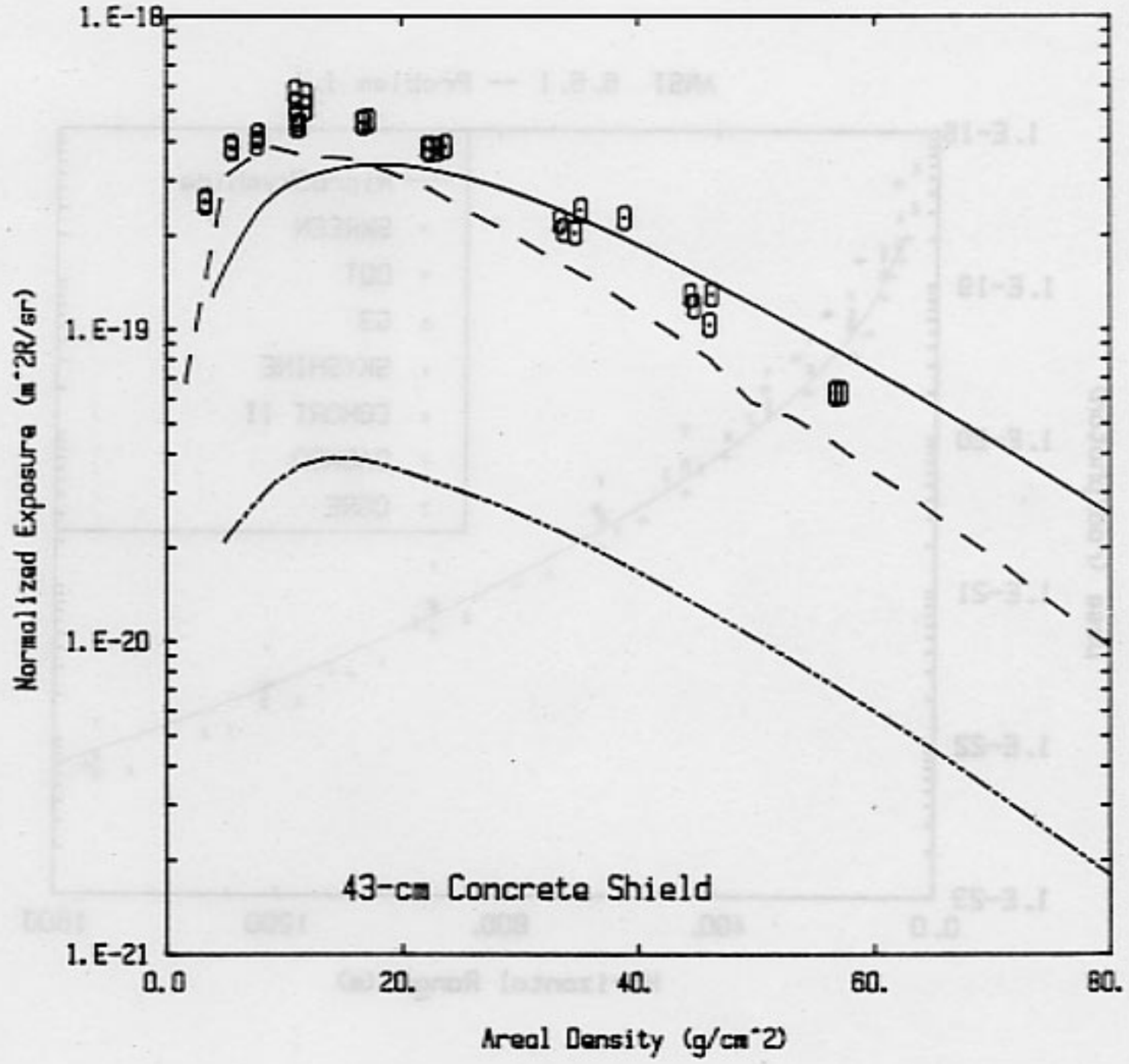

Fig. 6.5 Comparison of MicroSkyshine results with experimental data and results of other calculations for the conditions of the KSU benchmark skyshine experiments. A ^{60}Co source is within a cylindrical silo with a 150.5-degree full-angle of collimation and 42.8 cm of overhead concrete shielding. Solid line: MicroSkyshine. Broken line: G^3. Dashed line: 39-group DOT calculations.

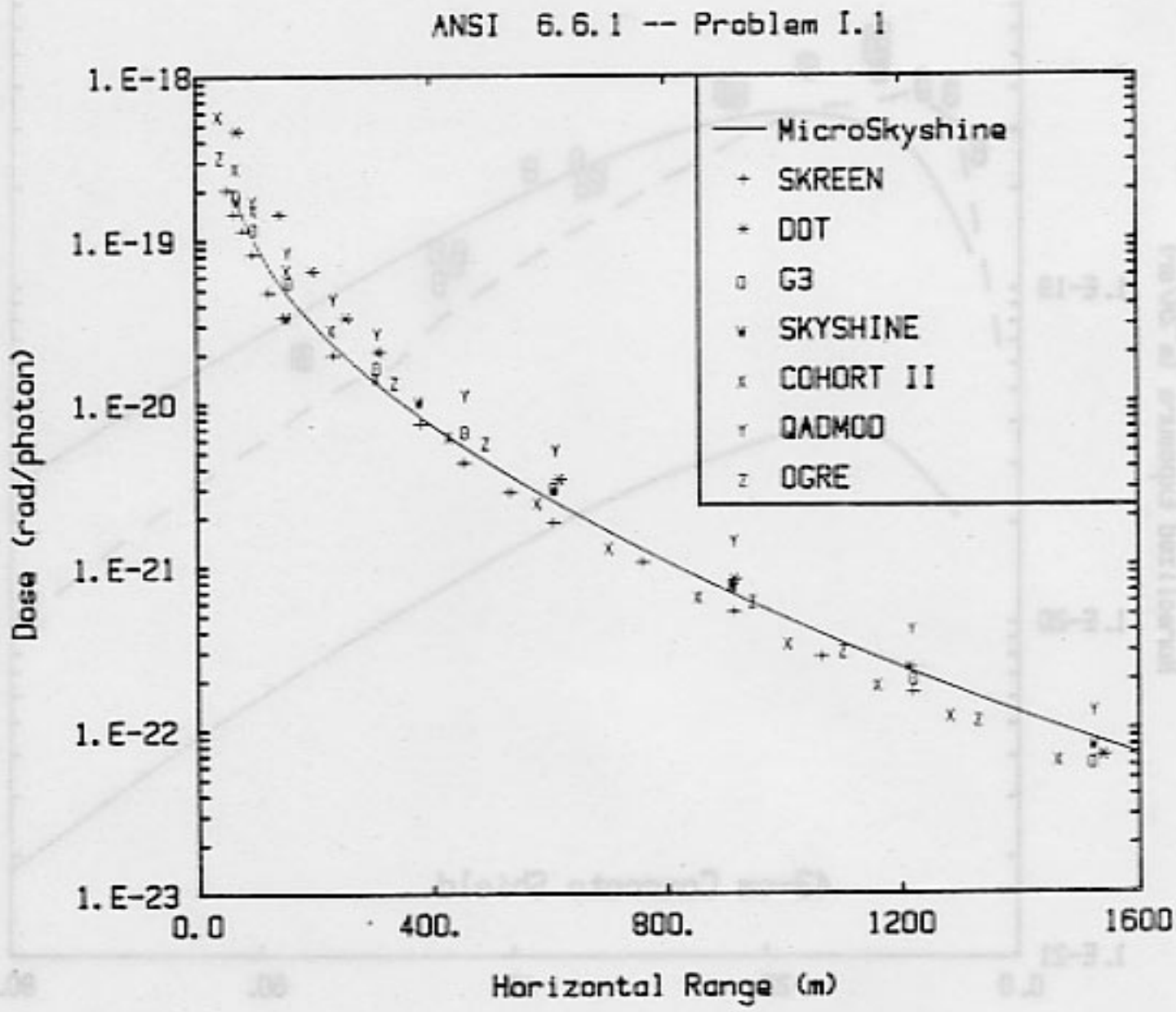

Fig. 6.6 Comparison of MicroSkyshine calculations with benchmark calculations for ANSI/ANS-6.6.1 Reference Problem I.1.

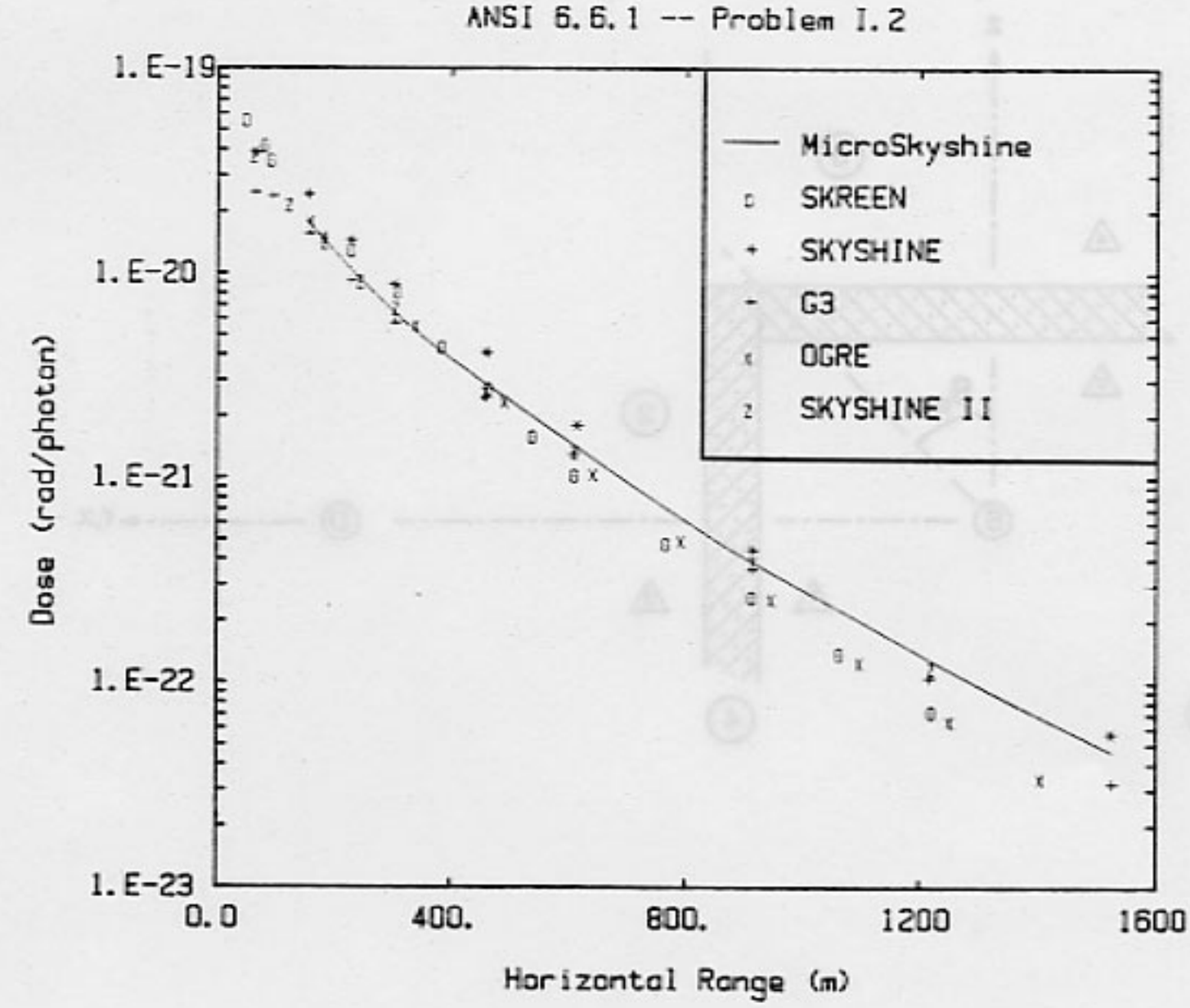

Fig. 6.7 Comparison of MicroSkyshine calculations with benchmark calculations for ANSI/ANS-6.6.1 Reference Problem I.2.

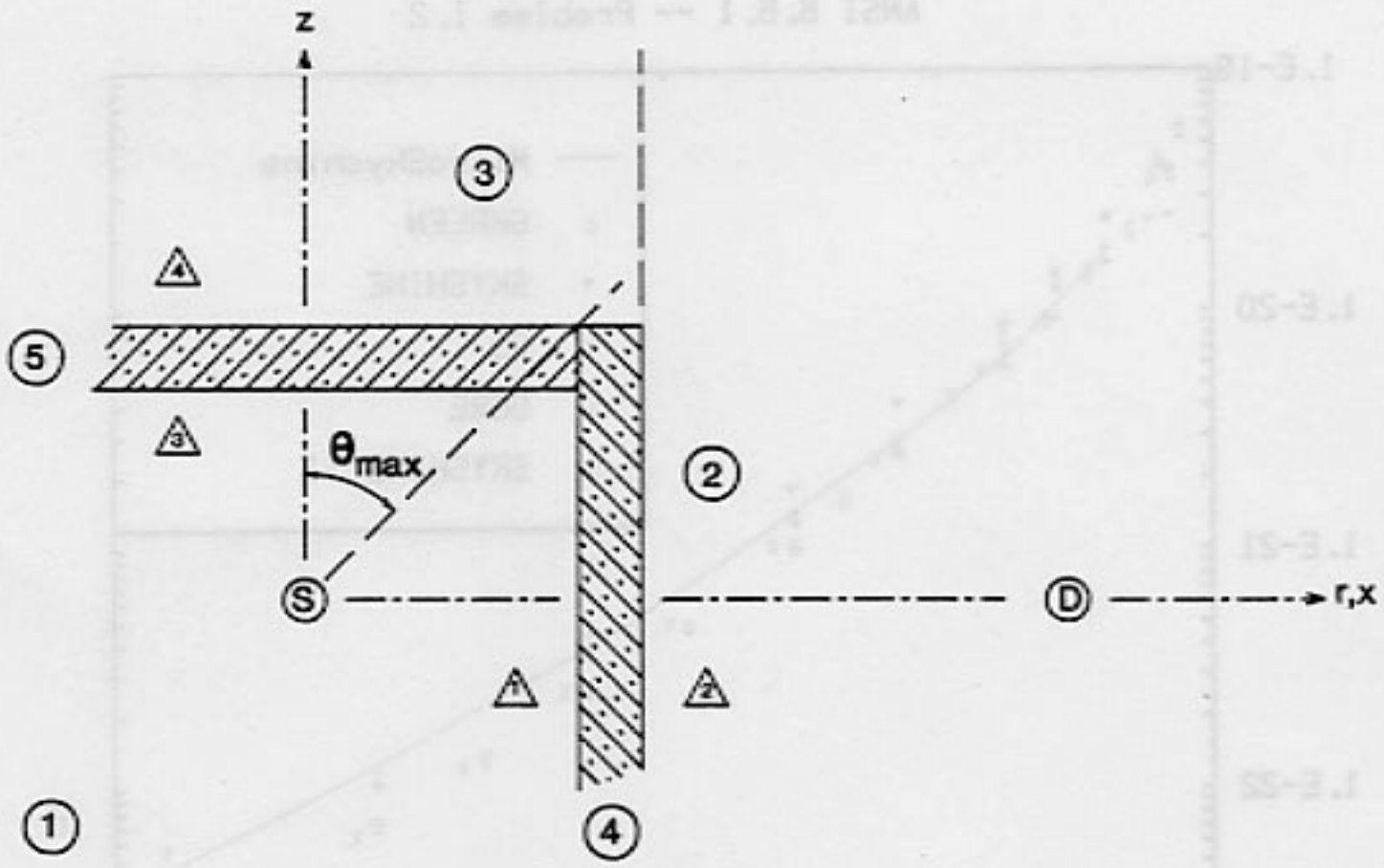

Fig. 6.8 Vertical section view of the geometry employed in G^3 calculations for the point source in a cylindrical silo shield. Notation is described in the text.

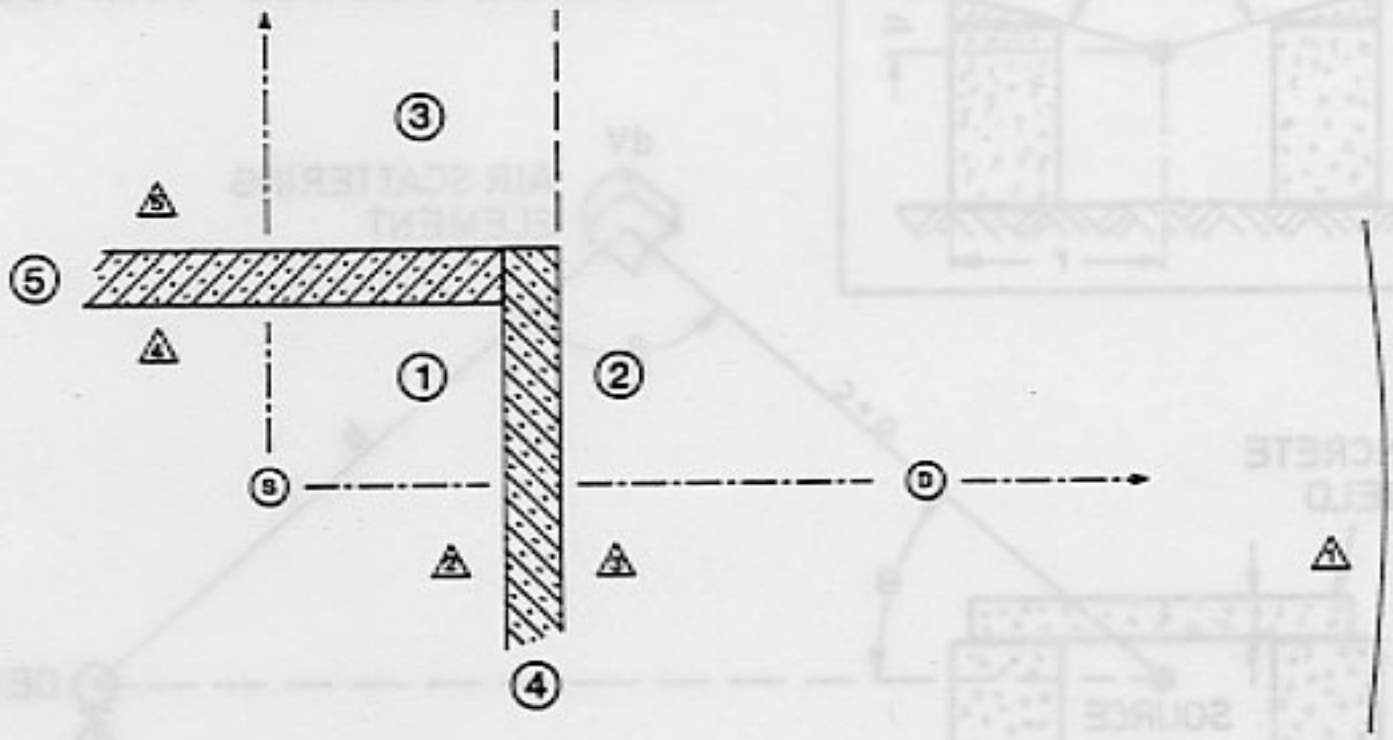

Fig. 6.9 Vertical section view of the geometry employed in G^3 calculations for the point source behind an infinite vertical wall.

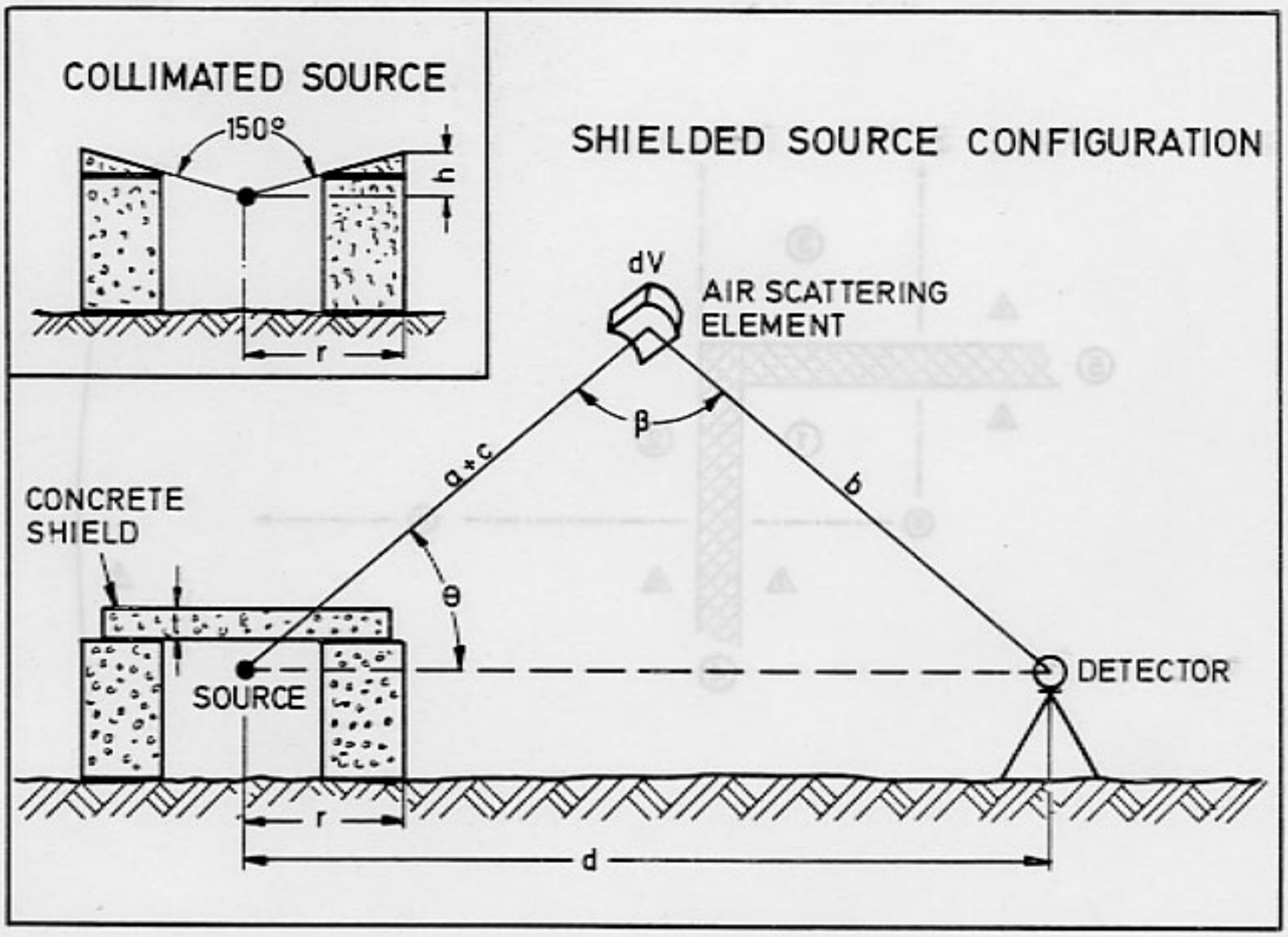

Fig. 6.10 Geometry for benchmark skyshine experiments. Source is in a concrete annular cylinder (2.5-m i.d., 4.35-m o.d., 2.29-m height) and either shielded from above by a concrete slab (21.0 or 42.8 cm thick) or collimated into a 150.5-degree vertical cone (inset). Distances a and b refer to the air path distances between the source and scattering element and between the scattering element and the detector respectively. Ray distance through concrete is denoted by c.

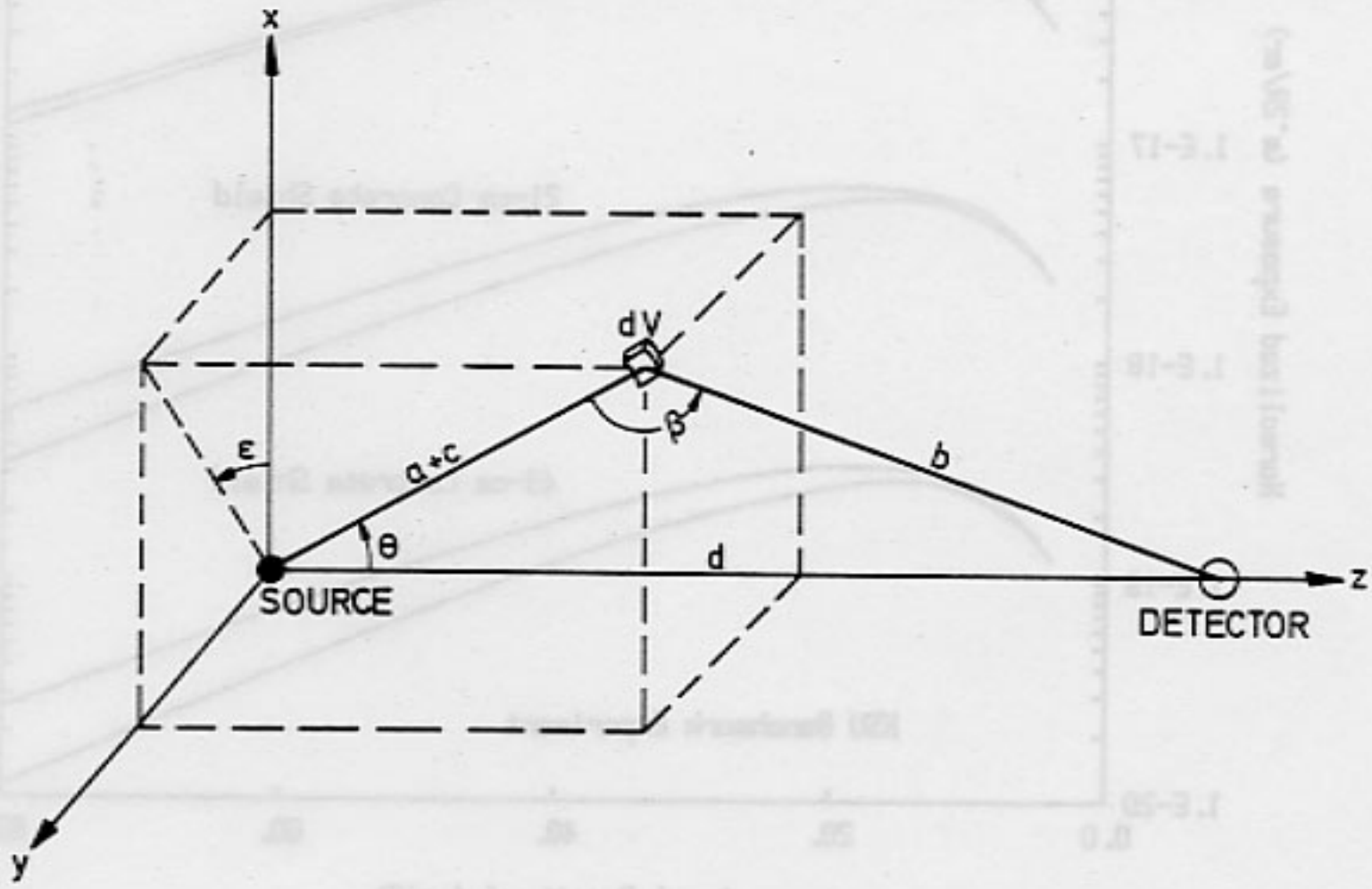

Fig. 6.11 Coordinate system for the K-SHINE single-scatter skyshine model.

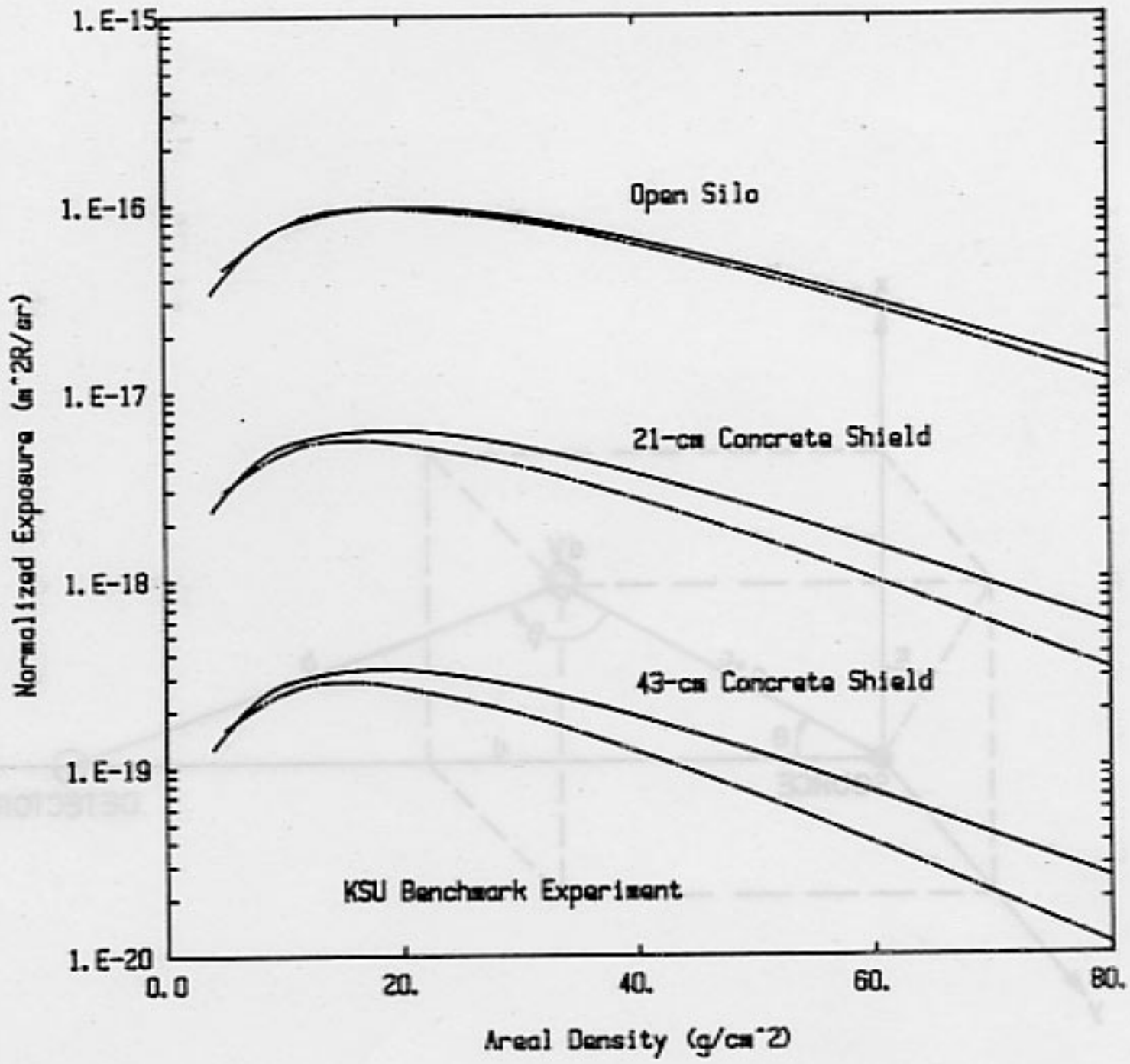

Fig. 6.12 Comparison of MicroSkyshine results (solid lines) with K-Shine results (broken lines) for the conditions of the KSU benchmark skyshine experiments.

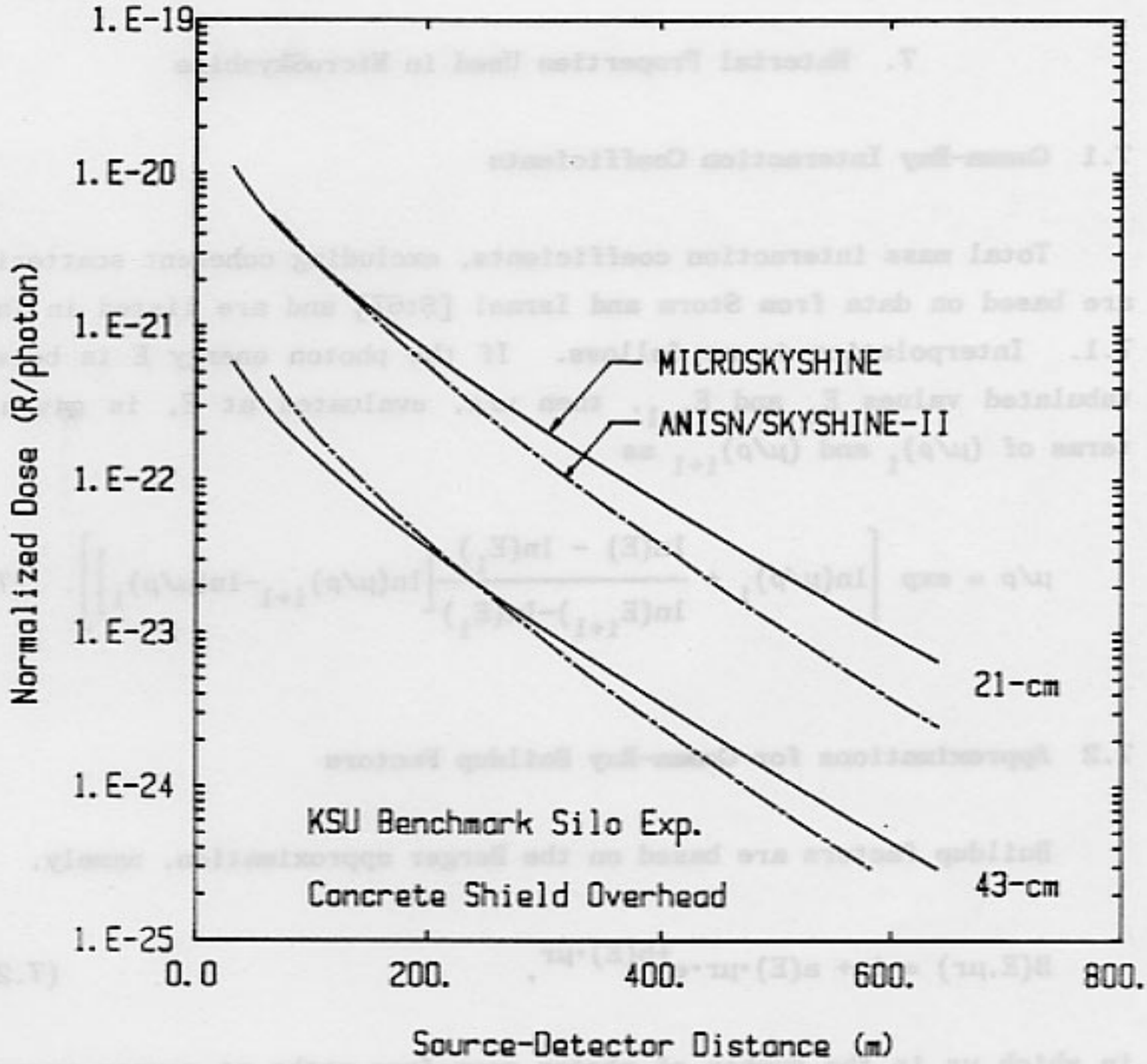

Fig. 6.13 Comparison of MicroSkyshine results (solid lines) with hybrid ANISN/SKYSHINE-II results [Ke82] (broken lines) for the conditions of the KSU benchmark skyshine experiments with overhead concrete shielding.

7. Material Properties Used in MicroSkyshine

7.1 Gamma-Ray Interaction Coefficients

Total mass interaction coefficients, excluding coherent scattering, are based on data from Storm and Israel [St67] and are listed in Table 7.1. Interpolation is as follows. If the photon energy E is between tabulated values E_i and E_{i+1}, then μ/ρ, evaluated at E, is given in terms of $(\mu/\rho)_i$ and $(\mu/\rho)_{i+1}$ as

$$\mu/\rho = \exp\left[\ln(\mu/\rho)_i + \frac{\ln(E) - \ln(E_i)}{\ln(E_{i+1})-\ln(E_i)}\left[\ln(\mu/\rho)_{i+1}-\ln(\mu/\rho)_i\right]\right]. \quad (7.1)$$

7.2 Approximations for Gamma-Ray Buildup Factors

Buildup factors are based on the Berger approximation, namely,

$$B(E,\mu r) = 1 + a(E)\cdot\mu r\cdot e^{+b(E)\cdot\mu r}, \quad (7.2)$$

in which μr is the number of photon mean-free-paths at source energy E and the coefficients a and b depend not only on the source energy E but also on the attenuating medium. The buildup factors employed in the MicroSkyshine method are air-kerma buildup factors which are suitable for exposure and dose equivalent [Ch84]. The coefficients listed in Table 7.2 are based on the work of Chilton, Eisenhauer, and Simmons [Ch75, Ch79]. Interpolation is as follows. If photon energy E is between tabulated values E_i and E_{i+1}, the the value of a (or b)

evaluated at energy E is given by

$$a = a_i + \frac{\ln(E) - \ln(E_i)}{\ln(E_{i+1}) - \ln(E_i)} \left[a_{i+1} - a_i \right]. \qquad (7.3)$$

Table 7.1. Gamma-ray mass interaction coefficients (total - coherent scattering) used in the MicroSkyshine Program [St67].

E	μ/ρ (cm^2/g)						
(MeV)	Air	H_2O	Concrete	Fe	Pb	Zr	UO_2
0.10	0.148	0.165	0.166	0.333	5.32	0.911	1.48
0.15	0.133	0.148	0.138	0.179	1.90	0.353	2.18
0.20	0.122	0.135	0.124	0.136	0.933	0.208	1.09
0.30	0.106	0.118	0.107	0.105	0.369	0.123	0.430
0.40	0.0954	0.106	0.0954	0.0913	0.215	0.0970	0.248
0.50	0.0868	0.0966	0.0871	0.0824	0.150	0.0845	0.172
0.60	0.0803	0.0895	0.0806	0.0758	0.117	0.0753	0.131
0.80	0.0705	0.0786	0.0709	0.0662	0.0840	0.0645	0.0922
1.00	0.0636	0.0707	0.0636	0.0594	0.0680	0.0572	0.0736
1.50	0.0516	0.0574	0.0518	0.0486	0.0509	0.0465	0.0538
2.00	0.0442	0.0493	0.0447	0.0424	0.0451	0.0412	0.0472
3.00	0.0357	0.0396	0.0364	0.0360	0.0416	0.0362	0.0496
4.00	0.0308	0.0340	0.0319	0.0331	0.0416	0.0347	0.0420
5.00	0.0275	0.0303	0.0289	0.0315	0.0424	0.0340	0.0423
6.00	0.0252	0.0277	0.0269	0.0305	0.0433	0.0339	0.0430
8.00	0.0222	0.0200	0.0244	0.0296	0.0456	0.0341	0.0448
10.00	0.0203	0.0222	0.0230	0.0298	0.0488	0.0352	0.0475

Table 7.2. Coefficients for the Berger form of the buildup factor as used in the MicroSkyshine method [Ch75, Ch79].

E	Air		Water		Concrete		Iron		Lead	
(MeV)	a	b	a	b	a	b	a	b	a	b
0.10	5.93	0.113	6.11	0.120	1.83	0.028	0.24	-0.030	0.20	0.479
0.15	4.70	0.121	4.88	0.125	2.19	0.054	0.52	-0.015	0.21	-0.075
0.20	3.94	0.113	4.13	0.118	2.20	0.065	0.77	0.004	0.08	-0.054
0.30	3.10	0.094	3.18	0.096	2.03	0.067	1.06	0.022	0.08	-0.040
0.40	2.61	0.079	2.67	0.080	1.87	0.061	1.15	0.033	0.11	-0.033
0.50	2.29	0.067	2.32	0.068	1.73	0.055	1.16	0.036	0.15	-0.028
0.60	2.05	0.058	2.07	0.059	1.60	0.049	1.14	0.036	0.19	-0.024
0.80	1.71	0.045	1.74	0.045	1.41	0.040	1.09	0.032	0.25	-0.019
1.00	1.50	0.035	1.50	0.036	1.27	0.032	1.03	0.028	0.30	-0.015
1.50	1.16	0.021	1.16	0.021	1.02	0.021	0.88	0.020	0.36	-0.007
2.00	0.97	0.013	0.97	0.013	0.89	0.014	0.76	0.018	0.38	0.004
3.00	0.75	0.005	0.74	0.005	0.71	0.007	0.66	0.014	0.37	0.019
4.00	0.61	0.001	0.62	0.000	0.59	0.004	0.56	0.015	0.31	0.038
5.00	0.53	-0.002	0.52	-0.002	0.49	0.004	0.49	0.017	0.24	0.062
6.00	0.47	-0.004	0.47	-0.005	0.45	0.002	0.42	0.021	0.19	0.082
8.00	0.37	-0.004	0.38	-0.006	0.36	0.001	0.33	0.028	0.11	0.125
10.00	0.31	-0.004	0.31	-0.005	0.30	0.003	0.25	0.039	0.07	0.161

8. Bibliography

An79 ANSI/ANS-6.6.1-1979, *American National Standard for Calculation and Measurement of of Direct and Scattered Gamma Radiation from LWR Nuclear Power Plants*, American Nuclear Society, LaGrange Park, Illinois, 1979.

Ch75 Chilton, A. B., C. M. Eisenhauer, and G. L. Simmons, "Point Isotropic Buildup Factors for Air, Water, and Iron," **Nucl. Sci. & Engg.**, 56, 263-270 (1975).

Ch79 Chilton, A. B., "Tschebycheff-Fitted Berger Coefficients for Eisenhauer-Simmons Gamma-Ray Buildup Factors in Ordinary Concrete," **Nucl. Sci. & Engg.**, 69, 436-438 (1979).

Ch83 Chou, Dong-Pao, Tsen-Pao Hsaio, and Guey-Her Lai, *SKYSHINE-P, A Point Kernel Computer Program for Calculating Skyshine Exposure Rates*, Report INER-0498, Institute of Nuclear Energy Research, Taiwan, Republic of China, 1983.

Ch84 Chilton, A. B., J. K. Shultis, and R. E. Faw, *Principles of Radiation Shielding*, Prentice-Hall, 1984.

Ge87 George, Darren, *Computational Techniques in Gamma-Ray Skyshine Analysis*, M.S. Thesis, Nuclear Engineering Department, Kansas State University, 1987.

Ke82 Keck, B., and P. Herchenroder, Nachrechnen eines Gamma-Skyshine-Benchmarkexperiments," **Atomwirtschaft**, May, 1982.

Ki68 Kitazume, Mitsuyuki, "A Simplified Calculation for Air-Scattered Gamma Rays," **J. Nucl. Sci. & Tech**, 5, 464-471 (1968).

La79 Lampley, C. M., The Skyshine-II Procedure: *Calculation of the Effects of Structure Design on Neutron, Primary Gamma-Ray, and Secondary Gamma-Ray Dose Rates in Air*, Report RRA-T7901 (NUREG/CR-0781), Radiation Research Associates, Fort Worth, Texas, 1979.

Ly58 Lynch, R. E., J. W. Benoit, W. P. Johnson, and C. D. Zerby, *A Monte Carlo Calculation of Air-Scattered Gamma Rays*, Report ORNL 2292, Oak Ridge National Laboratory, Oak Ridge, Tennessee, 1958.

Ma73 Malefant, Richard E., G^3: A *General Purpose Gamma-Ray Scattering Program*, Report LA-5176, Los Alamos Scientific Laboratory, Los Alamos, New Mexico, 1973.

My73 Mynatt, F. R., et al., *The DOT II Two-Dimensional Discrete-Ordinates Transport Code*, Report ORNL-TM-4280, Oak Ridge National Laboratory, Oak Ridge, Tennessee, 1973.

Na81 Nason, R. R., J. K. Shultis, R. E. Faw, and C. E. Clifford, "A Benchmark Gamma-Ray Skyshine Experiment," **Nucl. Sci. & Engg.**, 79, 404-416 (1981).

Pe65 Penny, S. K., D. K. Trubey, and M. B. Emmett, OGRE, *A Monte Carlo System for Gamma Ray Transport Studies, Including an Example, (OGRE-P1) for Transmission through Laminated Slabs*, Report ORNL-3905, Oak Ridge National Laboratory, Oak Ridge, Tennessee, 1965.

Pr76 Price, J. H., D. G. Collins, and M. B. Wells, *Utilization Instructions for SKYSHINE*, Report RRA-N7608, Radiation Research Associates, Fort Worth, Texas. 1976.

Rh73 Rhodes, W. A., and F. R. Mynatt, *The DOT-3 Two Dimensional, Discrete Ordinates Transport Code*, Report ORNL-TM-4280, Oak Ridge National Laboratory, Oak Ridge, Tennessee, 1973.

Ro73 Rogers, D.R., *BWR Turbine Equipment ^{16}N Radiation Shielding Studies*, Report NEDO-20206, General Electric Company, San Jose, California, 1976.

Ro80 Roseberry, M. L., *Benchmark Skyshine Exposure Rates*, M.S. Thesis, Nuclear Engineering Department, Kansas State University. 1980.

Ro82 Roseberry, M. L., and J. K. Shultis, "Point-Kernel Calculations of Skyshine Exposure Rates," **Nucl. Sci. & Engg.**, **80**, 334-338 (1982).

Rs75 *Documentation for CCC-75/G^3-6ED Code Package*, Report CCC-75, Radiation Shielding Information Center, Oak Ridge National Laboratory, Oak Ridge, Tennessee.

So75 Soffer, L., and L. C. Clemons, Jr., *COHORT-II: A Monte Carlo General Purpose Shielding Computer Code*, Report NASA-TN-D-6170, Lewis Research Center, Cleveland, Ohio.

St67 Storm, E., and H. I. Israel, *Photon Cross Sections from 0.001 to 100 MeV for Elements 1 through 100*, Report LA-3753, Los Alamos Scientific Laboratory, Los Alamos, New Mexico, 1967.

Tr61 Trubey, D. K., "The Single-Scattering Approximation to the Solution of the Gamma-Ray Air-Scattering Problem," Nucl. Sci. & Engg., 10, 102-116 (1961).

ACKNOWLEDGMENTS

The authors express their appreciation to Jeffrey C. Ryman of Oak Ridge National Laboratory for his very helpful advice during the course of this work. They also express their appreciation to C. A. Negin of Grove Engineering for his encouragement and advice during the course of this work, for his careful review of the manuscript, and for his many helpful suggestions. They also especially thank Richard Bowers of the Perry Nuclear Station for his review of the manuscript and for his valuable comments and suggestions.

APPENDICES

A. Tabulation of Results from MicroSkyshine Calculations

B. Line-Beam Gamma-Ray Response Functions

The following appendices are published as a separate supplementary document:

C. The K-SHINE Single-Scatter Codes

D. Tabulation of Results from K-SHINE Calculations

E. Tabulation of Results from G^3 Calculations

F. Tabulation of Results from MORSE Calculations

APPENDIX A

Tabulation of Results from MicroSkyshine Calculations

Table A6.1. Results of MicroSkyshine calculations for point sources collimated in 2π geometry. Air density = 0.00125 g/cm^3. Quadrature order = 16.

	Exposure (R) per Photon			
x (m)	0.1 MeV	0.2 MeV	0.5 MeV	1.0 MeV
25	4.354E-19	5.805E-19	5.193E-19	4.814E-19
50	1.116E-19	1.695E-19	2.137E-19	2.129E-19
75	4.362E-20	7.415E-20	1.168E-19	1.266E-19
100	2.014E-20	3.803E-20	7.091E-20	8.329E-20
200	1.801E-21	4.923E-21	1.425E-20	2.202E-20
300	2.660E-22	9.632E-22	3.679E-21	7.136E-21
400	5.126E-23	2.253E-22	1.067E-21	2.531E-21
500	1.170E-23	5.837E-23	3.333E-22	9.549E-22
600	2.999E-24	1.621E-23	1.099E-22	3.789E-22
700	8.343E-25	4.739E-24	3.784E-23	1.573E-22
800	2.470E-25	1.445E-24	1.349E-23	6.814E-23
900	7.679E-26	4.566E-25	4.958E-24	3.069E-23
1000	2.485E-26	1.487E-25	1.872E-24	1.432E-23

x (m)	2.0 MeV	5.0 MeV	10. MeV
25	6.270E-19	5.579E-19	7.010E-19
50	2.579E-19	2.286E-19	2.711E-19
75	1.471E-19	1.340E-19	1.523E-19
100	9.522E-20	9.000E-20	9.956E-20
200	2.696E-20	3.024E-20	3.263E-20
300	1.030E-20	1.382E-20	1.546E-20
400	4.478E-21	7.193E-21	8.539E-21
500	2.101E-21	4.037E-21	5.133E-21
600	1.038E-21	2.383E-21	3.257E-21
700	5.326E-22	1.460E-21	2.146E-21
800	2.814E-22	9.214E-22	1.454E-21
900	1.522E-22	5.959E-22	1.007E-21
1000	8.400E-23	3.937E-22	7.106E-22

Table A6.2. Normalized gamma-ray skyshine exposure as a function of areal density.separating source and detector. The source is Cobalt-60 and is collimated by a cone of 150.5-degree full angle. In one case, there is no overhead shielding, in another there is a 21-cm thick concrete shield, and in a third there is a 42.8-cm thick concrete shield. Concrete density is 2.32 g/cm^3 The normalized exposure is Roentgens per photon, multiplied by the square of the source-to-detector distance (m) and divided by the solid angle of collimation. Air density is 1.25 mg/cm^3 and the areal density is the product of the density and the source-to-detector distance. Calculations were performed using the MicroSkyshine program.

Areal Density (g/cm^3)	Source-Detector Distance (m)	Normalized Exposure (m^2 R/sr) [1.17-1.33 MeV Avg.] Open Silo	21-cm Concrete	43-cm Concrete
4	32	3.396E-17	2.398E-18	1.291E-19
8	64	6.434E-17	4.476E-18	2.424E-19
12	96	8.417E-17	5.734E-18	3.091E-19
16	128	9.427E-17	6.270E-18	3.359E-19
20	160	9.692E-17	6.287E-18	3.342E-19
24	192	9.438E-17	5.969E-18	3.148E-19
28	224	8.861E-17	5.461E-18	2.855E-19
32	256	8.100E-17	4.866E-18	2.521E-19
36	288	7.261E-17	4.252E-18	2.182E-19
40	320	6.411E-17	3.658E-18	1.860E-19
44	352	5.597E-17	3.113E-18	1.566E-19
48	384	4.841E-17	2.624E-18	1.306E-19
52	416	4.157E-17	2.196E-18	1.082E-19
56	448	3.550E-17	1.827E-18	8.899E-20
60	480	3.018E-17	1.513E-18	7.289E-20
64	512	2.557E-17	1.249E-18	5.943E-20
68	544	2.160E-17	1.028E-18	4.833E-20
72	576	1.821E-17	8.438E-19	3.919E-20
76	608	1.533E-17	6.919E-19	3.172E-20
80	640	1.289E-17	5.665E-19	2.563E-20

APPENDIX B

Line-Beam Gamma-Ray Response Functions

Table B1. Gamma-ray atmospheric scattering coefficients used in the PRIGAM data base of the RRA SKYSHINE-II code [La79].

Source Energy Range: 9 - 10 MeV

Angle Range (degrees)	Coefficient a	Coefficient b	Coefficient c
0 - 1	-0.96633	-2.22751	0.00124
1 - 2	-7.23194	-1.59176	0.00116
2 - 3	-10.55880	-1.03487	0.00228
3 - 5	-10.71092	-1.10146	0.00216
5 - 7	-15.95755	-0.16114	0.00399
7 - 10	-11.35975	-1.25891	0.00159
10 - 15	-10.74326	-1.49491	0.00144
15 - 20	-12.98317	-1.16770	0.00256
20 - 30	-14.41240	-1.03743	0.00298
30 - 40	-15.80386	-0.88826	0.00416
40 - 50	-15.84307	-0.96073	0.00479
50 - 60	-13.66694	-1.46949	0.00482
60 - 70	-17.69994	-0.66462	0.00743
70 - 80	-19.20303	-0.38074	0.00883
80 - 90	-16.58897	-1.03876	0.00657
90 - 100	-15.18189	-1.38329	0.00580
100 - 120	-17.58408	-0.82025	0.00921
120 - 140	-15.98180	-1.25561	0.00757
140 - 160	-17.44104	-0.96695	0.00862
160 - 180	-17.76595	-0.92762	0.00971

Source Energy Range: 8 - 9 MeV

Angle Range (degrees)	Coefficient a	Coefficient b	Coefficient c
0 - 1	-1.27643	-2.19521	0.00117
1 - 2	-6.02626	-1.86655	0.00034
2 - 3	-9.32754	-1.41189	0.00068
3 - 5	-10.08947	-1.22374	0.00188
5 - 7	-11.52567	-1.02790	0.00239
7 - 10	-12.54757	-0.95172	0.00256
10 - 15	-16.28294	-0.31207	0.00404
15 - 20	-12.47079	-1.27018	0.00210
20 - 30	-13.79041	-1.12887	0.00300
30 - 40	-13.44670	-1.35021	0.00308
40 - 50	-15.25742	-1.08369	0.00422
50 - 60	-15.89613	-1.03279	0.00527
60 - 70	-17.16479	-0.80018	0.00655
70 - 80	-16.28027	-1.07681	0.00599
80 - 90	-19.24190	-0.47628	0.00839
90 - 100	-19.02226	-0.58027	0.00797
100 - 120	-18.44720	-0.70765	0.00867
120 - 140	-17.89644	-0.89165	0.00817
140 - 160	-19.65666	-0.42998	0.01047
160 - 180	-15.62134	-1.48406	0.00565

Table B1. Gamma-ray atmospheric scattering coefficients used in the PRIGAM data base of the RRA SKYSHINE-II code [La79].

Source Energy Range: 7 - 8 MeV

Angle Range (degrees)	Coefficient a	Coefficient b	Coefficient c
0 - 1	-1.61453	-2.07488	0.00185
1 - 2	-6.32340	-1.76996	0.00078
2 - 3	-5.99313	-1.90355	0.00086
3 - 5	-10.52523	-1.13105	0.00211
5 - 7	-10.45683	-1.26182	0.00174
7 - 10	-9.85828	-1.47730	0.00158
10 - 15	-12.93887	-1.00588	0.00246
15 - 20	-15.12577	-0.67508	0.00348
20 - 30	-15.62516	-0.71210	0.00387
30 - 40	-14.92150	-1.02963	0.00367
40 - 50	-15.88956	-0.89034	0.00511
50 - 60	-18.57085	-0.41270	0.00684
60 - 70	-16.88673	-0.82599	0.00654
70 - 80	-17.29063	-0.75680	0.00758
80 - 90	-19.08473	-0.44583	0.00851
90 - 100	-19.62418	-0.27734	0.01072
100 - 120	-19.91608	-0.23485	0.01189
120 - 140	-18.55849	-0.64599	0.00947
140 - 160	-26.29880	1.04575	0.01546
160 - 180	-16.83810	-1.12779	0.00843

Source Energy Range: 6 - 7 MeV

Angle Range (degrees)	Coefficient a	Coefficient b	Coefficient c
0 - 1	-2.38309	-1.90294	0.00227
1 - 2	-4.80042	-2.06050	0.00030
2 - 3	-7.47771	-1.62820	0.00138
3 - 5	-8.84173	-1.44803	0.00170
5 - 7	-8.77149	-1.59304	0.00125
7 - 10	-17.85831	0.23745	0.00540
10 - 15	-11.52531	-1.23708	0.00229
15 - 20	-13.26708	-1.03658	0.00275
20 - 30	-14.59400	-0.88523	0.00359
30 - 40	-15.08376	-0.94101	0.00395
40 - 50	-15.26557	-1.02850	0.00436
50 - 60	-14.40582	-1.28041	0.00472
60 - 70	-17.16684	-0.70713	0.00727
70 - 80	-16.82616	-0.87989	0.00692
80 - 90	-17.77261	-0.70027	0.00781
90 - 100	-18.42287	-0.61044	0.00838
100 - 120	-17.43135	-0.82067	0.00893
120 - 140	-15.56391	-1.35470	0.00667
140 - 160	-20.75914	0.05193	0.01584
160 - 180	-22.50772	0.16286	0.01164

Table B1. Gamma-ray atmospheric scattering coefficients used in the PRIGAM data base of the RRA SKYSHINE-II code [La79].

Source Energy Range: 5 - 6 MeV

Angle Range (degrees)	Coefficient a	Coefficient b	Coefficient c
0 - 1	-1.17040	-2.17234	0.00171
1 - 2	-6.28665	-1.77324	0.00085
2 - 3	-6.92961	-1.70296	0.00138
3 - 5	-9.37788	-1.31503	0.00204
5 - 7	-9.19481	-1.50111	0.00152
7 - 10	-10.63778	-1.27132	0.00208
10 - 15	-12.49068	-1.02191	0.00286
15 - 20	-12.96586	-1.02922	0.00303
20 - 30	-12.74737	-1.24221	0.00294
30 - 40	-14.33475	-1.05459	0.00387
40 - 50	-15.27230	-0.94429	0.00499
50 - 60	-15.37394	-1.05225	0.00497
60 - 70	-15.79401	-0.98227	0.00612
70 - 80	-18.83327	-0.39076	0.00842
80 - 90	-16.85590	-0.88791	0.00704
90 - 100	-19.22762	-0.30986	0.01064
100 - 120	-16.74614	-0.96728	0.00832
120 - 140	-19.83728	-0.38135	0.00937
140 - 160	-20.87526	-0.08079	0.01287
160 - 180	-21.24854	-0.07652	0.01207

Source Energy Range: 4 - 5 MeV

Angle Range (degrees)	Coefficient a	Coefficient b	Coefficient c
0 - 1	-1.35251	-2.09433	0.00238
1 - 2	-6.39405	-1.64521	0.00188
2 - 3	-5.14678	-2.03407	0.00108
3 - 5	-13.22635	-0.45479	0.00436
5 - 7	-13.89037	-0.39186	0.00465
7 - 10	-12.03440	-0.91836	0.00329
10 - 15	-12.98685	-0.83081	0.00369
15 - 20	-14.23684	-0.72083	0.00396
20 - 30	-13.50491	-1.01001	0.00362
30 - 40	-13.50518	-1.17783	0.00370
40 - 50	-16.39047	-0.66536	0.00572
50 - 60	-16.86620	-0.65382	0.00626
60 - 70	-19.25792	-0.24138	0.00735
70 - 80	-17.19453	-0.59774	0.00913
80 - 90	-16.49124	-0.93109	0.00692
90 - 100	-20.81064	-0.05883	0.00936
100 - 120	-20.82613	-0.04857	0.01101
120 - 140	-18.14961	-0.67325	0.00935
140 - 160	-21.16092	0.17101	0.01616
160 - 180	-23.82805	0.80598	0.02023

Table B1. Gamma-ray atmospheric scattering coefficients used in the PRIGAM data base of the RRA SKYSHINE-II code [La79].

Source Energy Range: 3 - 4 MeV

Angle Range (degrees)	Coefficient a	Coefficient b	Coefficient c
0 - 1	-1.41427	-2.07019	0.00286
1 - 2	-5.33547	-1.84693	0.00191
2 - 3	-8.29190	-1.30205	0.00302
3 - 5	-7.58098	-1.61380	0.00204
5 - 7	-12.03496	-0.77352	0.00389
7 - 10	-11.16974	-1.03341	0.00350
10 - 15	-12.45923	-0.87951	0.00394
15 - 20	-11.64471	-1.19637	0.00326
20 - 30	-15.75365	-0.45302	0.00533
30 - 40	-13.30522	-1.14323	0.00410
40 - 50	-15.40535	-0.81598	0.00530
50 - 60	-15.36346	-0.90304	0.00564
60 - 70	-14.99603	-1.04959	0.00618
70 - 80	-14.69474	-1.13174	0.00705
80 - 90	-17.08331	-0.65098	0.00886
90 - 100	-17.31468	-0.67162	0.00886
100 - 120	-17.30241	-0.73850	0.00875
120 - 140	-17.00349	-0.88367	0.00879
140 - 160	-21.66013	0.16085	0.01294
160 - 180	-19.71294	-0.41913	0.00929

Source Energy Range: 2 - 3 MeV

Angle Range (degrees)	Coefficient a	Coefficient b	Coefficient c
0 - 1	-1.09777	-2.09146	0.00374
1 - 2	-5.87928	-1.65446	0.00310
2 - 3	-7.25144	-1.50154	0.00327
3 - 5	-9.75290	-1.09374	0.00397
5 - 7	-8.56222	-1.43949	0.00304
7 - 10	-10.45913	-1.12257	0.00384
10 - 15	-13.33892	-0.61638	0.00510
15 - 20	-14.00175	-0.62580	0.00498
20 - 30	-13.65808	-0.82971	0.00483
30 - 40	-14.28149	-0.83548	0.00510
40 - 50	-14.40747	-0.93293	0.00520
50 - 60	-14.93978	-0.87661	0.00644
60 - 70	-15.05494	-0.93686	0.00663
70 - 80	-16.73682	-0.60065	0.00866
80 - 90	-15.43850	-0.93736	0.00803
90 - 100	-18.04227	-0.25090	0.01270
100 - 120	-16.87531	-0.75006	0.00877
120 - 140	-15.51526	-1.16113	0.00759
140 - 160	-18.00386	-0.46767	0.01329
160 - 180	-18.27325	-0.51747	0.01210

Table B1. Gamma-ray atmospheric scattering coefficients used in the PRIGAM data base of the RRA SKYSHINE-II code [La79].

Source Energy Range: 1 - 2 MeV

Angle Range (degrees)	Coefficient a	Coefficient b	Coefficient c
0 - 1	-1.88207	-1.83160	0.00638
1 - 2	-6.15557	-1.55195	0.00442
2 - 3	-6.68954	-1.57096	0.00404
3 - 5	-7.61911	-1.43174	0.00479
5 - 7	-8.74499	-1.29698	0.00485
7 - 10	-10.51921	-1.02387	0.00529
10 - 15	-10.74390	-1.09209	0.00492
15 - 20	-12.33465	-0.82242	0.00584
20 - 30	-12.70635	-0.88981	0.00572
30 - 40	-12.41500	-1.07663	0.00568
40 - 50	-13.64023	-0.92274	0.00646
50 - 60	-14.84865	-0.73399	0.00754
60 - 70	-17.12921	-0.24467	0.01027
70 - 80	-14.29750	-1.03933	0.00677
80 - 90	-16.27524	-0.66829	0.00800
90 - 100	-15.49397	-0.85092	0.00832
100 - 120	-15.89609	-0.78414	0.00950
120 - 140	-17.14375	-0.53206	0.01147
140 - 160	-16.03120	-0.82810	0.01049
160 - 180	-13.88944	-1.46034	0.00697

Source Energy Range: 0.5 - 1 MeV

Angle Range (degrees)	Coefficient a	Coefficient b	Coefficient c
0 - 1	-1.70224	-1.88534	0.00706
1 - 2	-3.74522	-2.03614	0.00489
2 - 3	-6.78916	-1.40120	0.00749
3 - 5	-9.66956	-0.83778	0.00962
5 - 7	-10.30129	-0.82406	0.00905
7 - 10	-13.67237	-0.15578	0.01097
10 - 15	-12.91123	-0.51830	0.00809
15 - 20	-13.44011	-0.51253	0.00787
20 - 30	-16.17589	0.03926	0.01026
30 - 40	-14.68676	-0.36593	0.00975
40 - 50	-13.04298	-0.88446	0.00769
50 - 60	-14.44376	-0.62403	0.00914
60 - 70	-16.26572	-0.25079	0.01107
70 - 80	-15.89551	-0.39649	0.01097
80 - 90	-15.63542	-0.59517	0.00945
90 - 100	-15.25005	-0.55038	0.01278
100 - 120	-15.51944	-0.56528	0.01256
120 - 140	-16.45744	-0.48418	0.01152
140 - 160	-15.57878	-0.66388	0.01211
160 - 180	-14.66253	-0.93023	0.01075

Table B1. Gamma-ray atmospheric scattering coefficients used in the PRIGAM data base of the RRA SKYSHINE-II code [La79].

Source Energy Range: 0.1 - 0.5 MeV

Angle Range (degrees)	Coefficient a	Coefficient b	Coefficient c
0 - 1	-3.03216	-1.36209	0.01758
1 - 2	-4.02539	-1.95695	0.00743
2 - 3	-5.00325	-1.87462	0.00689
3 - 5	-7.79520	-1.32186	0.00879
5 - 7	-8.64205	-1.17512	0.00942
7 - 10	-9.09309	-1.15442	0.00919
10 - 15	-9.36501	-1.16253	0.00944
15 - 20	-11.28526	-0.75515	0.01147
20 - 30	-10.62629	-1.08614	0.00891
30 - 40	-12.17277	-0.71810	0.01192
40 - 50	-13.91578	-0.31443	0.01483
50 - 60	-12.97496	-0.73646	0.01128
60 - 70	-12.52756	-0.90100	0.01083
70 - 80	-12.80100	-0.93309	0.01002
80 - 90	-14.43838	-0.51621	0.01326
90 - 100	-13.30396	-0.81320	0.01255
100 - 120	-13.95091	-0.70494	0.01294
120 - 140	-13.42071	-0.89696	0.01199
140 - 160	-13.24349	-0.96503	0.01198
160 - 180	-14.60762	-0.45341	0.01852

Source Energy Range: 0.01 - 0.1 MeV

Angle Range (degrees)	Coefficient a	Coefficient b	Coefficient c
0 - 1	2.64685	-3.05353	0.00944
1 - 2	0.34319	-3.03892	0.00562
2 - 3	-2.23370	-2.43497	0.01010
3 - 5	-3.63825	-2.13858	0.01288
5 - 7	-5.68574	-1.73715	0.01361
7 - 10	-6.19980	-1.67393	0.01435
10 - 15	-7.36487	-1.45444	0.01539
15 - 20	-9.98350	-0.67649	0.02337
20 - 30	-7.86144	-1.55991	0.01343
30 - 40	-9.12073	-1.28620	0.01615
40 - 50	-8.91406	-1.48840	0.01327
50 - 60	-9.65228	-1.27510	0.01723
60 - 70	-8.75517	-1.69228	0.01234
70 - 80	-9.41166	-1.51541	0.01453
80 - 90	-10.59076	-1.14491	0.01910
90 - 100	-10.92487	-1.01646	0.02190
100 - 120	-10.87449	-1.13016	0.01969
120 - 140	-10.25175	-1.37627	0.01667
140 - 160	-10.00213	-1.49537	0.01582
160 - 180	-10.47370	-1.32353	0.01834